BERICHTE
aus dem MARUM und dem Fachbereich Geowissenschaften der Universität Bremen

No. 313

Stegmann, S.,

Baeten, N., Fleischmann, T., Kluger, M.O., Kreiter, S., Lange, M., Li, W., Roskoden, R., Rösner, A., Schunn, W., Völker, D.

Report and preliminary results of R/V POSEIDON cruise POS472

NORGEotech

Geotechnical in situ investigation of slope stability in Norway

Trondheim (Norway) – Tromsø (Norway)
27.07.2014 – 12.08.2014

Berichte, MARUM – Zentrum für Marine Umweltwissenschaften, Fachbereich Geowissenschaften, Universität Bremen, No. 313, 103 pages, Bremen 2017

ISSN 2195-9633

Berichte aus dem MARUM und dem Fachbereich Geowissenschaften der Universität Bremen

published by

MARUM – Center for Marine Environmental Sciences
Leobener Strasse, 28359 Bremen, Germany
www.marum.de

and

Fachbereich Geowissenschaften der Universität Bremen
Klagenfurter Strasse, 28359 Bremen, Germany
www.geo.uni-bremen.de

The "Berichte aus dem MARUM und dem Fachbereich Geowissenschaften der Universität Bremen" appear at irregular intervals and serve for the publication of cruise, project and technical reports arising from the scientific work by members of the publishing institutions.

Citation:

Stegmann, S., Baeten, N., Fleischmann, T., Kluger, M.O., Kreiter, S., Lange, M., Li, W., Roskoden, R., Rösner, A., Schunn, W., Völker, D.: Report and preliminary results of R/V POSEIDON cruise POS472, NORGEotech, Geotechnical in situ investigation of slope stability in Norway, Trondheim (Norway) – Tromsø (Norway), 27.07.2014 – 12.08.2014. Berichte, MARUM – Zentrum für Marine Umweltwissenschaften, Fachbereich Geowissenschaften, Universität Bremen, No. 313, 103 pages. Bremen, 2017. ISSN 2195-9633.

An electronic version of this report can be downloaded from:
http://nbn-resolving.de/urn:nbn:de:gbv:46-MARUM9

Please place requests for printed copies as well as editorial concerns with reports@marum.de

BERICHTE AUS DEM MARUM UND DEM FACHBEREICH GEOWISSENSCHAFTEN
DER UNIVERSITÄT BREMEN

Report and preliminary results of RV POSEIDON expedition POS472 NORGEotech

Geotechnical in situ investigation of slope stability in Norway

Trondheim (Norway) – Tromsø (Norway)

27/07/2014 – 12/08/2014

Stegmann, S. (Chief Scientist)

Baeten, N., Fleischmann, T., Kluger, M.O., Kreiter, S., Lange, M.,
Li, W.,Roskoden, R., Rösner, A., Schunn, W., Völker, D.

2017

Table of Content

1 Summary 3

2 Participants 5

3 Research Objectives of *POS472* 6

4 Introduction 7

5 Previous Work & Geological Setting of *POS472* Study Sites 9
5.1 Coastal Areas 10
5.1.1 Trondheim Harbour (TH) 11
5.1.2 Orkdalsfjorden (OF) 13
5.2 Open Ocean Setting 14
5.2.1 Lofoten Slope (LS) 14
5.2.2 Vesterålen Slope (VS) 15

6 Methods 17
6.1 Geotechnical in situ CPTu testing 17
6.1.1 Static CPTu Testing 17
6.1.2 Dynamic CPTu Testing (Free Fall-CPTu [FF-CPTu]) 20
6.1.2.1 Deepwater Free Fall CPTu (DW FF-CPTu) 20
6.1.2.2 Shallow-water Free Fall CPTu (SW FF-CPTu) 22
6.1.3 FF-CPTu Winch 23
6.2 Gravity Coring and Sediment Description 24
6.2.1 Gravity Coring 24
6.2.2 Sediment description 26
6.2.3 Physical properties 27
6.2.3.1 Cone penetrometer 27
6.2.3.2 Vane shear testing 28
6.2.3.3 Multi-sensor core logger (shore-based) 30
6.2.4 Pore Fluid Extraction and investigation of freshening 31
6.2.5 *In situ* temperature measurement 32
6.2.6 Bathymetry Site Survey 33

7 Measurements and Data 36
7.1 Data, Sample Storage & Availability 36
7.2 Preliminary Results 37

7.2.1 Coastal Setting 37
7.2.1.1 Trondheim Harbour (TH) 37
7.2.1.2 Orkdalsfjorden (OF) 43
7.2.2 Open Ocean Setting 48
7.2.2.1 Vesterålen Slope (VS) 48
7.2.2.2 Lofoten Slope (LS) 50

8 Station List 53

9 Acknowledgements 58

10 References 58

11 Appendix 62
11.1 Core Logs 62
11.2 Initial MSCL Logging Data 81
11.3 Bathymetry Maps (including track line) 101

1 Summary

The cruise NORGEotech / *POS472* (Trondheim [27/07/2014] – Tromsø [12/08/2014]) on RV Poseidon focused on the geotechnical *in situ* investigation of shallow failure and sediment deformation processes along the Norwegian continental margin.

Main important equipment for the working program was the static CPTu device GOST to identify and characterise failure prone sediments. The dynamic free-fall CPTu lance was a useful tool to profile the uppermost sediments (up to 6 mbsf), where surficial deformation processes are assumed. Gravity cores provide sediment for (i) laboratory-based deformation tests (e.g. shear test) to describe the mechanical behaviour in general as well the susceptibility to creep and for (ii) geochemical analyses to identify a contribution of fresh water. Multibeam bathymetry data were collected using the on-board *ELAC SB3050* system.

The expedition comprised four different study areas in two various physiographic settings.

The first part of the cruise (27/07 – 01/08/2014) was dedicated to the investigation of near-shore sediments along the coastlines of **Trondheim** and **Orkdalsfjorden** – both part of the Trondheimfjorden (Central Norway), which is intensively affected by ancient as well as recent failure processes. Here, soft and more sensitive clay-rich beds act as slide plane and, hence, control the location and the depth of the failures features. Pore pressure transients due to meteo-hydrological events (high precipitation, snow-melt), steep slope gradients (locally > 10°), creep processes as well as overloading of construction of infrastructure are responsible for landslide processes. Since the last century several collapses along the coastline resulted in high socio-economic loss.

Based on 8 static CPTu profiles with a maximum penetration depth of 20 mbsf, 15 FF-CPTu drops and 8 gravity cores, main preliminary findings can be summarised as follows:

- Static CPTu profiles in the Trondheim Harbour and Orkdalsfjorden reveal mechanically weak sediment layers accompanying with zones of increasing pore pressure. This layers coincide with glide planes of failure features.
- It is assumed, that groundwater flow occur within the prodeltaic deposits off Trondheim, which may generate pore pressure transients in the sediments. Initial analysis of pore fluids, extracted from cored sediments, reveal mixing processes of sea and fresh water within the sediments of the Trondheim Harbour.
- Gassy sediments, as identified by gas escape fractures and other extensional features in the cores after recovery and equilibration, were seen for the first time within the Orkdalsfjorden, The occurrence of gas may have a critical influence on the stability of the flanks of the fjord.
- In addition to the standard CPTu tests the Vibrotory CPTu mode was used at one location in the Orkdalsfjorden to evaluate the cyclic softening of fine-grained sediments *in situ.* From static and vibratory CPTu data a distinct drop in cyclic cone resistance in several silty layers represents a higher potential for cyclic softening compared to the surrounding fine-grained sediment. These findings highlight the potential of the GOST Vibratory CPTu testing mode for better identifying the vulnerability of marine fine-grained sediments to fail under seismic shaking.

- One study deals with the effect of the non-constant rate of the FF-CPTu lance during the penetration in the sediment on the soil classification. The latter one is an important parameter, which can be derived by the primary CPTu readings.

During the transit (02/08 – 03/08/2014) from the Trondheimsfjorden to the northern part of Norway three gravity cores were taken for a paleo-climate post-doc project by Johan Faust (NGU).

The sites we studied during the second part of the cruise (04/08 – 12/08/2014) are located along the Norwegian continental margin offshore **Lofoten** and **Vesterålen,** where the failure and deformation processes are yet poorly understood. Based on infinite slope stabilities analysis the Lofoten Slope as well as the Vesterålen Slope are *per se* stable. Therefore, external triggers (e.g. earthquake-induced shear strain) are needed to explain failures in this area (e.g. along the Vesterålen Slope). Other intriguing features and specific patterns in seabed geomorphology, like gullies, small graben-, cracks- or fracture-like features with variable dimensions (up to several hundred meter in width and 10-15m in thickness) delineate unstable sediment labs. These on-going sediment deformation processes could have severe implications for offshore infrastructure (e.g. pipelines).

- First main findings of the 6 static GOST-CPTu profiles we obtained within a small-scale failure feature along the Vesterålen Slope was the identification of mechanically weak zones. These zones are interbedded by coarser layers with high values of cone tip resistance q_t. The occurrence of sensitive fine-grained material may be responsible for the loss of strength in the deeper portion. 1D pseudo-static stability analysis (based on the CPTU data) attests that the Vesterålen slope to be stable except for exceptionally large earthquakes. The depth levels of the weak layers correspond well with the different glide planes of the slide complexes.
- 26 FF-CPTu drops and 13 gravity cores were located within the superficial deformation features along the Lofoten and Vesterålen Slope. Deformation and geotechnical experiments are still running in the laboratory of the MARUM working group “Marine Geotechnics”.

Based on a collaboration between the MARUM and other Norwegian Institutes (NGI, NGU, University Bergen, University Tromsø) data and findings obtained during *NORGEotech* / *POS472* will be incorporated into ongoing studies, which have been carried out in the frame of national Norwegian projects (SEABED, CDog and LOSlope [Vanneste et al. 2012]).

2 Participants

Name	Discipline	Institution
Stegmann, Sylvia, Dr.	Marine Geotechnics / Chief Scientist	MARUM
Baeten, Nicole, Dr.	Sedimentology, Observer	NGU Trondheim
Fleischmann, Timo	Technician	MARUM
Kluger, Max, PhD student	Geotechnics, Sedimentology	MARUM
Kreiter, Stefan, Dr.	Geotechnics, Sedimentology	MARUM
Lange, Matthias	Technician	MARUM
Li, Wie, PhD student	Geotechnics	MARUM
Roskoden, Robert, MSc. student	Geotechnics	MARUM
Rösner, Alexander, MSc. student	Sedimentology	MARUM
Schunn, Wolfgang	Technician	MARUM
Volker, David, Dr.	Bathymetry	MARUM

Participating Institutes

DFG-Research Centre MARUM, University Bremen, Leobener Strasse 8, 28359 Bremen, Germany

Geological Faculty, University of Bremen, Klagenfurter Strasse, 28359 Bremen, Germany

Geological Survey of Norway (NGU), Leiv, Eirikssons Vei 39, 7040 Trondheim, Norway

Norwegian Geotechnical Institute (NGI) - International Centre for Geohazards –, Postboks 3930 Ullevål Stadion, 0806 Oslo, Norway

University of Bergen, Allegt 41, NO-5020 Bergen

UiT University Tromsø – Institute of Geology, Postboks 6050 Langnes, N-9037 Tromsø, Norway

3 Research Objectives of *POS472*

The main scientific objective of *NORGEotech* / *POS472* was to complement and strengthen existing studies of shallow landslides along the Norwegian continental margin off Lofoten and Vesterålen as well as landslide studies in coastal areas (Trondheim Harbour, Orkdalsfjorden). Within the frame of national Norwegian projects (SEABED, CDog, LOslope) shallow landslide processes along the Norwegian margin off Vesterålen and Lofoten as well as landslide studies in coastal areas (Trondheim Harbour, Orkdalsfjorden) were studied intensively and provided a comprehensive data base consisting on bathymetry and seismic data, geotechnical and sedimentological data (for details and references please refer to Chapter 5).

Therefore overarching geotechnical aspects and goals represented the strategy of the working program during the cruise:

1) Identification and geotechnical *in sit*u characterisation of mechanical weak layers and pore pressure signatures using static and dynamic CPTu tools (GOST, FF-CPTu).

2) Recovery of gravity cores for geotechnical experiments in the NGI and MARUM laboratories (deformation tests, determination of soil index properties) and for ground-truthing at each CPTu location.

3) Comparison of rate-dependent CPTu probes: The FF-MARUM-Winch was used for the first time on a research vessel. This field activity was used to check i) the handling of the winch itself on a vessel, ii) the function of non-controlled lowering for free-fall tests with the FF-CPTu, and the accuracy of adjustment of velocity to lower an instrument.

4) Modification of some modules (CPTu cone, real-time data transfer unit, for details please refer to Chapter 6.1.2.1) of the Deep Water FF-CPTu has been done in the run-up of *POS472*. During the cruise these modified units were tested under different conditions (e.g. water depth). In addition to geotechnical aspects, the working program included also generic problems. The influence of the penetration rate on CPTu measurements is significant (see summary in Steiner et al., 2013). Since the 1970ies a wealth of study exists, that capture the influence of the penetration velocity on CPTu strength and pore pressure measurements empirically or numerically to perform strain-rate-correction of dynamic CPTu measurements relating to static CPTu standards (Lunne et al. 1997). The strain rate effect is complex as it depends on interactions of sedimentary conditions (e.g. grain size, state of consolidation, stiffness), the geometry of the cone and the penetration rate (drained / undrained conditions). Since the use of FF-CPTu instruments in the MARUM working group Marine Geotechnics, studies of strain rate dependency of dynamic FF-CPTu have been carried out in different settings (e.g. Stegmann et al. 2006, Steiner et al. 2013). With the availability of dynamic and static CPTu systems and the *MARUM FF-Winch* (see above) and sediment information based on gravity cores, the strain rate related data base was expanded

4 Introduction

The stability of marine sediment at ocean margins is a function of the intrinsic strength of the material and forces counteracting this strength (e.g. Hampton & Lee, 1996). When broken down to the particle scale, the strength is controlled by the friction coefficient for the individual mineral particles at a given confining stress, minus the pore pressure that is compensating for some of the external stress. This relationship, known as the effective stress (Terzaghi 1925), is a crucial aspect in slope stability since pore pressures may equal the overburden stress, exceed lithostatic values, and hence cause liquefaction (in coarse-grained sediment) or softening (in fine-grained material) by destroying the article network (e.g. Maltman, 1994; Moore et al., 1995). Both progressive soft sediment deformation (creeping, slumping, liquefaction) as well as brittle failure (faulting, hydrofracture) are important processes in mass wasting along continental slopes. The inherent mechanisms and factors governing slope stability and submarine landslides are known because of extensive research carried out by academia and industry (e.g. Hampton & Lee 1996; Leroueil 2001; Locat 2001; Locat & Lee 2002; Lee 2009), however, the temporal and spatial variability of landslide processes remain poorly understood. In general, submarine landslides occur in areas of weakness, often posed by the presence of weak mineral phases such as clay minerals, or by excess fluid that enhances pore pressure. Temporally, they are influenced by the sedimentology of depocenters as well as variations in seafloor pressure and temperature, seismicity and volcanic activity, or groundwater flow conditions (Lee 2009).

Although the abovementioned processes are broadly understood, the exact trigger mechanisms and their interaction of only a few given submarine landslides are known with certainty (Mienert 2004; Sultan et al. 2004). Slope failure is generally controlled by long-term governing factors and short-term triggers (Bjerrum 1967; Leroueil 2001; Locat 2001; Sultan et al., 2004; Petley et al. 2005). The first include topographic effects such as slope gradient, the geodynamic evolution of the margin (sedimentary or tectonic loading, unroofing, erosion, etc.) or other effects (glacial loading/unloading, marine transgression/regression, etc.; Lee 2009). The second group of trigger mechanisms act at a much shorter time-scale and usually cause a significant change in stress state. Among the processes most crucial to slope stability are (i) seismic loading (i.e. earthquakes), (ii) storm wave loading, (iii) rapid sedimentation (in deltas, through mass wasting, etc.), (iv) gas hydrate dissociation, (v) deep-seated fluid generation, upward migration and seepage, (vi) oversteepening, (vii) cyclic loading by tides, and (viii) charging and migration of fluids (e.g. free gas, groundwater) (see Locat & Lee, 2002 for details on many of those points). In the North Atlantic sector (incl. the Nordic Seas and Mediterranean Sea), numerous large landslides have been reported for the past 45 ka most likely associated with cryospheric-induced variabilities in isostatic energy, sedimentation rate and local sea level (isostatic uplift, postglacial seismicity, increase of sediment supply, release of free gas due to lowered sea level during the glacial (Maslin et al., 2004, Owen 2007).

Along the Norwegian margin, trigger mechanisms are strongly related to the sedimentary and erosional dynamics related to glacial-interglacial fluctuations during the Quaternary glacial period, and most recently to isostatic rebound and associated seismicity given the Arctic ice shield is retreating (also in Greenland). In addition to large-scale failure events (e.g. Storegga Slide [Bryn 2005], Traendadjupet Slide [Laberg & Vorren 2000], smaller-scale collapses of slope sediments occurred spaciously along the entire Norwegian

margin in shallow (Vesterålen Slope [Rise et al. 2012]) to intermediate (Lofoten Slope [Rise et al. 2009]) water depths, but also along the Norwegian coast and within fjords (e.g. Bjerrum 1971, Rygg & Oset 1996, Emdal et al. 1996, Longva et al. 2003) (Figure 1).

Considering the fact, i) that smaller-scale landslides show a high variety and complexity of morphology, pre-conditions and trigger mechanisms related to their geographical location (open ocean setting versus coastal setting), ii) that smaller-scale mass movements occur much more frequently than large-scale failure events and their impact may be significant along vulnerable portions of the coast and any submarine infrastructure (Lecomte et al. 2008), the approach of the cruise *POS472* is addressing both types of triggers (i.e. anthropogenic as well as natural) and further compares shallow landslides in coastal settings and at open ocean sites.

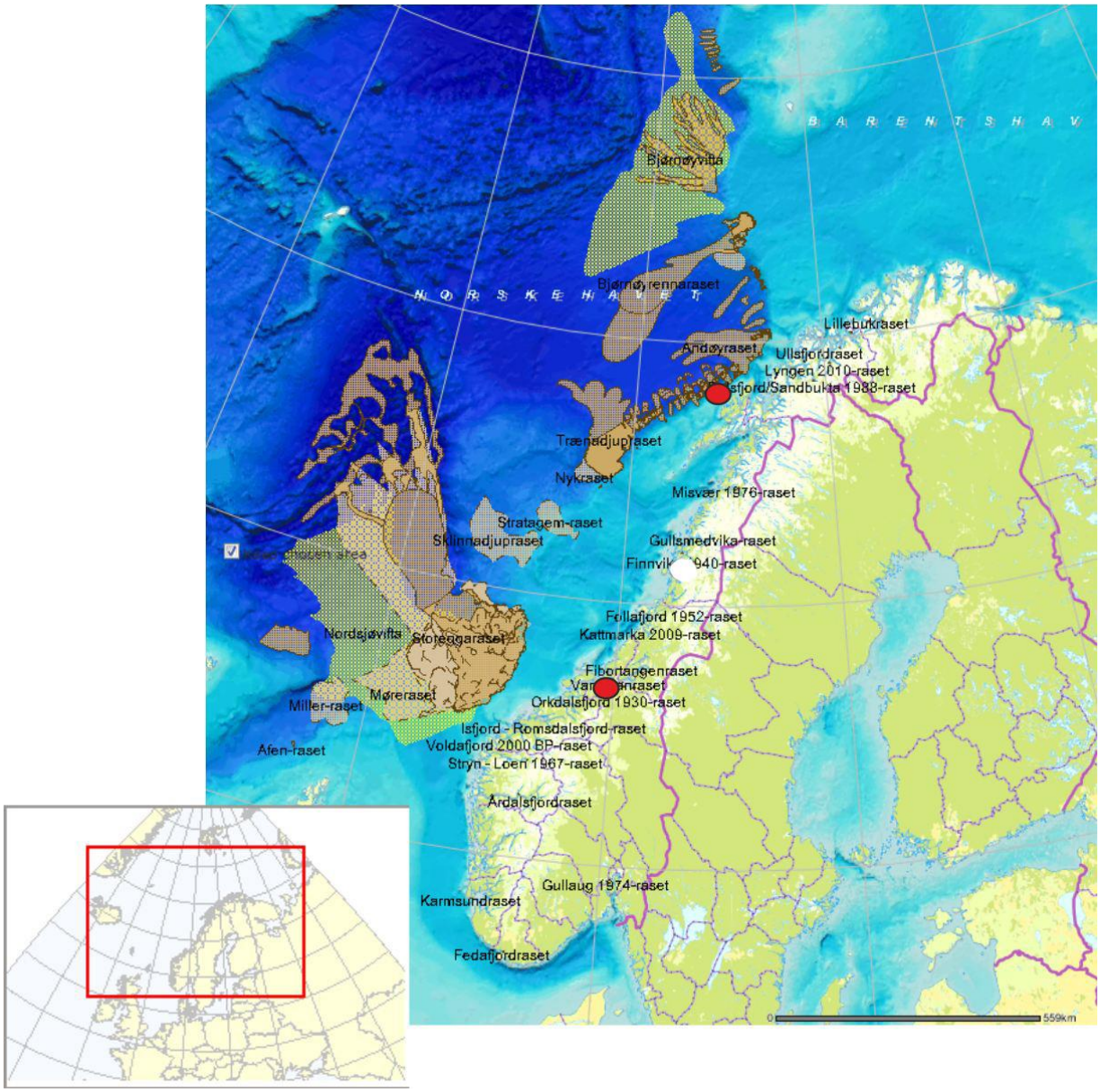

Figure 1 *Distribution of landslide and mass wasting events along the Norwegian Margin. Brown-shaded areas represent the surface extension of known submarine slides (www.mareano.no). Related to glacial-interglacial fluctuations submarine mass movements and failure events occurred along the entire Norwegian margin. These phenomena are located in open ocean realm as well as along the coastline. Our study areas are marked by the red circles.*

5 Previous Work & Geological Setting of *POS472* Study Sites

Focus of the *POS472* expedition was the investigation of various shallow landslide complexes in two different physiographic settings along the Norwegian margin (Figure 2). These include

1) coastal areas in the Trondheim Fjord with intensive anthropogenic impact, and

2) open ocean setting in shallow to intermediate water depth along the Norwegian slope off the Vesterålen and Lofoten.

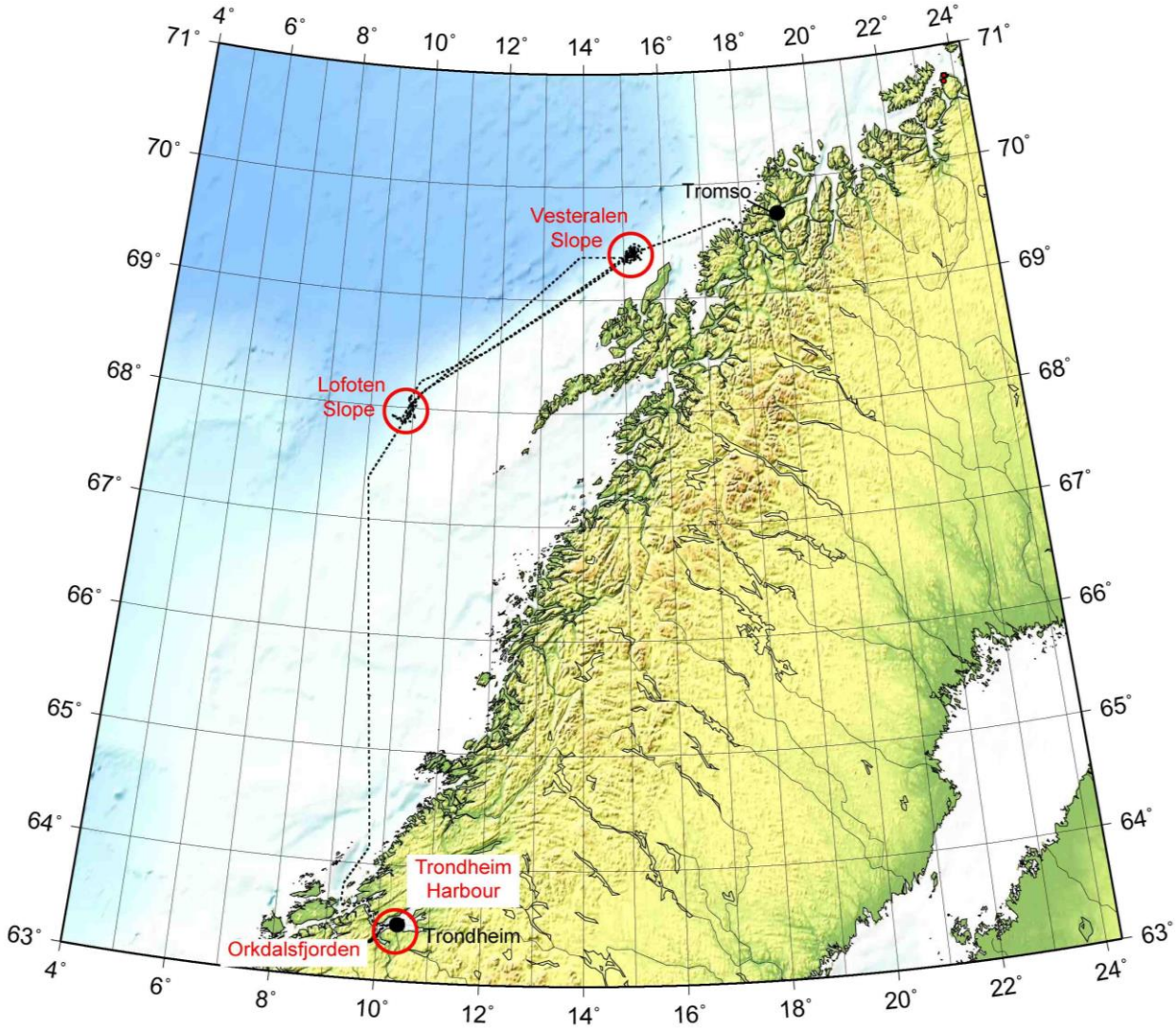

Figure 2 *Map of the four study areas of the POS472 expedition: Both coastal study sites were located within the Trondheimsfjorden (Trondheim Harbour, Orkdalsfjorden). The expedition POS472 started in Trondheim Harbour, which was also our first study area and ended in Tromsø Harbour. Dashed black line marks the track of R/V POSEIDON. (Source of map: Becker et al., 2009)*

5.1 Coastal Areas

The geological evolution for coastal areas of formerly-glaciated settings is related to the glacio-isostatic rebound associated with a significant fall of relative sea-level (Corner 2006) followed by the exposure of (glacio-) marine deposits with intensive fluvial erosion. The marine sediments were leached due to the contact by groundwater flow. This resulted in the evolution of quick clay, which represents a widespread coverage of mechanical weak sediments along continental slopes (L'Heureux et al., 2012).

The overall sedimentary strata is characterised by the deposits of (glacio-) marine sediments within the fjord-deltaic settings during and after the last glaciation. In the course of declatiation the glacio-isistatic rebound and the rapid drop of sea-level resulted in the shifting of river outlets and associated deposits and the progradation of Holocene deltas. Hydrographically connected to present-day fluvial systems, those geological strata can be considered as an aquifer system with a land-fjord directed groundwater flow along more permeable layers (see above).

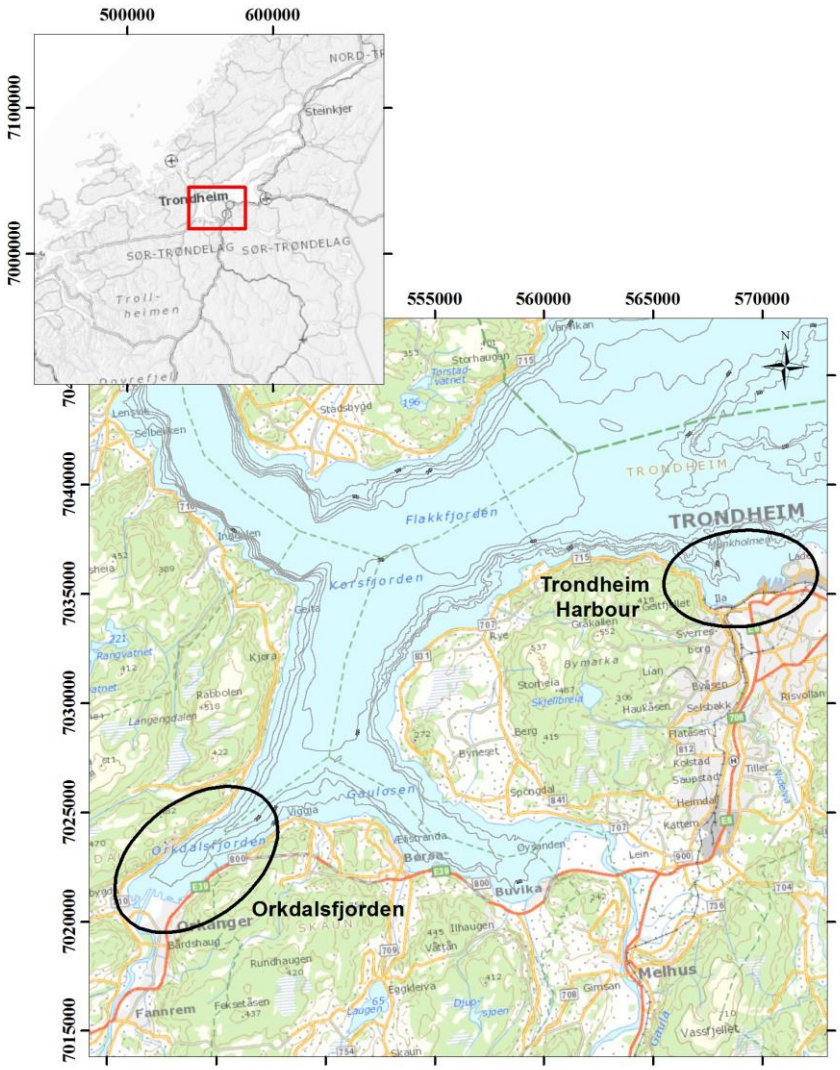

Figure 3 *POS472 NORGEotech Study Sites in the coastal setting. (Source of map: Kartverket (*http://www.kartverket.no/en/Maps--Nautical-Charts/Gratis-kartdata/Open-and-Free-geospatial-data-from-Norway/*)*

As a consequence of the increasing economic utilisation of fjords providing attractive human settlement conditions (access to the sea with protected ports, fertile soils in surrounding rough terrain) an increase of recurrence of slope failures along populated coastlines has been observed in several locations along the Norwegian coast (i.e. Trondheim Bay, Finneidfjord [Longva et al., 2003, L'Heureux et al., 2012, Vanneste et al., 2012]; for details see below). This correlation implies that man-made factors contribute to or trigger slope failures evidently and call for the need to understand the role and impact of anthropogenic factors in the already complex interaction of pre-conditions and the failure mechanics and dynamics. The long historical record of landslides along the coastline (e.g. Trondheim Bay [e.g. L'Heureux et al. 2010; 2011], Finneidfjord [e.g. Best et al. 2003; Longva et al. 2003; Cassedy et al. 2008; Vardy et al. 2012; L'Heureux et al. 2012]), combined with its accessibility and the availability of state-of-the-art-methodologies nearby, makes this site particularly interesting for improving the knowledge of shoreline mass wasting processes and can be considered as natural filed laboratories. Coastal study sites of *POS472* were located in the Trondheimsfjorden (Figure 3)

5.1.1 Trondheim Harbour (TH)

Trondheim located on the western coast of central Norway, is the third largest city of the country, and represents the economic and administrative center of Mid-Norway. In the last century with the beginning of urbanisation and land reclamation in 1875, the landslide-prone coastline along the Trondheim Bay was affected by three major retrogresssive landslides (1888, 1959, 1990; see map in Figure 4), resulting in material damage, generation of tsunami waves and the loss of life (Skaven-Haug 1955; Bjerrum 1971; Emdal et al. 1996; L'Heureux et al. 2007). The volume of mobilised sediment ranged between 3 x 10^6 m³ and 6 x 10^6 m³ (L'Heureux 2009). Along the Trondheim Bay the bedrocks are covered with a 125 m-thick sequence built up by glacio-marine clayey sediments, prodelta deposits (silt to sandy silt), steeply dipping delta foresets and gravel beach. Weak, clay-rich layers are interbedded in the prodeltaic and deltaic sediments deposited rapidely by turbiditic flows caused by large terrestrial quick-clay landslides (see Figure 4, and L'Heureux et al., 2011). The bay is separated by a shallow area into an eastern and western part. The present-day river Nidelva discharges in the eastern part. The western side is characterised by a deeply incised submarine channel (Nidelva Channel). Pockmarks with diameters of up to 15 m and less than one meter deep indicate fluid migration in the sediments.

During *POS472* geotechnical investigation was carried out in sediments affected the 1990 Slide and the Western Slide (W'Slide) (Table 1).

- The retrogressive, multi-phase slope failure event of 1990 occurred at the mouth of the Nidelva River. The collapse was initiated within the thin, laminated clay-rich beds, which are characterised by higher water content, higher sensitivity and lower shear resistance compared to the surrounding, more slowly deposited successions. Triggers are assumed to be the combination of pore pressure fluctuations due to intense rainfall, snow melting and a response to rapid loading from construction work (L'Heureux et al. 2010). The seafloor affected by the 1990 Slide has been divided into 4 areas characterized by different morphological features. There is one portion in the eastern part of the slide underneath the headscar represented with a flat, polished surface with slickenside structures. An overconsolidated, clay-rich layer acting as the glide plane for the failure is exposed

there. On the western part of the failure the surface of the seafloor is hummocky, the glide plane identified in the eastern part is absent (L'Heureux et al. 2010). After the mobilization of the material along the clay-rich weak layer, the slope failed in 3 different stages retrogressively in this portion along a secondary slide plane (L'Heureux et al. 2010).

- The W'Slide is situated along the flank of the Nidelva channel. The event is assumed to be a consequence of the 1888 Slide, when failed material run down within the Nidelva channel and undercut the slope along the flank of the channel (L'Heureux et al. 2010)

Table 1 *Summary of the landslide events along the coastline of the Trondheim Bay, which have been investigated during the POS472 expedition. Please refer to L'Heureux et al. (2010) for more details.*

Slide	Pre-conditions	Trigger Mechansim	Volume	Height	Length	Mean Slope Angle
Western Slide (W'Slide)	Occurrence of a 1.5 m thick clay-rich layer, which is assumed to be the slide plane	The failure event is related to erosion and undercutting by sediment gravity flow run down through the Nidelva channel after the 1888 slide.	1.x10^6 m³	5 – 10 m	1100 m	5° – 6°
1990 Slide	Unfavourable pore pressure conditions due to high precipitation events, occurrence of a weak layer	Rapid loading from construction work at shoreline, varies retrogressive failure stages after initial event	5,0–6,0 x 10^6 m³	Max. 28 m	800 m	2°-3°

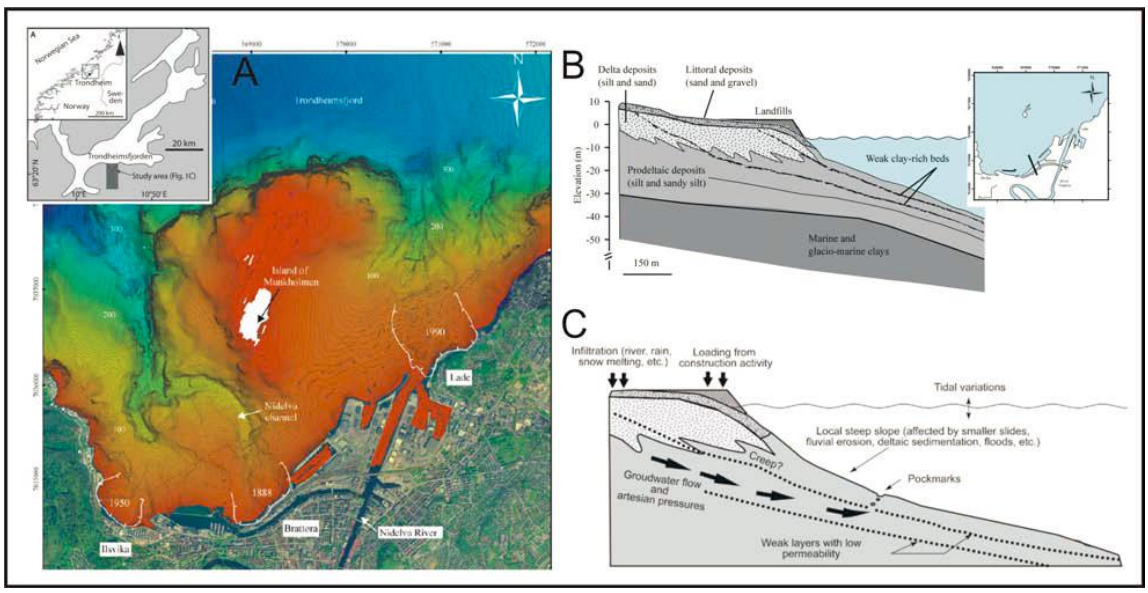

Figure 4 *Location of the Trondheim Fjord in central Norway. White lines indicate the landslide scars of the different failure events in 1888, 1950, 1990 (L'Heureux et al. 2011) b) Schematic cross-section of the sedimentological build-up of the Nidelva Delta (L'Heureux et al. 2011). The position of the profile is shown by the black line in the inset map; c) conceptual model of fluid migration (L'Heureux et al. 2011)*

5.1.2 Orkdalsfjorden (OF)

Orkdalsfjorden is a branch of the Trondheimsfjorden - located 25 km southwest to Trondheim - and presents a further location to study risk assessment due to landslide activity and tsunamigenic potential for coastal areas (Figure 3). In 1930 a landslide occurred in the vicinity of the river Orkla accompanied by a 15 m high tsunami wave (Figure 5). This event resulted in the loss of pier / harbour construction related to the initial failure and caused several cable breaks (18 km maximum northwards within the Trondheimforden) due to landslide propagation. Based on a combination of detailed eye witness documentation at that time and a data set recently acquired (bathymetry, high-resolution seismic reflection profiles and gravity cores) the timing of the different stages of the retrogressive failure process as well as pre-conditions and trigger mechanism have been figured out in a comprehensive study by L'Heureux et al. 2014).

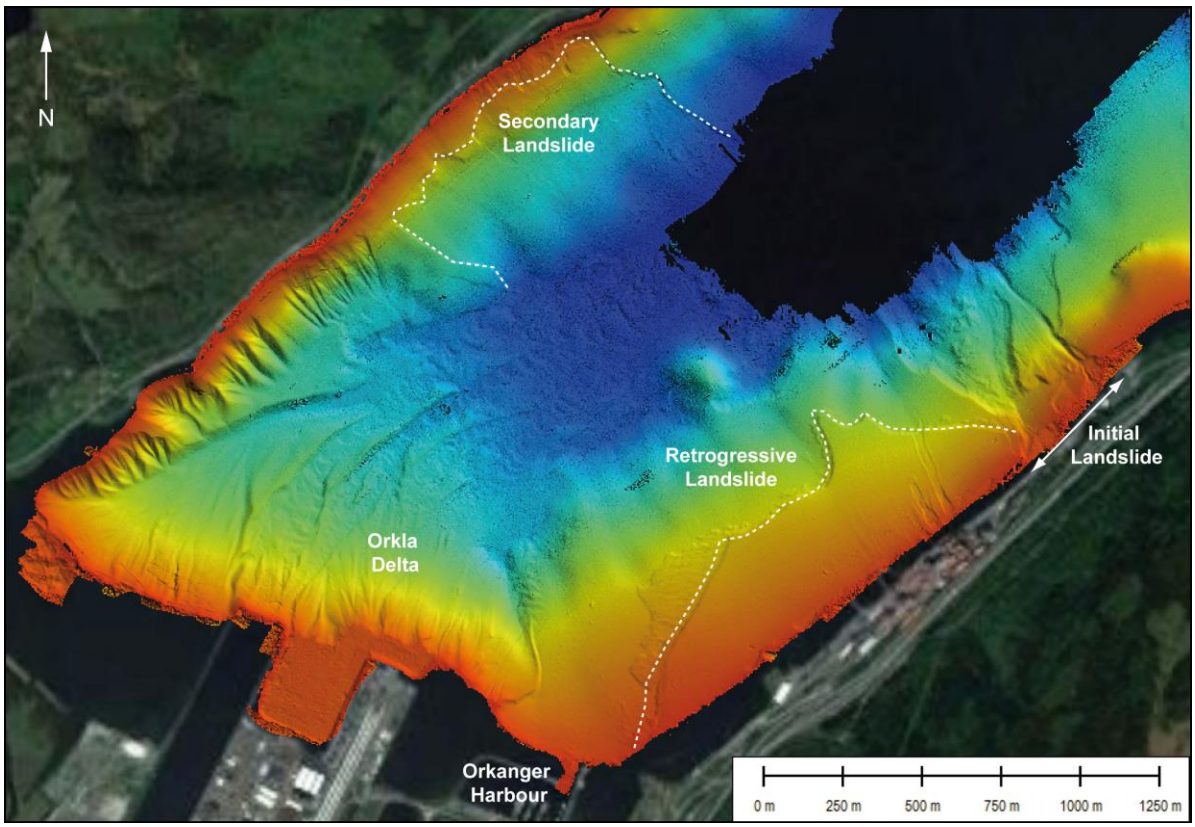

Figure 5 *The 1930 Orkdalsfjorden failure affected the southeastern flank of the fjord. The event was activated close at the shoreline from the area, where the collapse was initially activated to Along the southwestern flank of Orkdalsfjorden the headwall of the 1930 landslide stretches from the area, where the initial landslide was activated to the failure affecting Orkanger Harbour (L'Heureux et al. 2014).*

Steep flanks with slope angle ranging from 6° nearshore to 25° at the foot of the slope surround the fjord basin with water depth up to 400 m (L'Heureux et al. 2014). The strata is built up by i) fjord-marine sediments (silty clay), ii) landslide debris deposits consisting of silt, sand and gravel and clayey beds. These clayey sequences are assumed to be distal debris flows from terrestrial landslide, where quick-clay was displaced from the valley of Orkla into the catchment of the Orkdalsfjorden (L'Heureux et al. 2014).

Bathymetry data reveal morphological features like escarpments, detached slabs, channels and debris flow structures of both sides of the fjord flanks, which indicate mass

movement activity along the southwestern and northwestern portion of the fjord flanks (L'Heureux et al. 2014). The height of the scars reached 2 m in the northwestern part and varies between and 8 m to 12 m along the southwestern portion. Estimated total volume of failed material of both failure bodies is 16 – 18 x 10^6 m³. Clay-rich sequences represent the failure surface of the 1930 event. The occurrence of quick-clay deposits (see above) as well as steep slope gradients along the basin flanks represent failure pre-conditions. The trigger mechanisms of the 1930 event was a combination of building activity along the shoreline and high groundwater gradients along the slope (L'Heureux et al., 2014).

5.2 Open Ocean Setting

Variations in sediment supply during glacial periods related to ice-sheet dynamics alternated with periods of marine sedimentation (e.g. contourites, interglacials) created unstable slope conditions along the continental slope that developed into massive sediment failures under the influence of earthquakes, e.g. following isostatic rebound (Bryn et al., 2005), with devastating consequences. However, the Lofoten-Vesterålen slope with narrow shelf and modest dip angles developed differently due to its separation from the mainland by the island chain. There was no massive glacial sediment inflow in this area. Elongated contourite drifts containing sandy mud with ice-rafted debris dominate the late Cenozoic succession off Lofoten (Laberg et al., 2005). Also laminated muds occur, likely related to melt-water plumes. A thin, Holocene sandy mud (winnowing) drapes the seabed. Sedimentation rates are higher during glacials compared to the Holocene (Laberg and Vorren, 2004). Off the Vesterålen Islands, well-developed canyon systems contribute to mass transfer from the mainland to the deep ocean (Laberg et al., 2007). In between the canyons, topography is relatively undisturbed, and little glacial debris is deposited on the slope (Rise et al., 2009, 2012). Landslide investigation along in the open ocean setting is limited to bathymetry and high-resolution sidescan sonar and sedimentary data as well as occasional gravity cores (Vanneste et al. 2012, Laberg et al., 2011). *I*n situ investigation of expedition POS472 is designed to complement the abovementioned, existing data set. Geographical locations of the two different study areas in open ocean realm are given Figure 3.

5.2.1 Lofoten Slope (LS)

The Lofoten Slope (LS) is characterised by complex mass wasting processes with different failure features in deep water ranging between 800 and 1000 m on shallow slope with mean dip < 4°. The seafloor deformation structures include i) large-scale landslides, ii) stair-case pattern of escarpements with headwalls and further escarpments several tens of metres high (Baeten et al. 2013), iii) small graben- or fracture-like features with variable dimensions (up to several hundreds of meters in width and 10-15 m in thickness) and iv) gullies (Vanneste et al., 2012; Baeten et al. 2013). The remobilised mass was more or less completely evacuated, resulting in much longer run-out distances and deposition into the far deep sea (Figure 6A).

The sediments are predominantly normally-consolidated clays (in places silty and/or sandy), with variable clast content and laminations. Geotechnical investigations characterise strain-softening behaviour in different units (undrained triaxial shear and direct simple shear testing) and define higher sensitivity of clay intervals (about 8, mean sensitivity about 3) (Vanneste et al. 2012). Infinite slope equilibrium analysis using the

preliminary shear strength data yields also for the Lofoten margin a factor of safety (FS) well above 1. Therefore, external triggers (e.g. seismicity) are needed to explain failure processes in this area. Higher-resolution side-scan sonar images reveal other intriguing features and specific patterns in seabed geomorphology (for location of the high-resolution side-scan sonar survey please refer to Figure 6).

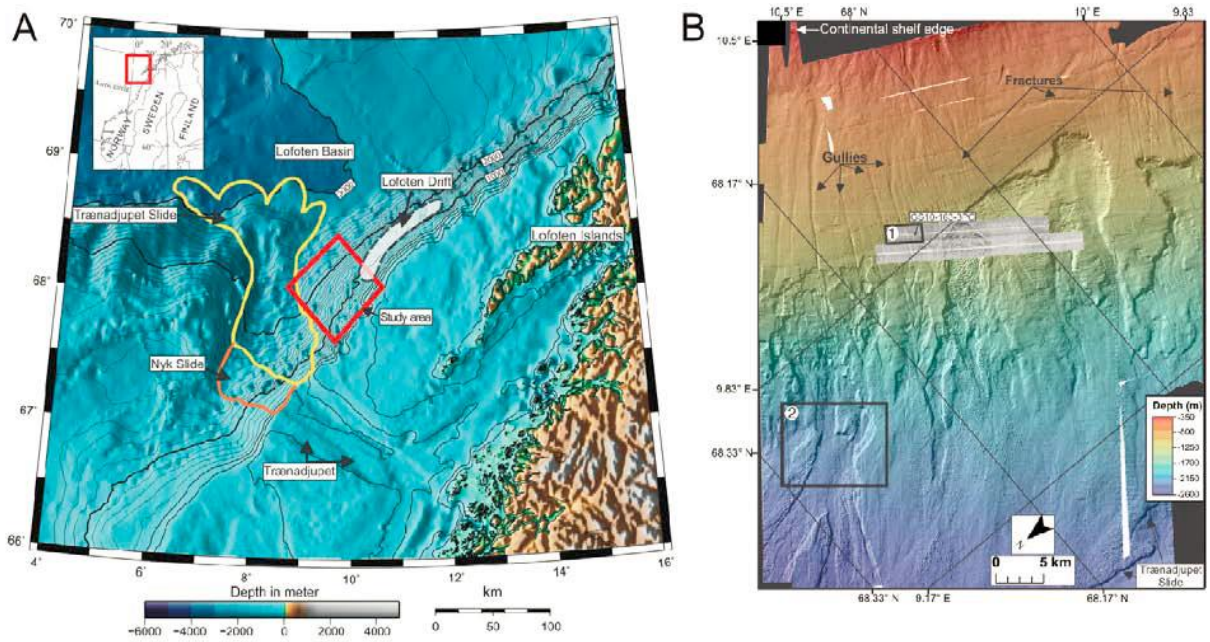

Figure 6 *Overview map of the continental slope off Norway (A) Red-coloured inset shows map in panel B, where gullies, fractures and several slope failures can be seen. Squares 1 in the map of panel B) indicates the positions of target areas during POS472. Both maps are published in Baeten et al. 2013.*

5.2.2 Vesterålen Slope (VS)

Isolated landslide features have been observed in bathymetry data on the gentle dipping slope (3°-4°) off Vesterålen close to the 500m isobath. The landslides are apart from canyon systems and they are not linked with the glacial termini further upslope (Laberg et al. 2007). An important observation by Vanneste et al. (2012) is the limited displacement of the mobilized mass. The landslides occur in an area essentially devoid of topographic relief (Figure 7). However, just upslope from the landslide areas, a change in seafloor dip occurs, and geomorphology upslope is hummockier, likely as a result of erosion under the influence of the Norwegian Atlantic Current or iceberg scouring and furrowing. Fractures of different size, often slope-parallel, may be related to ongoing stability, as is suggested by a slope equilibrium analysis indicating stability with a factor of safety (FS) not much larger than 1 (Vanneste et al. 2012). Sediment cores from undisturbed slopes are glacimarine (silty to sandy) clays, highly various density and water content, and containing variable amounts of clasts, interpreted as ice-rafted debris (Vanneste et al., 2012). It is unclear, however, whether the sliding planes of the slides are different in composition. Current data suggest that the clays are normally-consolidated with intermediate plasticity, but there are outstanding layers with decreasing pore pressure evolution, plasticity index and sensitivity with axial strain (Vanneste et al., 2012).

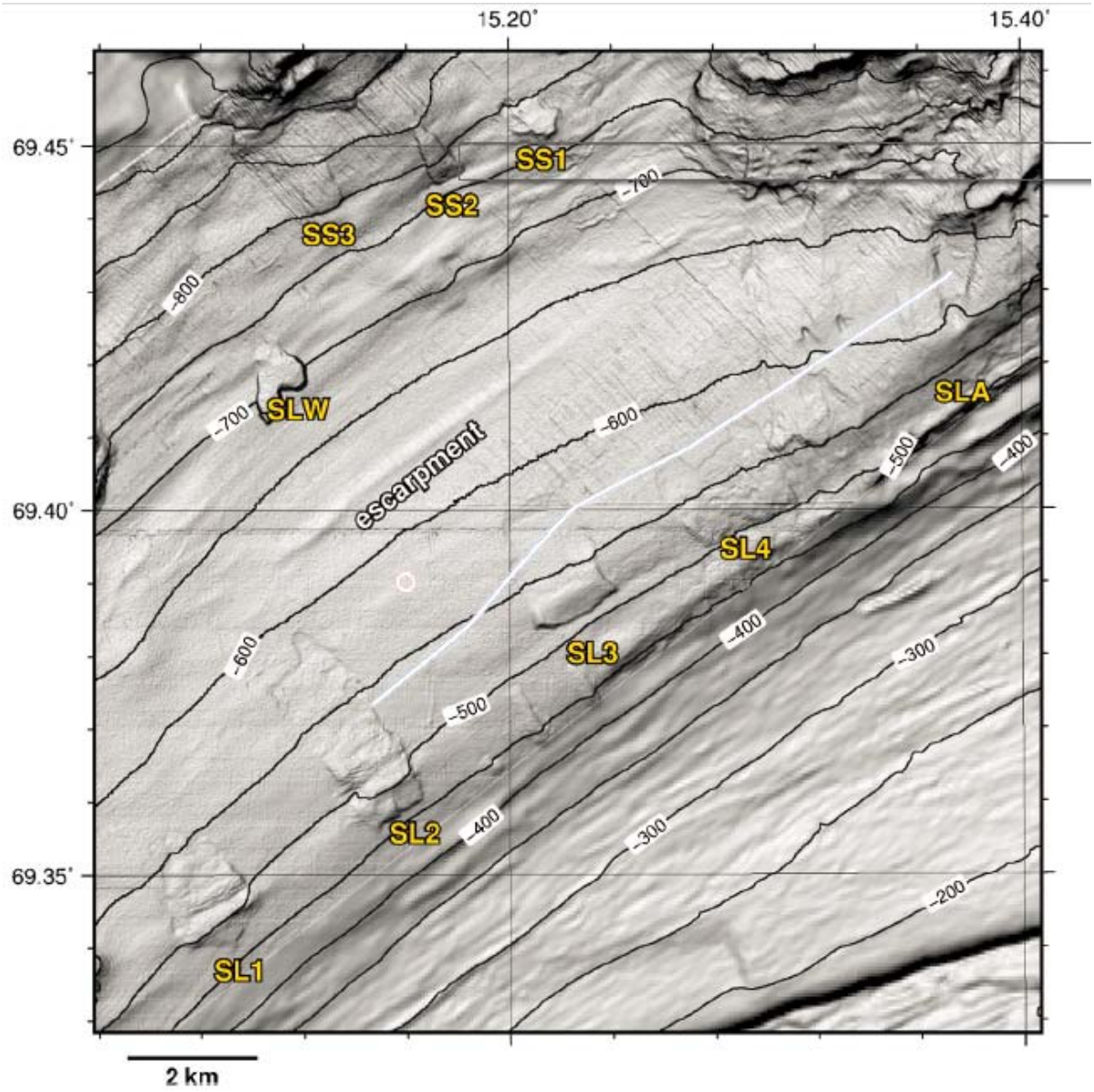

Figure 7 *Isolated deformation and failure features along the continental slope off Vesterålen in intermediate water depths (Vanneste et al. 2012).*

6 Methods

In this chapter, the methods of measurements are described, which were relevant for *NORGEotech*. In accordance to the geotechnical focus of *POS472* (see Chapter 3) static and dynamic CPTu systems (Cone Penetration Testing) represent the centrepiece of the campaign and were used to determine *in situ* physical properties of sediments in a depth up to 20 mbsf.

Gravity cores provided sediments of the upper 6 mbsf maximum for geotechnical and sedimentological laboratory-based analyses.

Bathymetry mapping was carried out in order i) to complement existing bathymetry charts by NGI and NGU, ii) to identify adequate spots for CPTu profiles and gravity cores.

6.1 Geotechnical in situ CPTu testing

6.1.1 Static CPTu Testing

(W. Schunn, S. Kreiter, M. Kluger)

Static *in situ* CPTu testing was conducted with the **G**eotechnical **O**ffshore **S**eabed **T**ool (*GOST*), which is an innovative instrument to characterise the sediment-mechanical properties of the subsoil by means of 'push-in tools', i.e. cone penetration testing along with pore pressure measurements (CPTu). The primary focus of GOST is offshore site investigation (Figure 8), but due to its modular layout, the system also works onshore, for instance mounted on a truck. *GOST* can be operated from almost any platform which can handle around 9 tons of weight. The system was recently designed and constructed at MARUM, Univ. Bremen. For further details and specification of the tools, please refer to: *https://www.marum.de/Binaries/Binary4710/Geotechnical_Offshore_Seabed_Characterization_Tool_-_GOST_Flyer.pdf*.

The system is equipped with a custom-built compressional 5 cm² digital CPTu probe, which is mounted on the rod. The probe measures the cone resistance q_c and sleeve friction f_s of the sediment (Figure 9), while the rod is pushed with a constant penetration velocity into the sediment by an hydraulic unit. Pore pressure u is measured differentially. The CPTu cone is filled with oil, while the inside of the cone is connected to the ambient pressure by the water filled rod. Thus the pressure transducer quantify the difference between the pressure port located at the standard u_2 location (see Lunne et al. 1997) and the pressure in the rod. In addition to the geotechnical parameters the tilt and the temperature of the cone is measured. All geotechnical sensors are digitised by 24 bit D-A converter in the cone transferred digitally to the main control unit with ~30 Hz leading to a sub-millimeter resolution at 2 cm/s penetration velocity. *GOST* is designed for a high push capacity of 80 kN and uses straight 23 mm diameter rods of tempered high performance steel. The maximum tool weight is 9 tons, for the *POS472* cruise *GOST* was used in a 3.6 ton configuration. The system is lowered in the water by a threefold pulley system with the rod in its center to stabilise the unit in the water column during operation. Power and communication is provided by a high voltage coaxial cable. Depending on the geological and sedimentological conditions of the test site the final length of the rod is defined and rigged from the working platform during lowering the GOST unit through the

water column (Figure 8). During *POS472* the length of the mounted rod was 20 m, which defined the maximum penetration depth. In the course of operation the rod was held upright by a constant-tension winch from the ship (Figure 8). When *GOST* reached the seafloor the CPTu probe is pushed quasi-statically into the soil with a penetration velocity of 2 cm/s in increments of 25 cm.

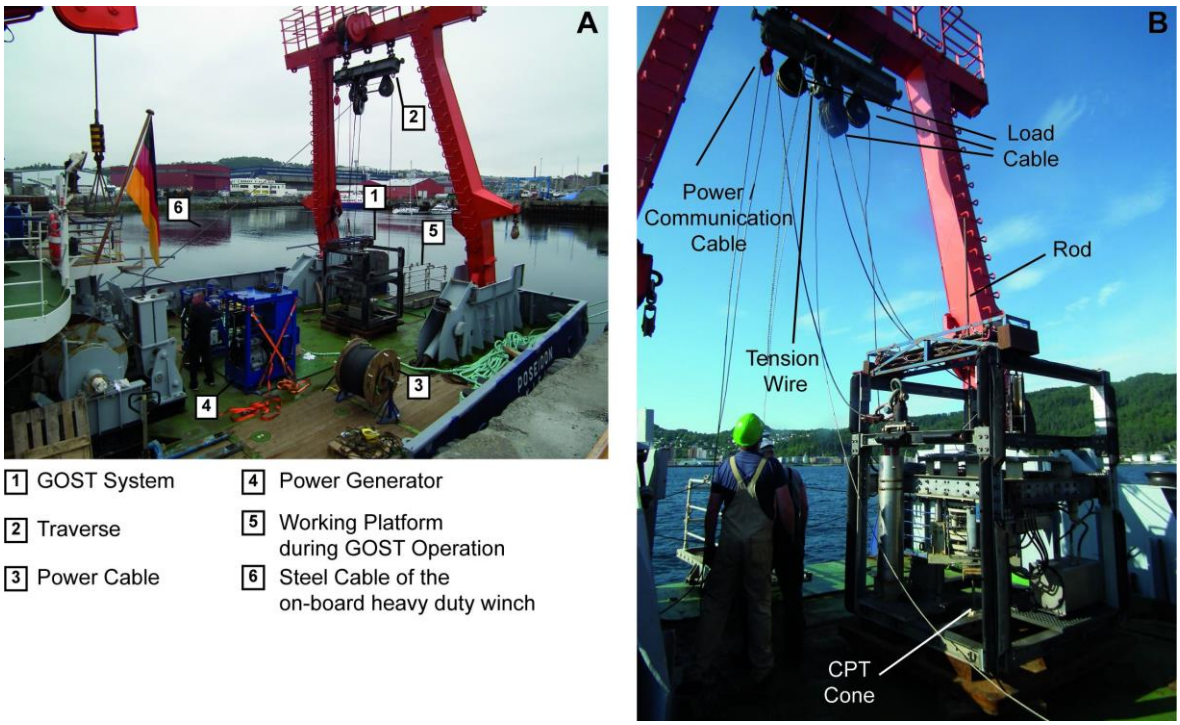

Figure 8 *Setup of the GOST system on R/V Poseidon*

During the *POS472* CPTu surveys in the coastal as well as open ocean settings, the tool was lifted for slightly from the seafloor, while the vessel drifted to the next CPTu location ("dangling operation"). This time-efficient operation mode *GOST* avoided a full recovery until all sites have been measured.

Figure 9 *Digital pressure-compensated compression CPTu cones, as installed in the GOST system.*

Vibratory CPTu Testing (VCPTu)

The aim of Vibratory Cone Penetration Tests (VCPTu) testing is to assess i) the liquefaction potential of sand (Sasaki et al. 1984; Youd et al., 2001) or ii) the cyclic softening behaviour in cohesive material (Boulanger and Idris, 2006, 2007). VCPTu measures the resistance of soil/sediment to cyclic loading (e.g. Jorat et al., 2014). The *Gost* system can be used as vibrotory CPTu, where the average penetration speed of 1.35 cm/s is modulated by a 5 Hz sine wave with an amplitude of 0.38 cm. For characterisation of the vulnerability of soil to cyclic loads standard CPTu and VCPTu tests are conducted in close vicinity. Liquefiable and cyclic softening soils are characterised by a decrease of vibratory cone resistance q_{cv} in comparison to the standard cone resistance q_{cs}.

Data handling and derived parameters

Primary CPTu parameters (q_c, f_s, u) as well as tilt and temperature are recorded continuously during penetration. Tilt and temperature are important parameter defining the quality of measurement. The data from the begin of the push is discarded where the push velocity is not yet 2 cm/s and were the cone resistance is influenced by relaxation This data gap is usually smaller than 5 mm. Penetration depth has been tilt-corrected.

Following CPTu parameters are presented here in the report:

- Corrected cone resistance q_t:

The corrected total cone resistance is given by the equation $q_t = q_c + u_2 (1-a)$. The cone area ratio a is calculated form the geometry of the cone to 0.5.

- Sleeve friction f_s
- Differential pore pressure u_2
- Undrained shear strength s_u:

Undrained shear strength was calculated by $s_u = (q_t-\sigma_{v0})/N_{kt,}$ using the static cone factor N_{kt} =10, 12, 15 (Lunne et al., 1997). Here the mean total vertical stress σ_{v0} =1.9 g/cm³ is used. Normalized undrained shear strength ($s_u/\sigma'v_0$) provides the state of consolidation. For normally-consolidated soil, this ratio typically falls in the range of 0.2 - 0.3 (Karlsson and Viberg 1967). A ratio exceeding 0.3 may indicate over consolidation.

Exceptional Operations during POS472

The distance sensor, which controls the hydraulic push process of *GOST* was damaged on the transport from Bremen to Trondheim. During the time of mobilisation in Trondheim Harbour the depth control unit of *GOST* was modified during the time of mobilisation in Trondheim Harbour. A time-controlled push mode was developed, in which the hydraulic valve received a constant signal that in turn provided a constant movement of the hydraulic unit during penetration. This constant signal was calibrated to reach a penetration velocity of 2+-0.05 cm/s with a stop watch. Some extra time was given to

assure full strokes and the hydraulic moved with the same speed also in the unclamped move resulting in a longer operation time. This operation mode was used for the first four locations in Trondheim Harbour (stations GeoB18608, -09, -11 and -11). Then the broken sensor was replaced by a sensor, which had been delivered to Trondheim Harbour and was used for the further ten locations in Orkdalsfjorden (deployments GeoB18624-1, -24-2, -25, and -27-1) and along the Vesterålen Slope (stations GeoB18633, -34, -35, -38, -39, and -40).

6.1.2 Dynamic CPTu Testing (Free Fall-CPTu [FF-CPTu])

(T. Fleischmann, M. Lange, R. Roskoden, W. Li, S. Stegmann)

6.1.2.1 Deepwater Free Fall CPTu (DW FF-CPTu)

The free-fall CPTu (FF-CPTu) instrument for deep water (DW) (up to 4000 m water depth) use consists of a 15 cm^2 CPT cone manufactured in the MARUM working group Marine Geotechnics and a water-proof housing containing a microprocessor, volatile memory, battery, and accelerometer (see Figure 10A; and Stegmann and Kopf, 2007 for details). The CPTu cone measures cone resistance and is equipped with two pore pressure port (u_1 and u_3). The stainless steel pressure-tight housing containing a microprocessor, standard secure digital memory card (SD), tiltmeter, accelerometer, power supply (battery packages), absolute and differential pore-water sensors as well as power and data interface module (PDIM). The tiltmeter (dual-axis tilt sensor) monitors the penetration angle at +/-45° relative to vertical. Five different accelerometers with different ranges (+/-1.7g, +/-18g, +/-35g, +/-70g and +/-120g) provide information about the de/acceleration behaviour of the DWFF-CPTU instrument upon penetration. Acceleration data allow the researcher calculation of penetration velocity and depth by 1st and 2nd integration. The reference pore-water pressure port at the pressure-tight housing is equipped with an absolute 40 MPa (400 bar) pressure sensors (*WIKA ECO-1*). The pore-water pressure ports at the tip (u_1) and 0.75 m behind the tip (u_3) are connected to the differential pore-water pressure transducers (*VALIDYNE P55D*) via stainless steel tubing. Pore-water pressure changes can be monitored over a range of 85 kPa (12.5 PSI) to 140 kPa (20.0 PSI) with a resolution between 8.0 - 15.0 Pa. The sensors are protected with valves if high excess pore-water pressures are met (e.g. owing to blocked hydraulic tubes). They are further used to bleed the tubing in case of gas is trapped inside, especially during the initial phase of deployment when the instrument is lowered through the water column.

The DW-FF-CPTu instrument is used in an autonomous mode, at which all sensor and transducer information will be recorded on a standard secure digital memory card (SD) with a very high sampling frequency (up to 1 kHz) using an AVISARO microcontroller. The frequency of data acquisition is variable depending on the operation mode (e.g. sub-seafloor profiling or pore-water pressure dissipation test) as well as the penetration rate of the DWFF-CPTU test. After the CPTu operation the data are downloaded via W-LAN to a PC. Two non-volatile battery packs available performance times of about eight to twelve hours, respectively. A self-developed deck interface box is used to download the recorded data and to charge the battery packs.

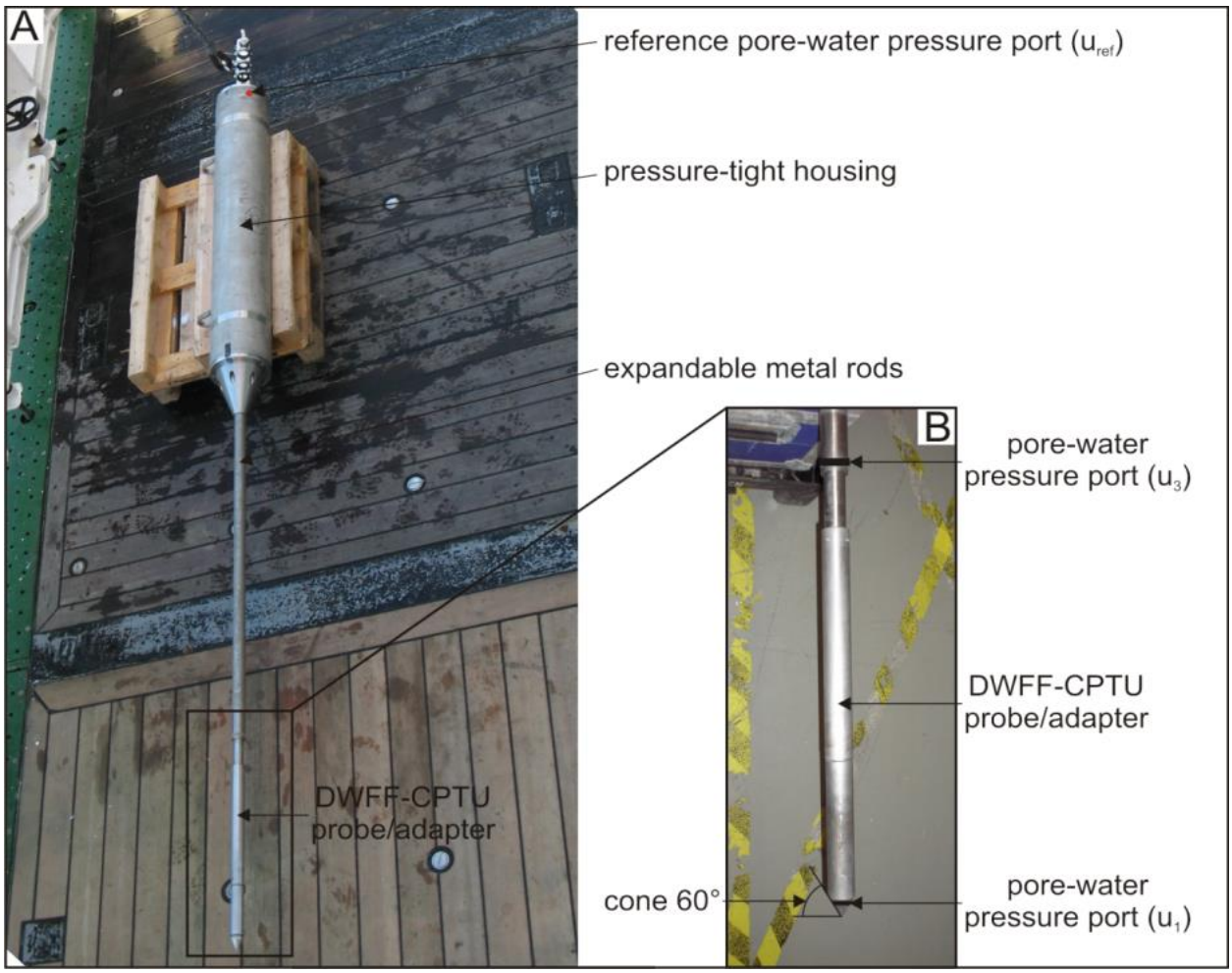

Figure 10 *Deep-water FF-CPTu instrument (A). Panel (B) shows blow up of the frontal portion with the pore pressure ports.*

Real-time data acquisition (lower sampling frequency 1Hz) and control of the instrument during deployment (e.g. operation of the valves) is provided by a data transmission telemetry system (*Seabird Electronics SBE36 CTD*) consisting of a deck unit (*SBE36 CTD*) and a *PDIM*, which is implemented in the head of the lance and a SHDSL Ethernet Extender (*IEX-402-SHDSL Series*) (Figure 11). The latter one was previously added additional to the *Seabird* telemetry to increase the data rate. The DW-FF-CPTu was used with that configuration for the first time during *POS472*.

The length of the DW-FF-CPTu instrument is variable from 4.1 m to a maximum length of 6.8 m depending on what type of sediment is anticipated. Hence, the weight of the DWFF-CPTU instrument ranges from approx. 500 kg to max. 550 kg.

During the cruise the DW-FF-CPTu instrument was deployed as individual measurement or pogo-style. The DW-FF-CPTu instrument was veered at 1.2 m/s winch speed to a level 30 – 50 m above the seafloor, then the winch speed was reduced to 0.5 m/s until the DWFF-CPTU probe hits the seafloor and dynamically decelerated until its penetration depth of several meters sub-seafloor (a fix winch speed for each location). The instrument was recovered after some minutes.

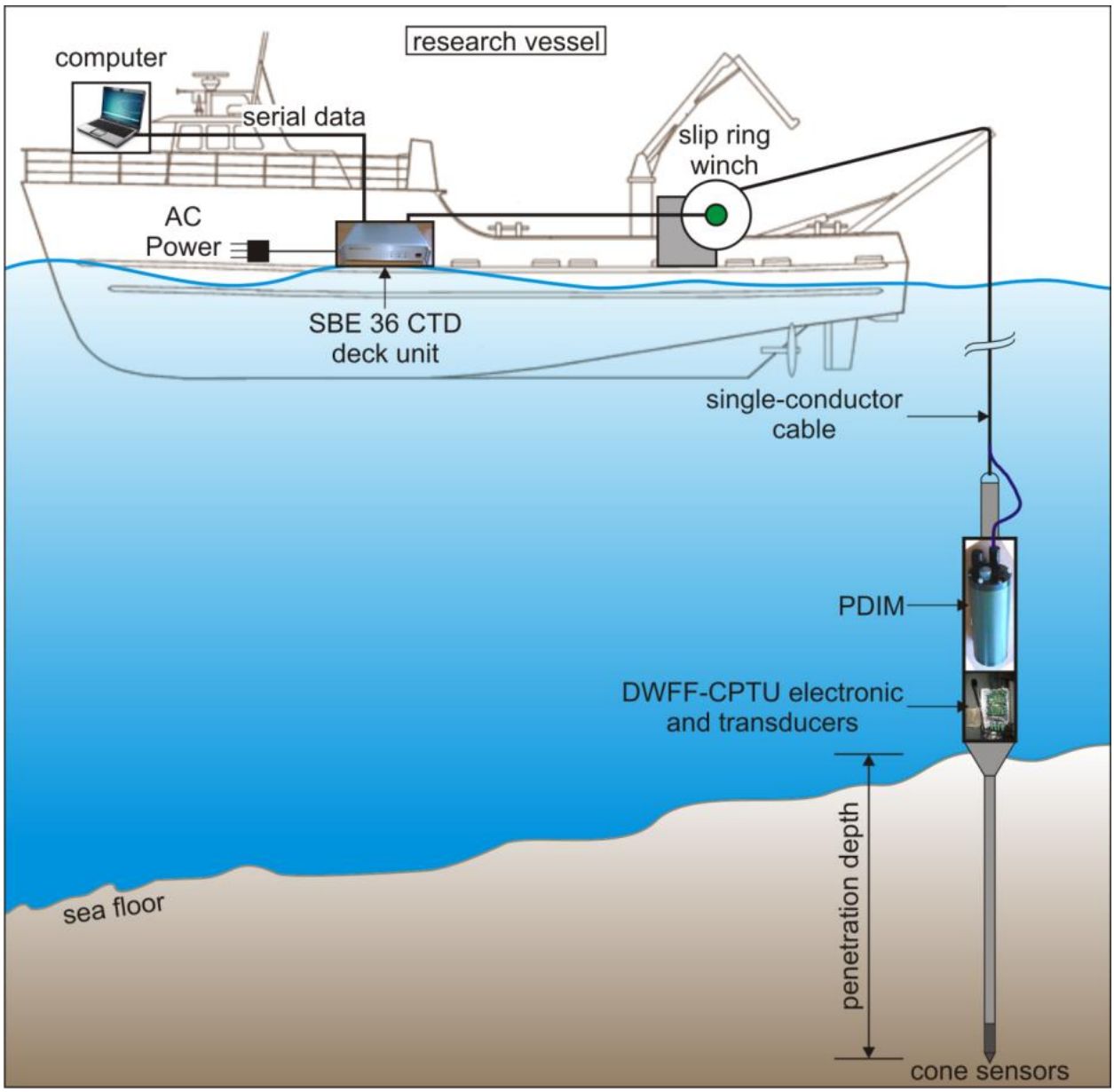

Figure 11: *Schematic of SBE36 CTD and PDIM telemetry system.*

6.1.2.2 Shallow-water Free Fall CPTu (SW FF-CPTu)

The lightweight SW-FF-CPTu instrument for shallow marine use consists of an industrial 15 cm^2 piezocone and a pressure-tight housing containing a microprocessor, standard secure digital memory card (SD), battery package and accelerometer (see Figure 11, top; and Stegmann et al., 2006). Strain gauges inside of the FF-CPTu probe measure the total cone resistance and sleeve friction by subtraction. A single pore pressure port (u_2) is equipped with absolute 1 MPa (CPTu - 25), 2 MPa (CPTu-100) or 5 MPa pressure sensors. An inclinometer is installed to monitor the penetration angle at +/-20° relative to vertical. Five different accelerometers with different ranges (+/-1.7g, +/-18g, +/-35g, +/-50g and +/-120g) provide information about the descent deceleration behaviour of the FF-CPTu instrument upon penetration. These data allow the researcher to calculate penetration velocity and depth during multiple deployments by 1st and 2nd integration. The

aluminium pressure tight housing tolerates a minimum 5 MPa confining pressure (approx. 500 m water depth) and hosts the power supply and microprocessor.

The frequency of data acquisition is variable and depends on the operation purpose of the FF-CPTu instrument (e.g. sub-seafloor profiling or pore pressure dissipation). Binary data are temporarily stored on a standard secure digital memory card (SD) and then downloaded to a personal computer (PC). The three non-volatile battery packs available provide performance times of about twelve and twenty-four hours, respectively. The length of the FF-CPTu instrument is variable from 0.5 m to a maximum length of 6.5 m depending on what type of sediment is anticipated. The extension is accomplished by adding 1.0 m long metal rods and internal extension data/power cables within them. Hence, the weight of the FF-CPTu instrument ranges from approx. 40 kg to max. 110 kg. If deep penetration is desired, modular weight pieces (15 kg each) can be mounted to the pressure-tight housing at the top, then reaching a max. 170 kg. The FF-CPTu instrument is deployed as individual measurement or pogo-style and remains in the sub-seafloor for appx. 15 minutes.

Processing of FF-CPTu Data

Additional to the primary CPTu data (q_c, f_s, u), temperature and acceleration are recorded during profiling. Penetration rate as well as penetration depth are calculated by the first and second derivation, respectively. As the penetration rate influences the primary CPTu parameter significantly (see Chapter 3), the strain-rate effect was recalculated using the empirical relationship by Dayal & Allen (1975).

6.1.3 FF-CPTu Winch

The *MARUM FF-CPTu*-Winch is capable of doing veer velocities up to 5 m/s in a controlled manner and is applicable for shallow water depth up to 200 m (Figure 12). This rate is close to what some free-fall penetrometers reach before they impact the seafloor. It was developed to carry out rate-dependent tests with the FF-CPTu probes in the MARUM “Marine Geotechnics” group in order to thoroughly assess how the strain rate affects the CPTu parameter and to improve the strain-rate correction.

The winch as well as the aggregate is designed with a footprint of a standard Euro-palette, and the winch itself can be put either next to the aggregate, or on top of it (see Figure 12). The frame is equipped with leashing points, where the winch was fixed on the working deck of RV POSEIDON. Electrical power was provided by the aggregate of the *GOST* system.

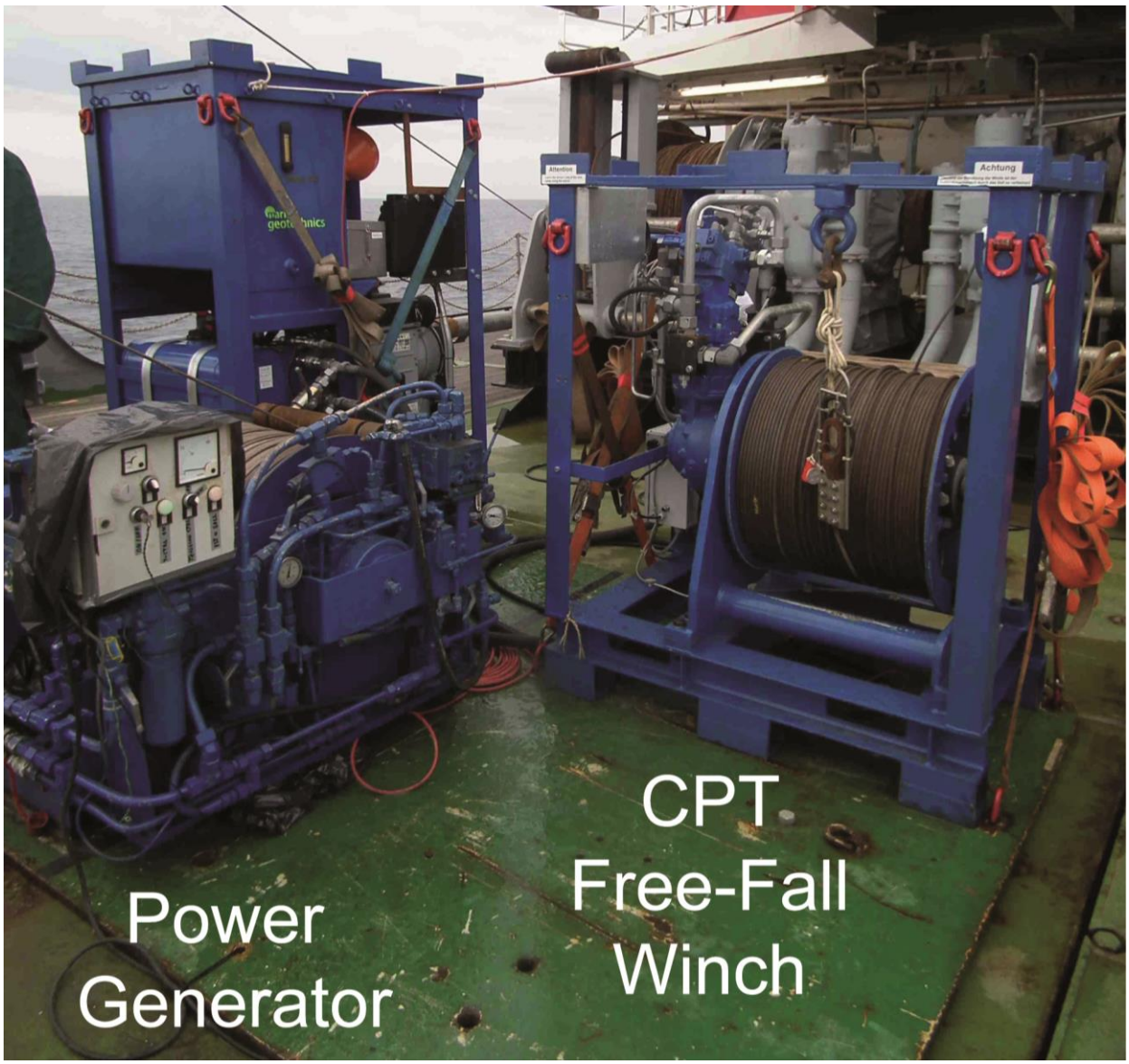

Figure 12 *New MARUM FF-CPTu-Winch 200 m (left) and entire assembly together with hydraulic aggregate (right).*

6.2 Gravity Coring and Sediment Description

6.2.1 Gravity Coring

(T. Fleischmann, N. Baeten, S. Kreiter, A. Rösner, M. Kluger, W. Li, R. Roskoden)

A gravity corer with tube lengths of 6 m and a weight of approximately 1.5 tons was used during cruise *POS472* (Figure 13). Plastic liners were marked lengthwise with a straight line in order to retain the orientation of the core and then placed inside the steel tube of the gravity corer.

Figure 13 *Gravity corer on board RV Poseidon.*

After recovery the sediment cores were cut into sections of 1 m length on deck, closed with caps on both ends and labelled according to a standard scheme (Figure 14). The half core with the marked line was stored as archive half (AH), while description, sampling, etc. were carried out on the remaining half (working half [WH]). For the detailed procedures each working half core underwent, see below.

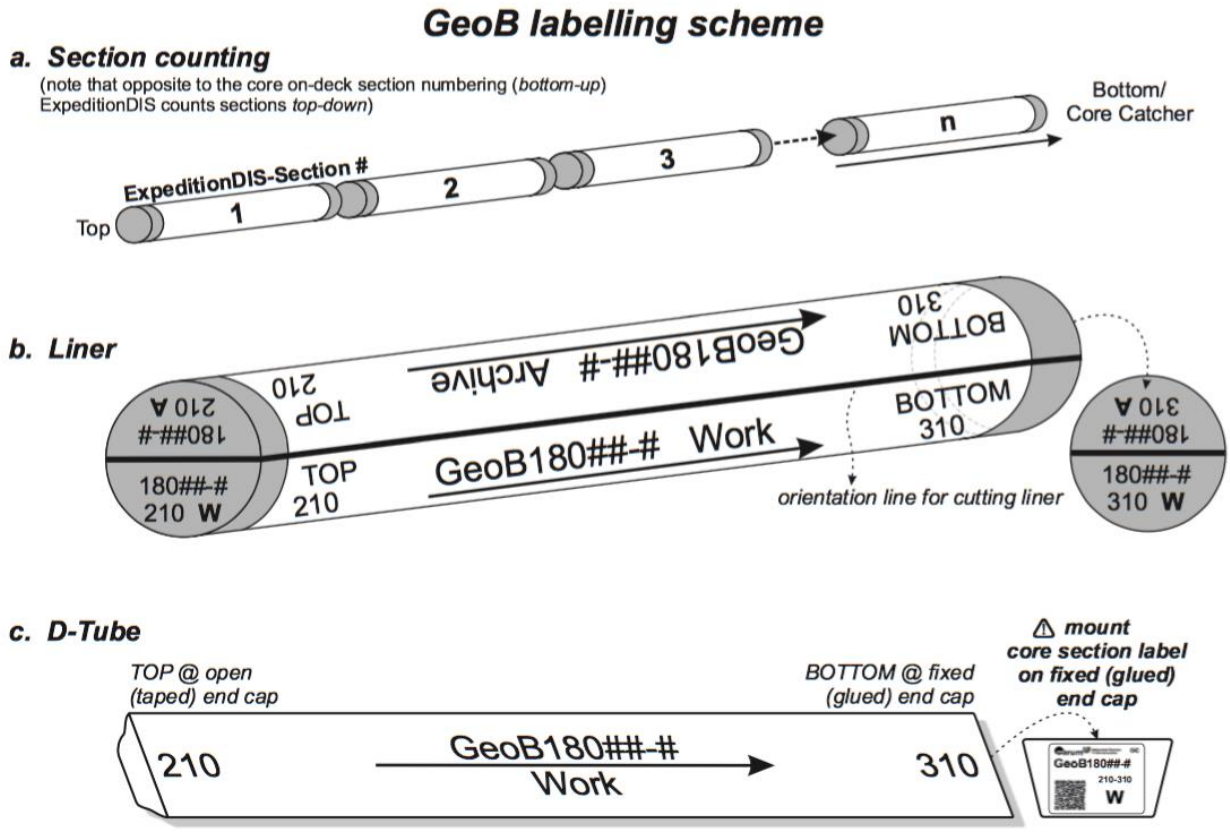

Figure 14 *Inscription scheme of gravity core segments following the GeoB Standard.*

6.2.2 Sediment description

(N. Baeten, M. Kluger, S. Kreiter, A. Rösner)

The split WH core segments were photographed using a single-lens reflex camera installed on a fixed frame. Sediment description was carried out largely from a sedimentological standpoint and based on the visual determination of lithological units and grain size. Therefore the grain size was assessed based on Wenthworth's (1922) classification. The colour of each lithological section was determined using Munsell's soil colour chart nomenclature. Sedimentary signature and biogenetic structures were determined. Sediment samples were taken with equidistant spacing for grain size and water content analysis.

For each core, a one-page log sheet was compiled. It combines photographs of the core next to a graphical log showing: i) the assigned lithological unit related to grain size classes (visually determined), and ii) distinct sedimentological structures related to e.g., mass movement events, deformation structures or bioturbation. The core log is combined with results from fall cone penetration and vane shear tests conducted on-board (see Appendix). Figure 15 summarises the list of patterns and symbols used on the barrel sheets. All core logs are provided in Appendix.

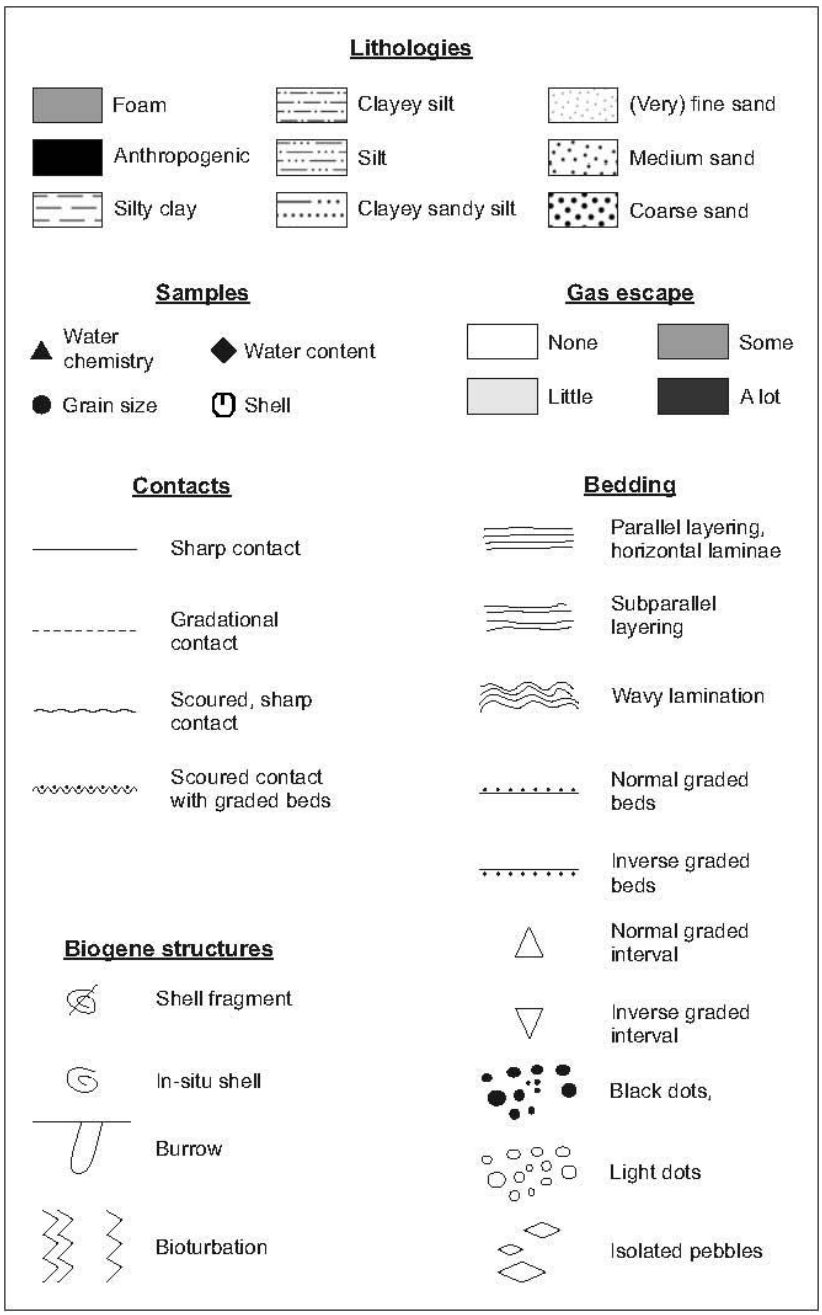

Figure 15 *List of patterns and symbols used on the barrel sheets.*

6.2.3 Physical properties

Since no container with a Multi-Sensor Core Logger (MSCL) could be placed on board RV *Poseidon*, MSCL measurements on the undisturbed archive half of the cores were carried out immediately after the cruise shore-based at MARUM Bremen (see Chapter 6.2.3.3).

The on-board investigation was limited to measurements of the undrained shear strength (s_u) using a fall-cone and vane shear device (Figure 16). The tests were realised on the working half of the sliced gravity cores. However in some cases the measurements were performed on the archive half of the cores in case the working half was disturbed by the slicing process. Fall-cone measurements were performed with a spatial resolution of 5 cm over the complete length of the core. Vane shear experiment are related to the lithologically interesting units (upper and lower boundary of the unit), which results in an average spacing of 33 cm.

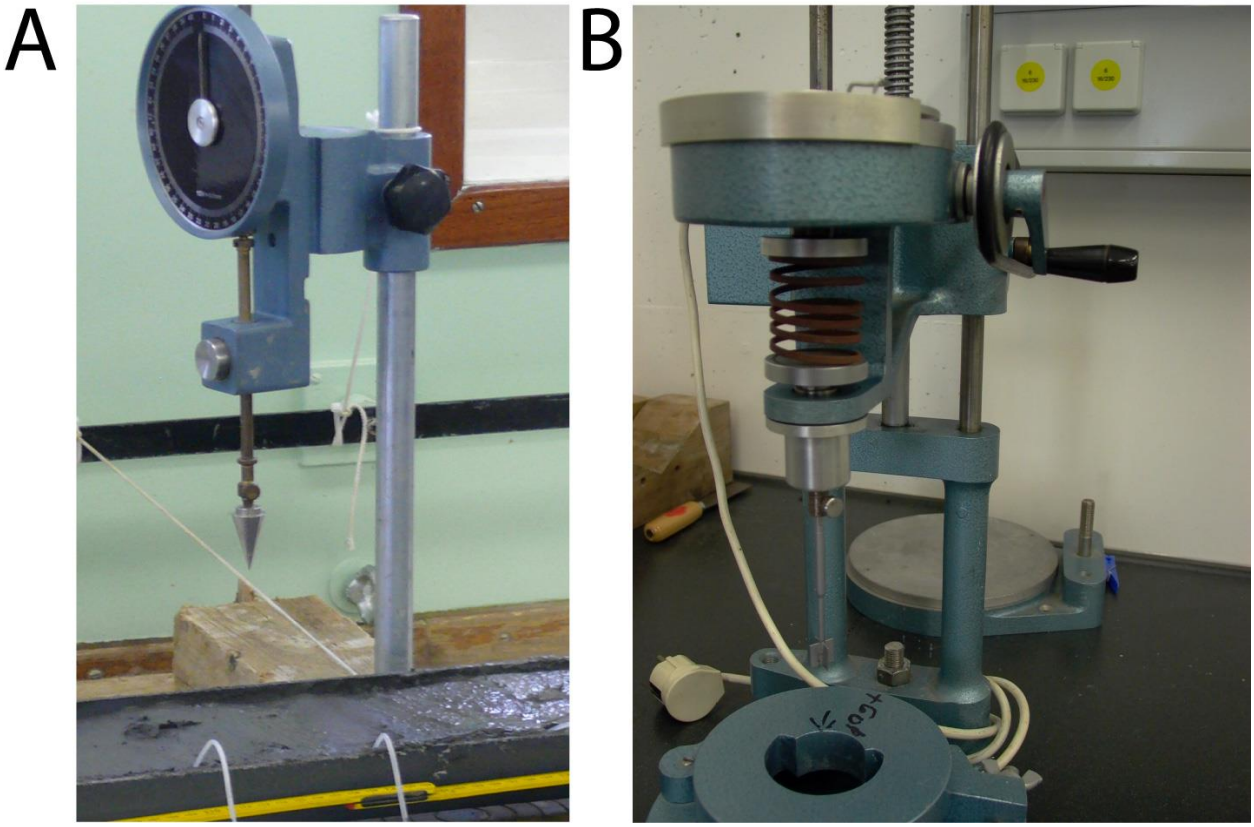

Figure 16 *(A) Falling cone penetrometer and (B) vane shear device used on the split core surface.*

6.2.3.1 Cone penetrometer

(A. Rösner, R. Roskoden)

The geotechnical properties along the sediment cores were determined according to British Standards Institutions (BS1377, 1975). *A Wykeham-Farrance cone penetrometer WF 21600* fall-cone penetrometer was used to determine the first-order undrained shear strength of the sediment. The shear strength (s_u) is measured by placing the sample

underneath the fall-cone penetrometer, whereas the cone tip touches the split core sediment surface (Figure 17). Before the experiment starts the initial depth (d_i) is measured; afterwards the cone is released and it penetrates the sediment. After five seconds of penetration the penetration depth (d_p) is measured. Finally the initial depth (d_i) is subtracted from the penetration depth (d_p), to calculate the relative penetration depth (d).

Undrained shear strength (c_u) is calculated by the formula modified after Wood (1985),

$$c_u = \frac{k * m * g}{d^2}$$

where (k) is the cone factor, (m) the cone mass, (g) the earth acceleration and (d) the relative penetration depth of the cone. The cone factor is dependent on the cone angle (α) and the friction between the soil and the cone (Wood 1985).The tests were performed with a 30° cone with a mass of 82.95 g. After Wood (1985) the average value of the cone factor is 0.85, which was used for the calculation.

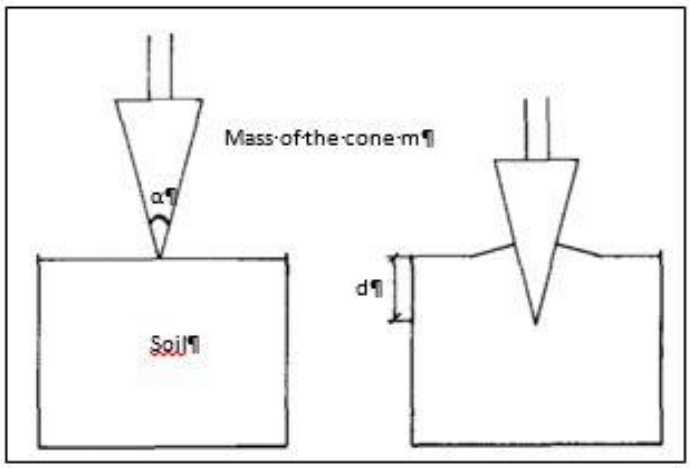

Figure 17 *Diagram of fall-cone tests after Wood, 1985.*

6.2.3.2 Vane shear testing

(A. Rösner, R.Roskoden)

In addition to the Cone Penetrometer a *Wykeham Farrance Vane shear 27-WF1730/2* with four different springs and three different vanes was used for the determination of the undrained peak shear strength (Figure 16b). **Fehler! Verweisquelle konnte nicht gefunden werden.** summarises the different springs and vanes used in the experiments. The right spring has to be chosen before the experiment starts. The stiffness increases from spring No. 1 to No. 4, that is why No. 1 is used for very soft sediment and No. 4 is used for stiff sediments.

Table 2 *Summary of springs and vanes used in the experiments on-board.*

Spring number	Serial number		Vane	Geometry [height x diameter]
No. 1	994		Small	12.7 mm x 12.7 mm

No. 2	402		Medium	18.99 mm x 12.7 mm
No. 3	402		Large	25.4 mm x 12.7 mm
No. 4	402			

The split core was placed below the vane and the pointer has to be in contact with the carrier. Afterwards the carrier is rotated by hand until the pointer is brought to zero on the inner scale. Then the handle is used to rotate the pointer to zero on the outer scale (Figure 18). Finally the top hand knob is used to lower the vane into the sediment core to a depth where shearing can take place on the horizontal edges of the vane (Controls Group 2007). When the sediment fails the torque angle of failure is measured in degrees on the inner scale. Therefore the calibration sheets (note that springs of different production series are related to different calibration sheets) provided by the manufacturer should be used to convert torque angle of failure into torque (T) which has the unit Nm. The equation below is used to calculate the undrained shear strength (c_u) in $N*m^{-2}$,

$$c_u = \frac{T}{K}$$

where (K) is the vane constant in m^3 (Blum 1997). The vane constant depends on the geometry of the vane as well as on the penetration depth of the vane (fully inside the sediment or with visible front face). Blum (1997) presented a formula to calculate the vane constant with the vane fully submerged into the sediment. The formula below is derived from his formula to calculate the vane constant with visible front face

$$K = \pi(\frac{1}{4} * d^2 * h + \frac{1}{6} d^3)$$

where (d) is the diameter and (h) is the height of the vane in meter. Depending on the type of sediment, a different setup of springs and vanes was used on board (see Table 2). The large vane was almost used in every experiment.

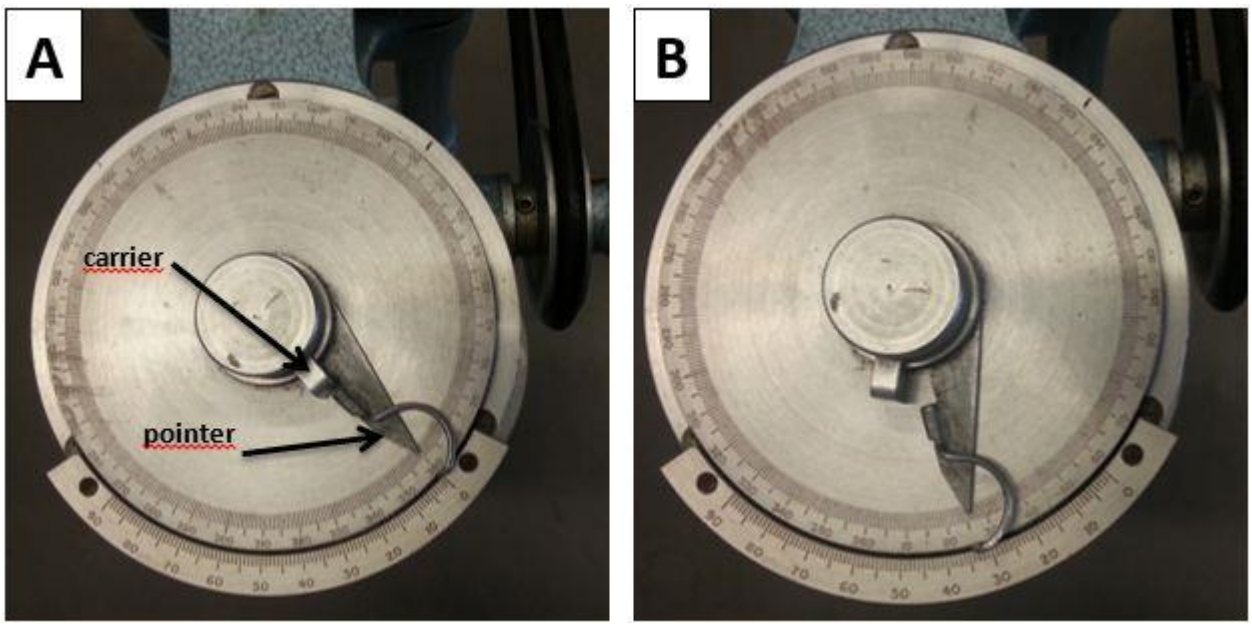

Figure 18 *A shows the experiment setup: Inner scale 0° is placed on the outer scale 0°. Pointer starts at 0°/0° and touches carrier. B shows the setup after obtaining peak shear strength: Carrier does not touch any more the pointer and the pointer shows peak shear strength (inner scale).*

6.2.3.3 Multi-sensor core logger (shore-based)

(T. Fleischmann)

The *GEOTEK* MSCL device at MARUM Bremen combines three sensors on an automated track (Figure 19).

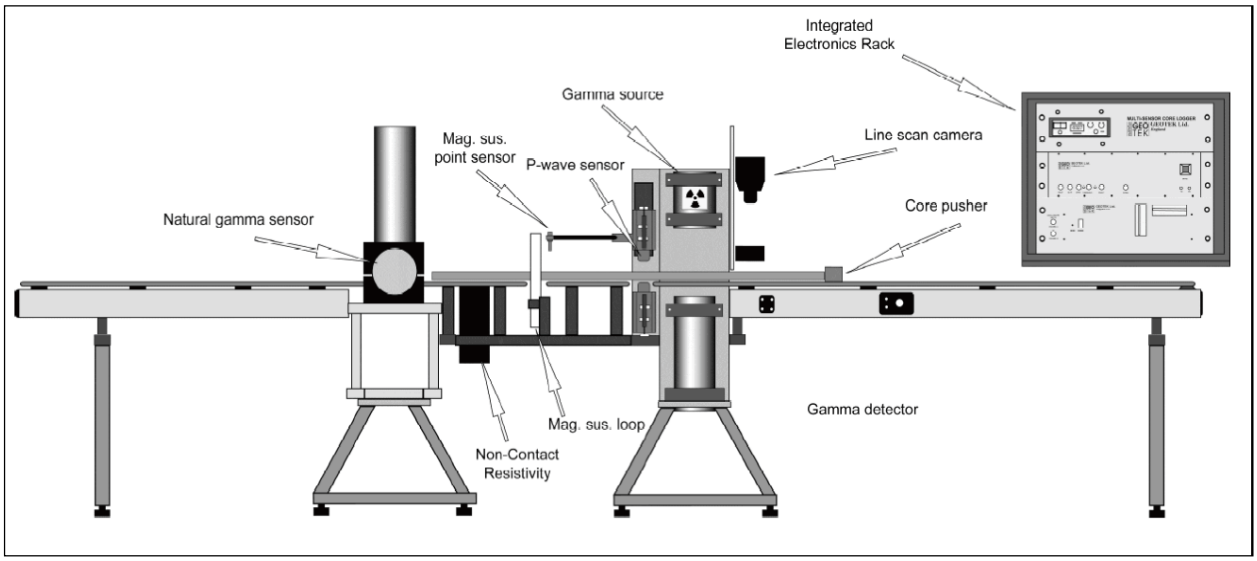

Figure 19 *Schematic drawing of the Geotek Multi Sensor Core Logger (MSCL).*

During logging the P-wave velocity, gamma ray attenuation (bulk density), and the magnetic susceptibility were recorded. From this data the fractional porosity and impedance were derived. RGB images were also produced with a full color digital line scan imaging system. Magnetic susceptibility, bulk density, and line scan photography were generally measured on all cores.

Magnetic Susceptibility

Magnetic susceptibility was measured with a *Bartington point sensor MS2* using an 80-mm internal diameter sensor loop (88-mm coil diameter) operating at a frequency of 565 Hz and an alternating field of 80 A/m (0.1 mT). The sensitivity range was set to the low sensitivity setting (1.0 Hz). The sample period and interval were set to 2 s and 4 cm, respectively, unless noted otherwise. The mean raw value of the measurements was calculated and stored automatically. The quality of these results degrades in XCB and RCB cores, where the core may be undersized and / or disturbed. sturbed. Nevertheless, general downhole trends are useful for stratigraphic correlations. The MS2 meter measures relative susceptibilities, which have not been corrected for the differences between core and coil diameters.

Gamma-Ray Attenuation

Bulk density was estimated for split core sections as they passed through the GRA bulk densiometer using sampling periods and intervals of 2 s and 4 cm, respectively, unless

noted otherwise. A thin gamma beam from a Caesium-137 source with energies around 0.662 MeV is passed through the core and the relative intensity of this beam can be used to measure the gamma density. These photons are scattered by electrons in the core and loose some of their energy. To determine the gamma density the number of unscattered electrons is measured by counting photons with the same principle energy as the photon source. The gamma density of an aluminum billet of stepped thickness is used to obtain calibration equations to convert gamma density into actual density values.

P-Wave Velocity

The P-wave velocity is measured at 4-cm intervals and 2-s periods using two PWL transducers. The PWL measured P-wave velocity across the unsplit core sections. In order to determine the P-wave velocity, the PWL transmits 500-kHz P-wave pulses through the core at a frequency of 1 kHz. The transmitting and receiving transducers are aligned perpendicular to the core axis while a pair of displacement transducers monitors the separation between the P-wave transducers. Variations in the outer diameter of the liner do not degrade the accuracy of the velocities, but the unconsolidated sediment or rock core must completely fill the liner for the PWL to provide accurate results. During this measurement good acoustic coupling between the core liner and transducer is achieved by adding water to the contact points.

6.2.4 Pore Fluid Extraction and investigation of freshening

(S.Stegmann)

During *POS472*, pore water analysis was conducted mainly to find indications for freshening related to seaward directed groundwater flow within more permeable layer along coastal sediments (see Chapter 5).

Pore water was extracted using pore water rhizon samplers (~0.4 µm) on the split working half of the core. The vacuum necessary to operate the rhizon samplers was created by pulling up 10 ml plastic syringes. The amounts of pore water retrieved by this method were between 5 and 10 ml. Depth levels of pore water sampling are represented in the lithology logs (see Appendix). A first-order determination of salinity was carried out using a handheld salinity refractometer (Figure 20A). For the measurement the sample plate has to be opened and some drops of the pore fluid has to be added on the plate (Figure 20B). After closing the sample plate, you hold the refractometer up to a natural light source. The instrument measures the refractive index of the sample and displays the result in parts per thousand and specific gravity (d20/20). This method is highly sensitive to temperature. Temperature about the sample has to be 20°C.

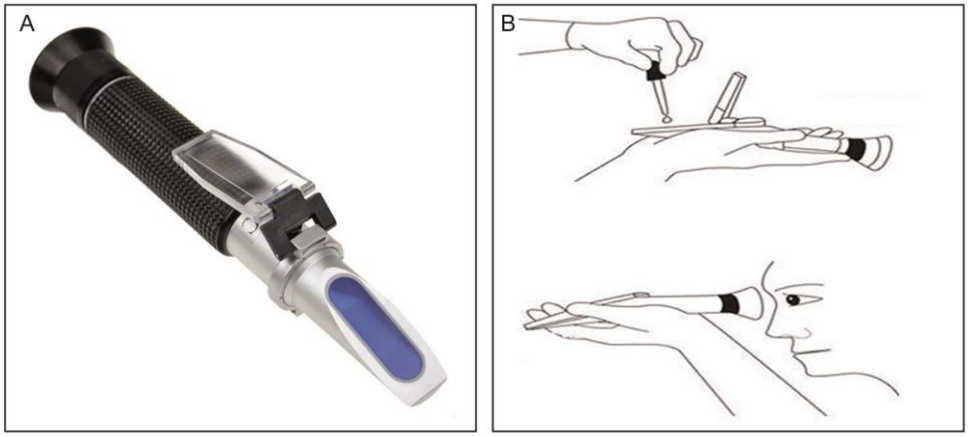

Figure 20 *A) Photo of a handheld salinity refractometer, which was used for a first-order determination of salinity of pore fluids during POS472. B) Procedure of measurement.*

6.2.5 *In situ* temperature measurement

(T. Fleischmann)

The *in situ* temperature gradients within the superficial portion of sediments were measured routinely when gravity cores were taken using autonomous **M**iniature **T**emperature **L**oggers (*MTL*s). For technical specifications and detailed information, refer to Pfender & Villinger (2002). Measurement of temperature within the sediments (seafloor penetration) was realised by mounting the MTLs to the gravity core barrel using fins and receptacles and get gradient at the chosen spacing as well as reference temperature in the water column *(*Figure 21*).* The probe remains in the seafloor sediment for 5 mins to allow for some dissipation of artificial frictional heat from inserting the gravity corer. The sampling rate of the logger is 1sec. For each depth temperature is plotted as a function of time. The data are available in the open-source data base PANGEA (www.pangea.de)

Figure 21 *MTL mounted on the gravity corer on cruise P472. The pointy end with the thermistor is facing downward.*

6.2.6 Bathymetry Site Survey

(D. Völker, W. Li, T. Fleischmann)

We used the on-board multibeam sonar system *Multibeam 3050* from *L-3 Communications ELAC Nautik*. This system has been installed on RV POSEIDON in October 2010 and was still in the testing phase.

The *Multibeam SB 3050* system on POSEIDON is designed to operate in depths from 3 m to approximately 3000 m. The operating frequency is in the 50 kHz band. Maximum ping rate is 50 swaths per second and the maximum number of beams is 315. The maximum across-ship swath coverage sector is 140 degrees.

The hardware components of the *Seabeam 3050* system include a motion sensor, a positioning system, a sound velocity profiler and a surface sound velocity sensor. An operating computer receives the preprocessed data stream. Bathymetric data can be visualised in real time using the *Hypack* (2) mapping tool. A schematic diagram of these different components can be seen in Figure 22.

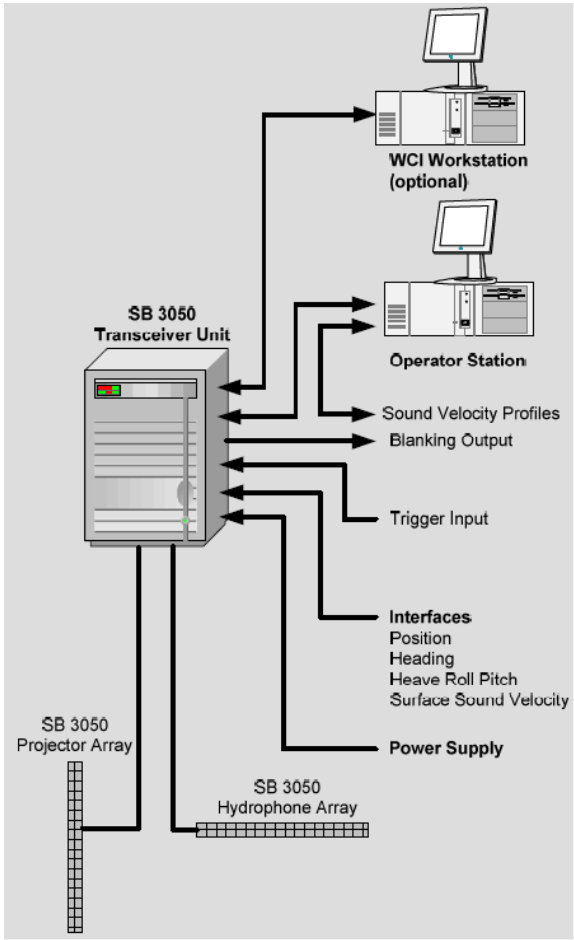

Figure 22 *Layout of the Multibeam system recently installed on RV Poseidon.*

Operating problems during POS472

Right from the start, we encountered a severe software problem that affected the Integrated Navigation System IMU (*F180 system*).This caused erroneous navigational data to be written into the data records. Rendering them virtually was useless. The problem had to be overcome by a firmware update provided by *CODA OCTOPUS*. Once solved, the multibeam system worked reliably. The software configuration, consisting in the interplay of two separate programs (*HydroStar, HyPack*) proved rather counterintuitive and prone to erroneous handling for inexperienced watchmen. In particular, the real-time display of the data during mapping campaigns in map form, necessary for the control of track overlap was tricky.

The signal backscatter information was recorded for later creation of maps of the backscatter properties of the seafloor. Unfortunately, at present the software module (MB-System module) to read out this information is not yet available.

Processing of the data

Standard processing of the multibeam data requires two sequences of processing steps including a profile–oriented sequence followed by area-based processing. The profile-oriented processing of the data comprises the check of navigation data, interpolating missing navigation values, the calculation of water depth and positions of the footprints of the beams by raytracing through the water-column taking into account the sound velocity profile, and removing artefacts and erroneous data points. Area-based processing comprises the calculation of a digital terrain model (DTM) and the visualisation of the data. For easier integration of other data from different systems in various data formats, the “open source software” packages MB-System [Caress and Chayes, 1996] and GMT [Wessel and Smith, 1998] were used for the processing of the multibeam data. In the MB-System software, the raw data format that is provided by the *HydroStar* program (the binary format XSE or Data xchange format) is defined as format 94.

When post-processing the data, first auxiliary files are being created, containing meta-information for each file. In MB-System the management of the data is maintained by so-called data-list files that contain names, paths, format-ID and a weighting factor for each file. Data-list files are set up recursively, i.e. entries in a data-list refer to other data-lists that point to the actual data files. This structure helps to keep track of the data files which grow to several thousands of files for a normal-sized project. The creation of ancillary files and the set up or updating the respective data-list files is accomplished by shell scripts.

The cleaning of the raw data by flagging outliers and artefacts is done with the programs mbclean and mbedit for each of the raw data files. This time-consuming step is done in various iterations, first by automatic filters (mbclean) that are adjusted to remove unlikely data (e.g. spikes) but later by visual inspection of all pings and beams in each raw data file (mbedit). Following this, the navigation is checked interactively with the programme *mbnavedit* for each raw data file. The interactive editor programmes do not modify the data files, but store the edit instructions to separate files. Following the interactive editing, the data files are processed by a call to the programme *mbprocess*. After successful completion of *mbprocess* the profile-oriented data processing is finished.

The creation of grids and maps is performed using *mbgrid* and integrating additional existing data sets such as the MAREANO data set that was provided by NGI/NGU (www.mareano.no).

7 Measurements and Data

7.1 Data, Sample Storage & Availability

Measurements of the cruise *POS472* concentrated on i) the *in situ* investigation of sediments related to shallow landslide events in coastal as well as open ocean settings to complete existing studies (see Chapter 5), ii) testing the recently modified DW-FF-CPTu, and iii) the collection of a data set for generic CPTu studies.

A selection of data and preliminary results is presented in Chapter 7.2.: i) Lithology logs based on visual description of the gravity cores, ii) physical properties of cored sediments obtained by shore-based MSCL logging, and iii) bathymetry maps including the track line of the mapping survey are summarised in the Appendix.

Gravity cored samples are stored in the MARUM GeoB core repository. Lists of measurements on sediment and pore fluid samples are stored in the GeoB database system (www.marum.de/MARUM_GeoB_Kernlager.html).

Given that there was neither a full-time position nor a dedicated PhD project associated with that cruise, the work in the four study areas was done incrementally. Following data work and studies are already published related to *POS472* data:

Dynamic FF-CPTu tests carried out in Trondheim Harbour were analysed considering the strain-rate-effect on cone resistance and soil classification:

> **Roskoden**, R., 2015. Cone penetration tests: The soil classification and analytic assessments of dynamicand static penetrometer test data. Unpubl. MSc thesis, Univ. Bremen.

Results based on Vibratory CPTu testing in Orkdalsfjorden were published in the context of a PhD thesis by M. O. Kluger. The study contains also laboratory determination of geotechnical index properties as well as triaxial deformation tests of sediments recovered during *POS472:*

> **Kluger**, Max Oke, et al. 2016. "In situ cyclic softening of marine silts by vibratory CPTU at Orkdalsfjord test site, mid Norway." *Submarine Mass Movements and their Consequences*. Springer International Publishing, 2016. 201-209.

An on-going study focuses on the analysis and correlation of static CPTu profiles along the shoreline of Orkdalsfjorden.

Initial results of static CPTu data taken on the slope off Vesterålen as well as slope stability evaluation was studied and published by S. Stegmann:

> **Stegmann**, S., Kreiter, S., L'Heureux, J. S., Vanneste, M., Völker, D., Baeten, N. J., ... & Haflidason, H. (2016). First Results of the Geotechnical In Situ Investigation for Soil Characterisation Along the Upper Slope Off Vesterålen: Northern Norway. In *Submarine Mass Movements and their Consequences* (pp. 211-219). Springer International Publishing.

An interpretation of geotechnical data (plasticity index, sensitivity) based on laboratory tests on slope sediments of Vesterålen were summarized in a Bachelor thesis:

Koopmann, S., 2016. Geotechnische Untersuchungen an marinen Sedimenten des von Hangrutschungen gekennzeichneten norwegischen Kontinentalhangs vor den Vesterålen. Unpubl. BSc thesis, Univ. Bremen.

7.2 Preliminary Results

7.2.1 Coastal Setting

7.2.1.1 Trondheim Harbour (TH)

In the Trondheim Bay geotechnical investigation was carried out on six sites. The strategy of geotechnical measurement of sediments in the Trondheim Bay was concentrated on the characterisation of:

i) undisturbed material directly behind the scar of the W'Slide (TH01),
ii) undisturbed glacio-marine sediments for reference (TH02),
iii) on two failed blocks, which fail in different stages during the 1990 Slide (see Chapter 5.1.1; TH03 & TH04),
iv) the intact portion related to the 1888 failure (TH05), and
v) the sediments along the western flank of the Munkholmen Island (TH06).

Site locations are shown in Figure 23.

Static CPTu testing

In total, 4 static GOST CPTu profiles were carried out with a penetration depth ranging between 10 and 19.5 mbsf. A selection of the data is presented here. Because of the low water depth, the proximity to the shoreline and the high frequency of shipping traffic some initially planned static CPTu locations had to be cancelled or even modified. The intended static CPTu profils at site TH02 and TH05 were rejected, as the locations were on the main route of the shipping traffic within the harbour or too close to the shoreline, respectively. Location TH04 was shifted seawards to reach adequate water depth for GOST operations (> 35 m). Static CPTu profiles at the four sites were successful. Penetration depth ranged between 8.5 mbsf and 19.5 mbsf.

The CPTu profile GeoB18608 at site TH01 characterises the non-failed portion behind the W'Slope on the plateau in between the Nidelva channel system (Fig. 23). The corrected cone resistance q_t reflects well interbedded strata comprising i) the background sediment, which increases linearly up to ~800 kPa at 19.5 mbsf, ii) stiff layers with q_t -values up to 5.25 MPa, and iii) material, where q_t decreases relatively and indicates a certain loss of sediment-mechanical strength. In accordance to q_t, these portions reveals low values of sleeve friction f_s (Figure 24). These portions are highlighted by orange-colored corridors in the plot (Figure 24). Pore pressure measurement indicates no zone of overpressure. High values of q_t coincides with significant loss of pore pressure. This is the typical signal for dilative shearing behaviour when the CPTu penetrates coarser-grained or overconcolidated sediment.

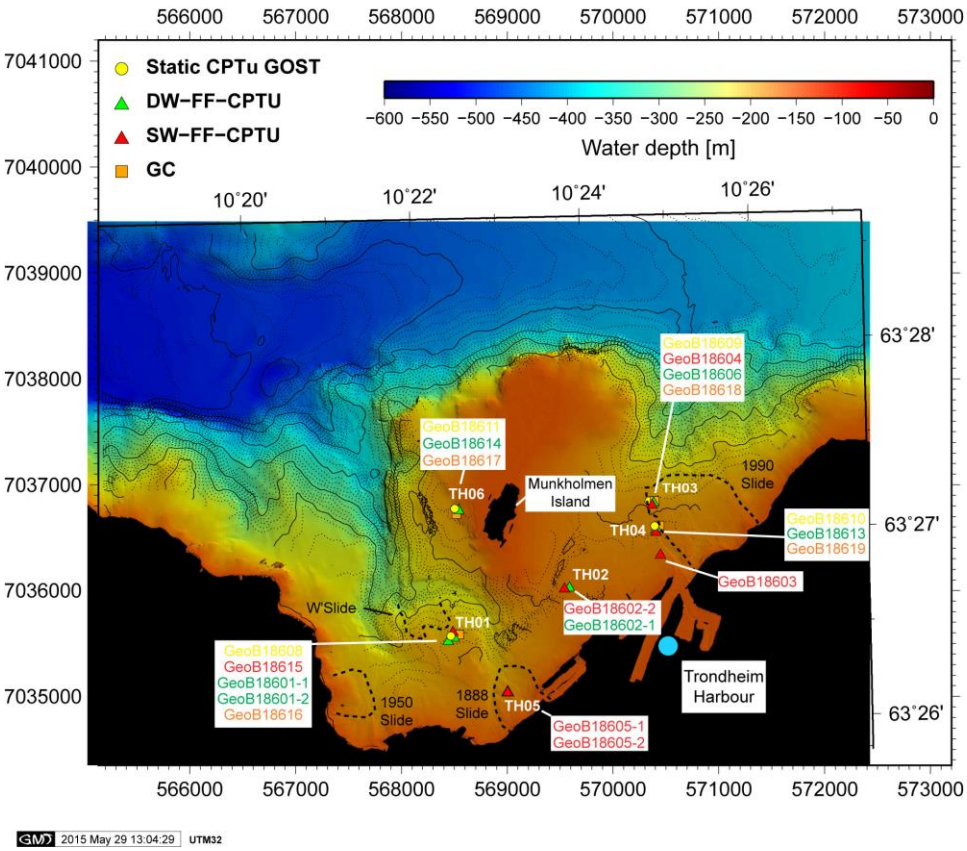

Figure 23 *Location of geotechnical in situ investigation using CPTu systems and gravity coring off Trondheim. Dashed, black lines indicate the scar of the coastal slope failure events along the shoreline of Trondheim. The combination of static and dynamic CPTu profiling and gravity coring was carried out at site TH01 (W'Slide), TH03 (1990 Slide), TH04 (1990 Slide) and TH06 (western slope of the Munkholmen Island). Bathymetry data are provided by NGU Trondheim.*

CPTu Profiles GeoB18609 and GeoB18610 were carried out at site TH03 and TH04, respectively. The CPTu operation (GeoB18609) was stopped at 8.5 mbsf when the resistance of the sediments on the cone increased more than 20 MPa to avoid bending or breaking of the rods.

Due to the close proximity of the sites TH03 and TH04 the accurate positioning for CPTu profiling was not easy. Similar signatures of the penetrated sediments can be observed in the CPTu readings of profile GeoB18609 and GeoB18610. Three different units can be distinguished from sediment-physical CPTu properties. In contrast to Unit I (up to 6.5 mbsf) and Unit III (14 mbsf – 18.5 mbsf) the sedimentary succession of Unit II (6.5 mbsf – 14 mbsf) represents minor mechanical strength due to low values of q_t and an increase of pore pressure u_2 (Figure 29). Here, maximum value of pore pressure u correlates with lowest values of cone resistance q_t and sleeve friction f_s.

CPTu profile GeoB18611 is located on a submarine terrace between the western flank of the Island Munkholmen and the Nidelva channel in the East (see Figure 23). Penetration depth was 18.5 mbsf. Penetration depth was 18.5 mbsf. Quality of the GeoB18611 data is limitid: i) The tiltmeter recorded an inclination up to 90° in the upper section (up to 10 mbsf). But no bending or breaking of the rods has been observed. ii) q_t, f_s as well as u show no reliable data underneath 10 mbsf (Figure 26). Cause for this data is not reproducible, as the *GOST* system worked well after recovery.

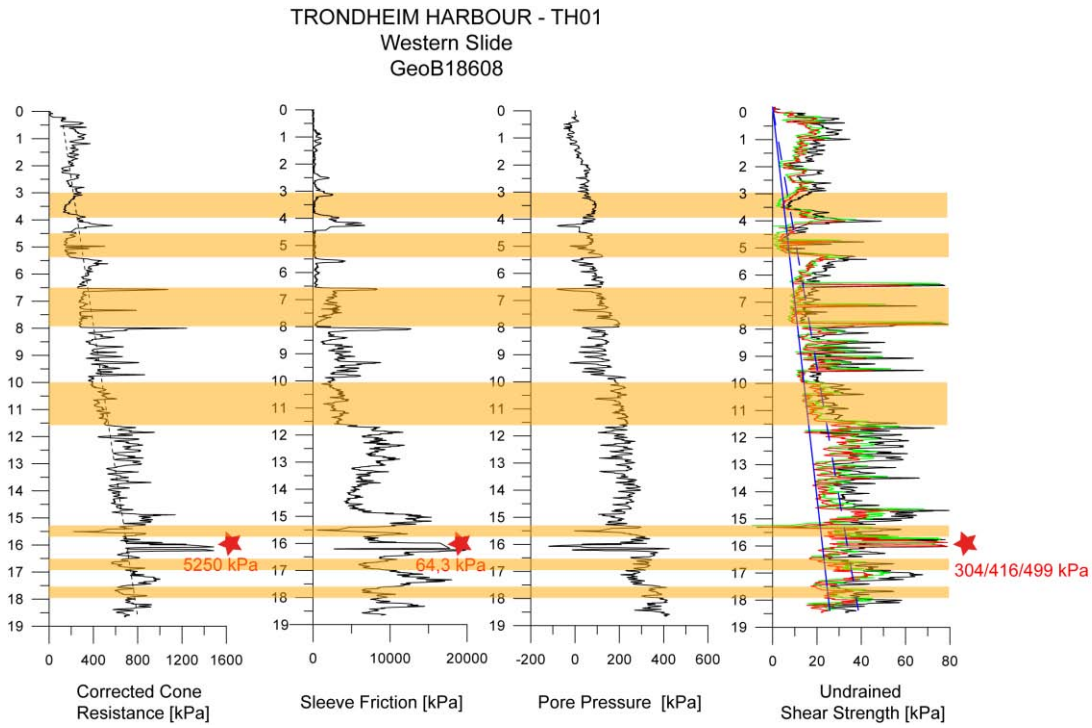

Figure 24 *Data plot of the static CPTu profile GeoB18608. Red-coloured stars mark data peaks, which have been clipped for better illustration. The number specify the value of the peak. Blue lines indicate the ratio of undrained shear strength over the depth of the profile (continuous line: su ratio =0.2; dashed line: su ratio = 0.3, see Chapter 6.1.1))*

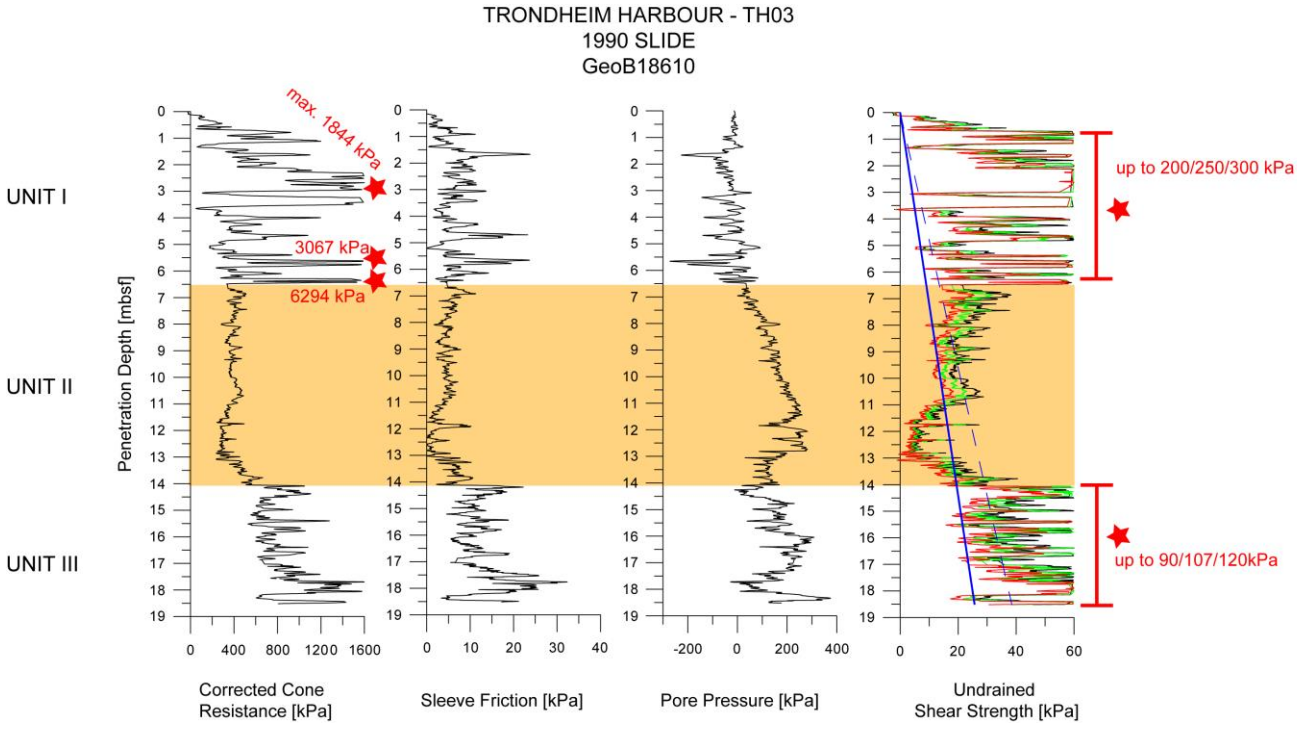

Figure 25 *Data plot of the static CPTu profile GeoB18610. Red-coloured stars mark data peaks, which have been clipped for better illustration. The number specify the value of the peak. Blue lines indicate the ratio of undrained shear strength over the depth of the profile (continuous line: su ratio =0.2; dashed line: su ratio = 0.3, see Chapter 6.1.1))*

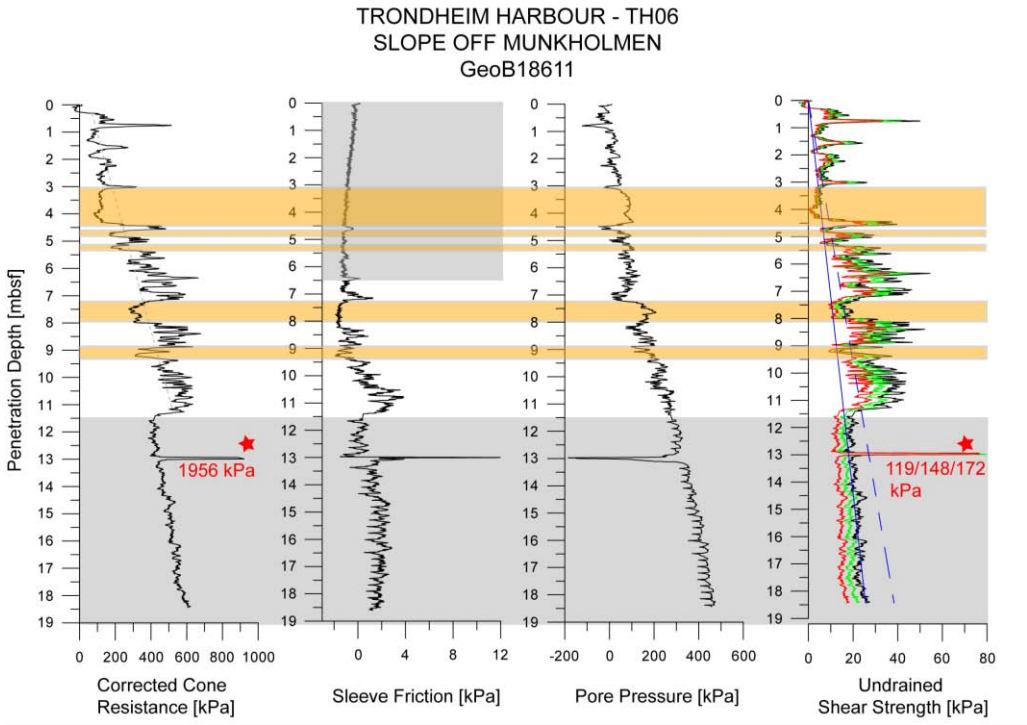

Figure 26 *Data plot of the static CPTu profile GeoB18611. Red-coloured stars mark data peaks, which have been clipped for better illustration. The number specify the value of the peak. Blue lines indicate the ratio of undrained shear strength over the depth of the profile (continuous line: su ratio =0.2; dashed line: su ratio = 0.3, see Chapter 6.1.1))*

Dynamic FF-CPTu testing

In addition to gravity coring and static CPTu testing, dynamic FF-CPTu profiles were carried out at each site (Figure 23). Penetration depth ranged between 0.3 and 4.6 mbsf. Good weather conditions and low water depth within the Trondheim Bay facilitated appropriate conditions for (generic) testing of the dynamic FF-CPTu systems (SW and DW, see Chapter 6.1.2).

The DW-FF-CPTu was deployed to check the real-time communication unit SHDSL Ethernet Extender between the CPTu tool and the vessel. This unit was recently added and tested for the first time on a vessel. The DW-CPTu instrument was deployed at 6 sites (Figure 23). Real-time data transfer during the CPTu operations worked well. Constant negative pore pressure values may indicate deficient saturation of the tubing related to low water depth.

At study site TH01 16 SW-FF-CPTu deployments were obtained using the MARUM FF-Winch. The winch was used for the first time on research vessel. The FF-Winch was placed on the working deck of *R/V POSEIDON* (see Figure 12). The cable of the FF-Winch run over the A-Frame of the vessel to deploy the SW-FF-CPTu from the aft deck. CPTu testing with the FF-Winch was limited to coastal settings carried out in coastal settings as the length of the cable of the FF-Winch is limited to 200 m.

SW-FF-CPTu profiling in the Trondheim Bay focused on i) the test of the *MARUM FF-Winch*, which was used for the first time on a research vessel. At site TH01 16 SW-FF-

CPTu deployments were performed using the *MARUM FF-Winch* with velocities ranging between 0.5 m/s and 3 m/s. This experiment provides the data set for the generic approach to study the influence of the strain rate effect on CPTu parameters in different types of sediments (silt, clay) within a natural realm. Composition of the sediments and thickness of the strata is provided by the gravity core GeoB18616 for reference. Figure 27 summarises the variable deployments of the CPTu lance, where five different groups of initial penetration rate (0.5, 1, 1.5, 2.5 m/s) are shown.

Penetration depth ranged from 0.9 mbsf and 3.7 mbsf (Figure 27). The variability of penetration depth increased for the deployments with v = 0.5 m/s (black-coloured lines, 0.9 mbsf – 2.9 mbsf) and v = 3 m/s (purple-coloured lines, 3.1 mbsf – 3.7 mbsf).

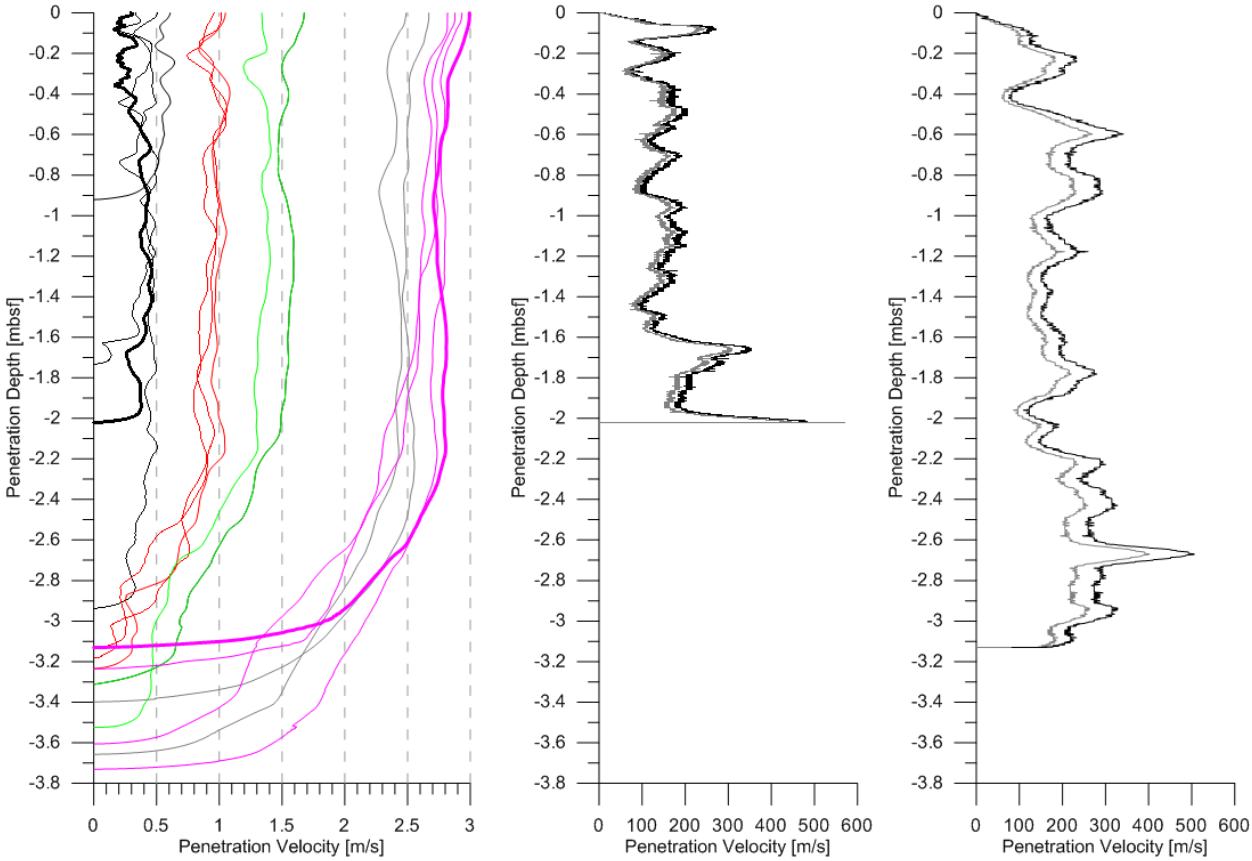

Figure 27 *Rate-dependence CPTu testing with the FF-SW-CPTu lance at site TH01. A) Illustrations of the various initial penetration rate (0.5, 1.0, 1.5, 2.5 & 3 m/s), which was used for the 16 dynamic CPTu drops, and the resulting penetration depth. For each "velocity group" the CPTu deployment was carried out four times. This plot contains only successful deployments. B) Difference between rate-corrected and non-rate-corrected values of cone resistance for different initial penetration velocities. Profiles shown here are highlighted in panel A by a heavy line.*

Gravity cores

Four gravity cores with a maximum length of 5 mbsf were recovered in the Trondheim Bay (see Appendix).

Sediments of undisturbed portions (stations GeoB18616, -17) comprised silty clay and silt with sandy layers. Stations GeoB18618 and -19 are located at Site TH03 and TH04. Increase of content of sandy deposits is significant higher than in GeoB18616 and -17, which results in lower coring depth (max. 2.38 mbsf). Deformation structures related to gas escape after splitting the gravity cores can be observed at site TH01 (GeoB18616), TH03 (GeoB18618) and TH04 (GeoB18619).

First-order determination of salinity of extracted pore fluids using a handheld salinity refractometer reveal freshening of fluids within the core taken nearby the coastline (GeoB18616, -18, -19, Figure 28A). Here values of salinity decrease up to 28 ‰ minimum in core GeoB18616 at site TH01. Salinity of pore fluids obtained from Core GeoB18617, located at the western flank of the island Munkholmen attest sea water conditions (salinity ~ 35 ‰). Further geochemical analyses will be carried out in the MARUM laboratory.

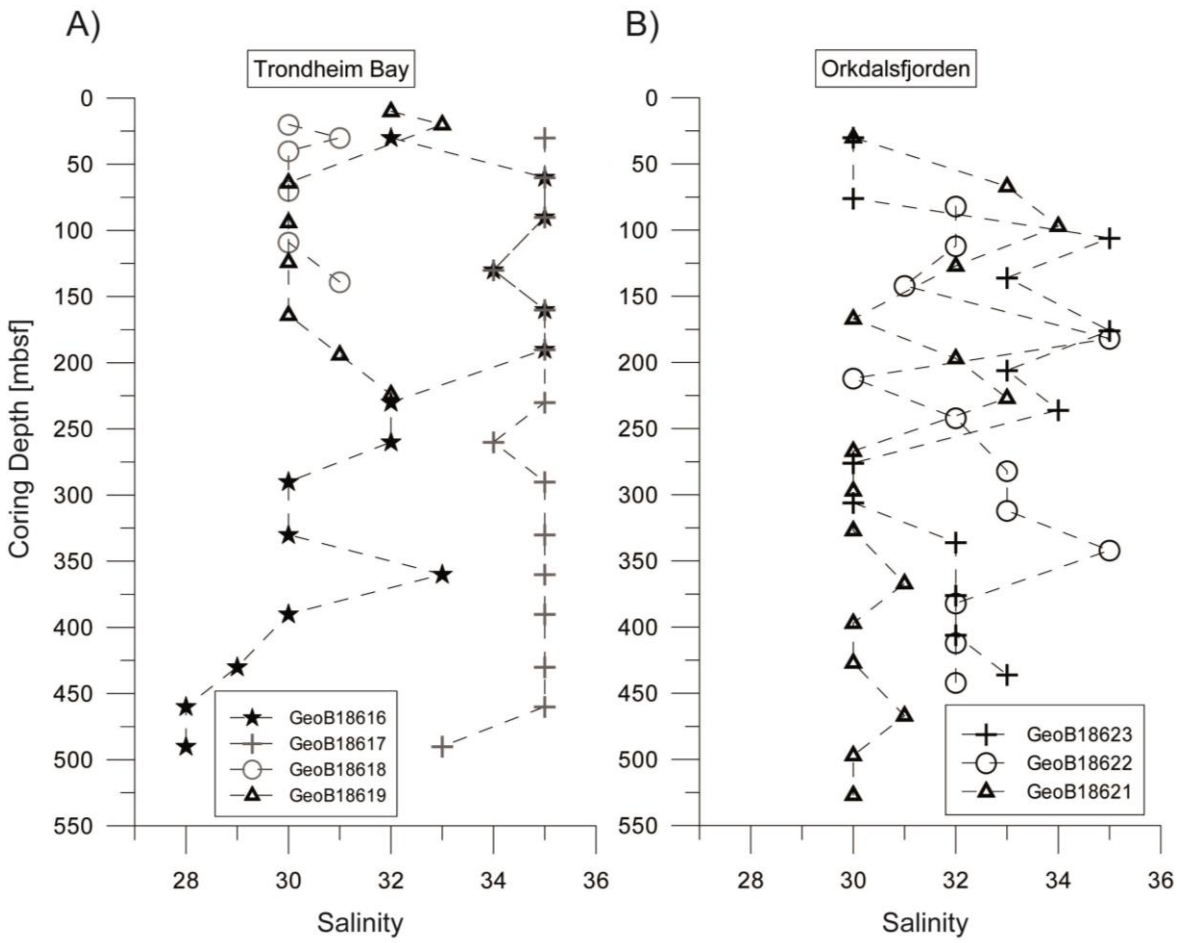

Figure 28 *Values of salinity measured on pore fluids extracted from gravity cores taken within the Trondheim Bay and Orkdalsfjorden.*

7.2.1.2 Orkdalsfjorden (OF)

Strategy of the geotechnical *in situ* investigation of sediments on the flank of Orkdalsfjorden, which have been affected by the 1930 failure running retrogressively parallel to the shoreline, aimed to characterise:

i) intact portions of sediment along the headwall, where the failure event was initialised (OF02) as well as where a stable segment of the slope resist the deformation forces (OF01, “stable nose”)
ii) the geotechnical conditions of the sliding surface of the 1930 failure event. Height of the headwall spans from 8 m to 12 m (L’Heureux et al. 2014).Thus this zone was profiled by static *GOST* CPTu profiles reaching a penetration depth of 18.5 mbsf.
iii) material, which was directly affected by the retrogressive failure process at site OF03. This site - located, where the failure was initialised – was chosen to reach strata underlying the sliding surface.

Locations of the study sites and measurements are illustrated in Figure 29.

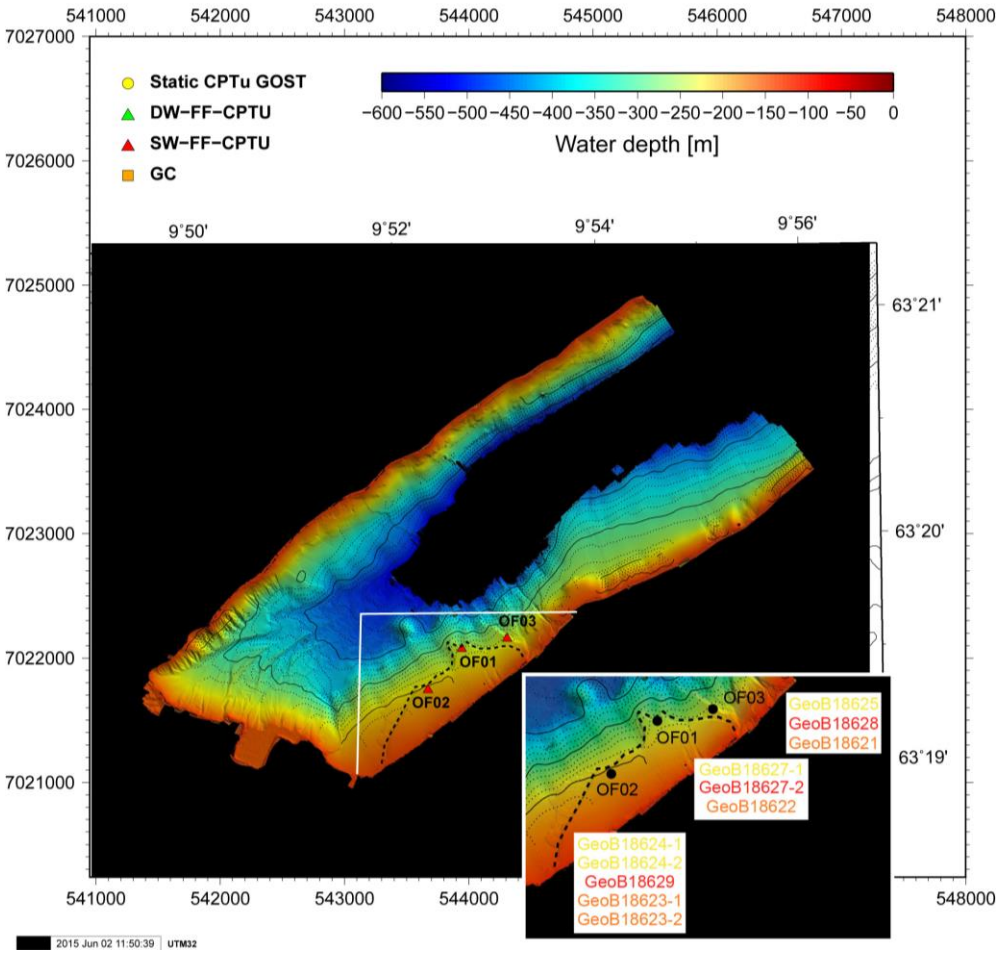

Figure 29 *Location of geotechnical in situ investigation and gravity coring within the Orkdalsfjorden (Source of bathymetry data: NGU Trondheim). Dashed, black lines indicate the scar of the tsunamigenic slope failure event running retrogressively along the eastern shoreline. The combination of in situ measurement (static and dynmaic CPTu) as well as gravity coring was done at site OF01, OF02 and OF03. In addition to three static CPTu profiles with a penetration depth about 19 mbsf, we obtained at site OF02 one vibratory CPTu (VCPTu) profile (GeoB18624-2) using the seismic mode of the GOST system.*

Static CPTu profiles

Three static CPTu profiles with a penetration depth between 18.3 and 18.9 mbsf were carried out at site OF1, OF2 and OF3. Profile of deployments GeoB18624-1 (OF2) and -27-1 (OF1) represents the geotechnical characterisation of undisturbed sediments directly behind the headwall of the 1930 Slide (Figure 29). Both profiles reveal the occurrence of mechanically weak layer (see orange-coloured zones in Figure 30 and Figure 31) between ~8 and 16 mbsf. In the CPTu deployment GeoB18627-1, however, this kind of zone ranged continuously from 7.5 mbsf up to 14.5 mbsf (Figure 31). In accordance with the loss of sedimentary strength, pore pressure increased significantly (Figure 31), which indicates the occurrence of clay-rich layers. The mechanically weaker portion at may be assumed to correlate with the sliding surface of the 1930 failure event (see L'Heureux et al. 2014).

Profile 18625 is located at OF3, where the initial failure occurred and sediments were mobilised (see Figure 29 and L'Heureux et al. 2014). Here, we reached a sedimentary portion of sediment underneath the sliding surface with a thickness of 8 m (Figure 32). Pore pressure can be used to distinguish between different units (Figure 32). In the upper 12 mbsf pore pressure increased slightly or remained constant. In deeper strata the general trend of pore pressure increased significantly (Figure 32).

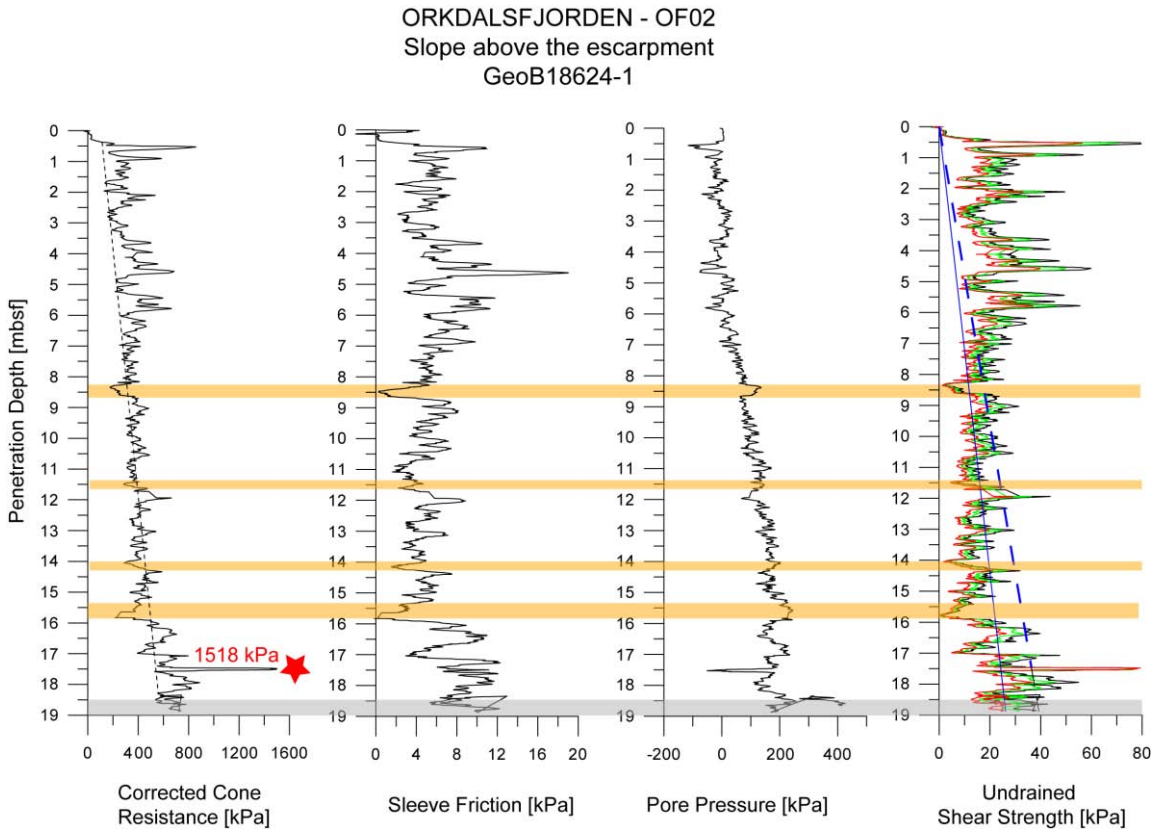

Figure 30 *Data plot of the static CPTu profile GeoB18624-1. Red-coloured stars mark data peaks, which have been clipped for better illustration. The number specify the value of the peak. Blue lines indicate the ratio of undrained shear strength over the depth of the profile (continuous line: su ratio =0.2; dashed line: su ratio = 0.3, see Chapter 6.1.1). Orange-coloured bar represents mechanically relative weaker layers defined by decreasing* q_t.

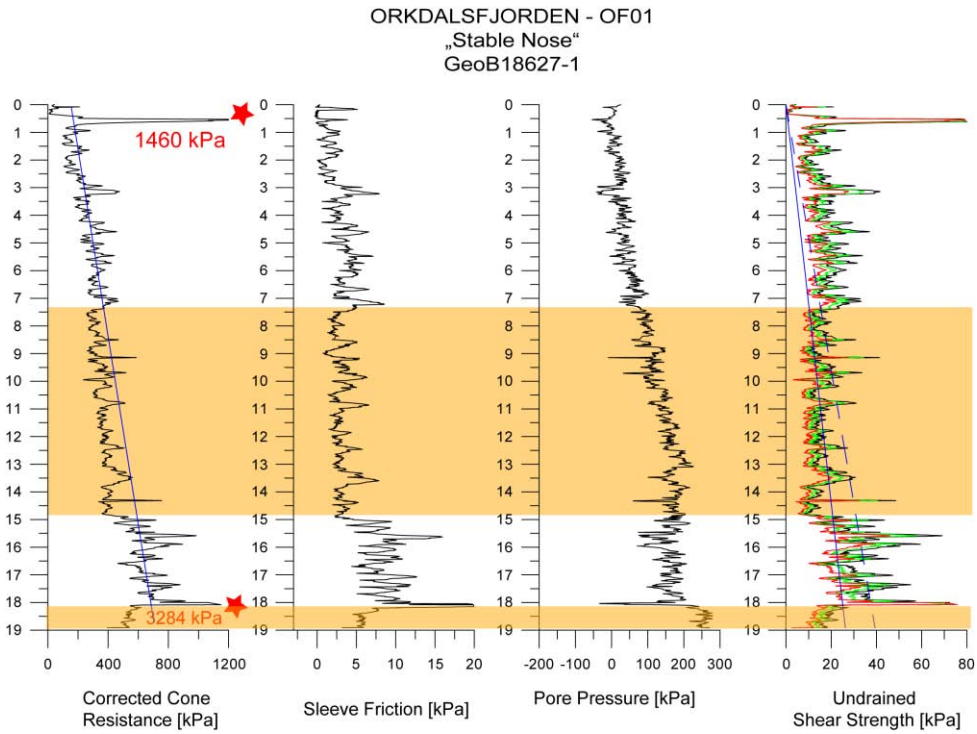

Figure 31 *Data plot of the static CPTu profile GeoB18627-1. Red-coloured stars mark data peaks, which have been clipped for better illustration. The number specify the value of the peak. Blue lines indicate the ratio of undrained shear strength over the depth of the profile (continuous line: su ratio =0.2; dashed line: su ratio = 0.3, see Chapter 6.1.1)). Orange-coloured bar represents mechanically relative weaker layers defined by decreasing* q_t.

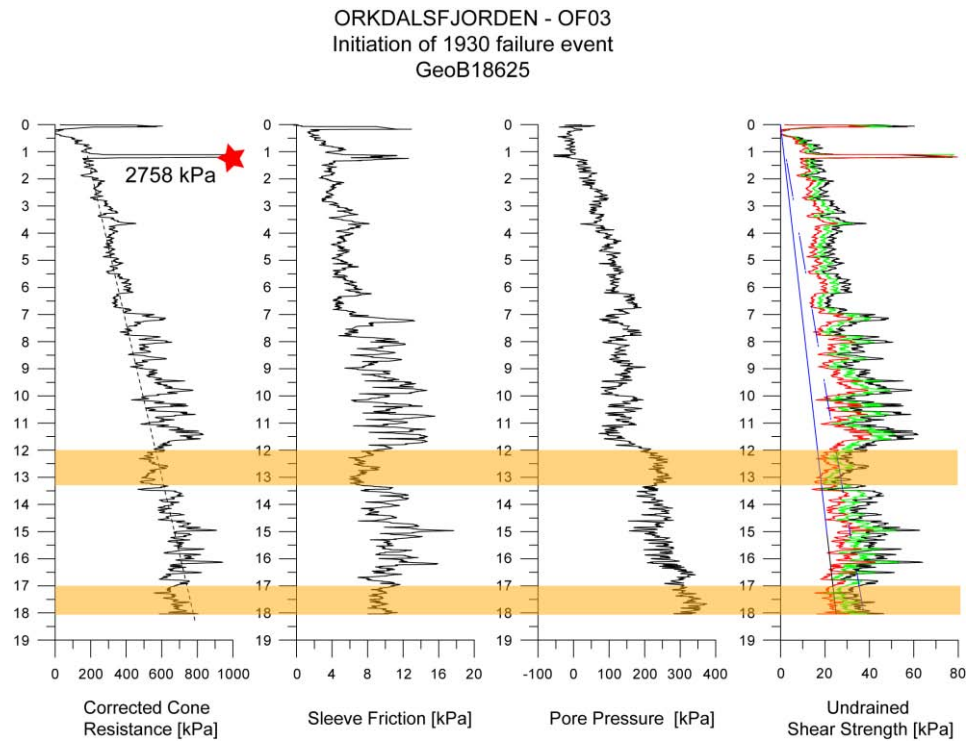

Figure 32 *Data plot of the static CPTu profile GeoB18625. Red-coloured stars mark data peaks, which have been clipped for better illustration. The number specify the value of the peak. Blue lines indicate the ratio of undrained shear strength over the depth of the profile (continuous line: su ratio = 0.2; dashed line: su ratio = 0.3, see Chapter 6.1.1)). Orange-coloured bar represents mechanically weaker layers defined by decreasing* q_t.

Vibratory CPTu profiles

In addition to the static standard CPTu profile GeoB18624-1 a VCPTu profile (GeoB18624-2) was carried out at site OF2 with the *GOST* system reaching a penetration depth of 19 mbsf (Figure 33).

This was the first *GOST* VCPTu test in marine realm. The operation provided i) a successful test of the VCPTu modul of *GOST* in marine settings and ii) a trustworthy data set to analyse the mechanically behaviour of fjord sediments due to cyclic loading. Here, the CPTu cone was moved with a sinus-shaped cyclic amplitude of 0.38 mm and a frequency of 4.9 Hz during penetration. Penetration speed was reduced to 1.35 cm/s due to limited hydraulic force supply.

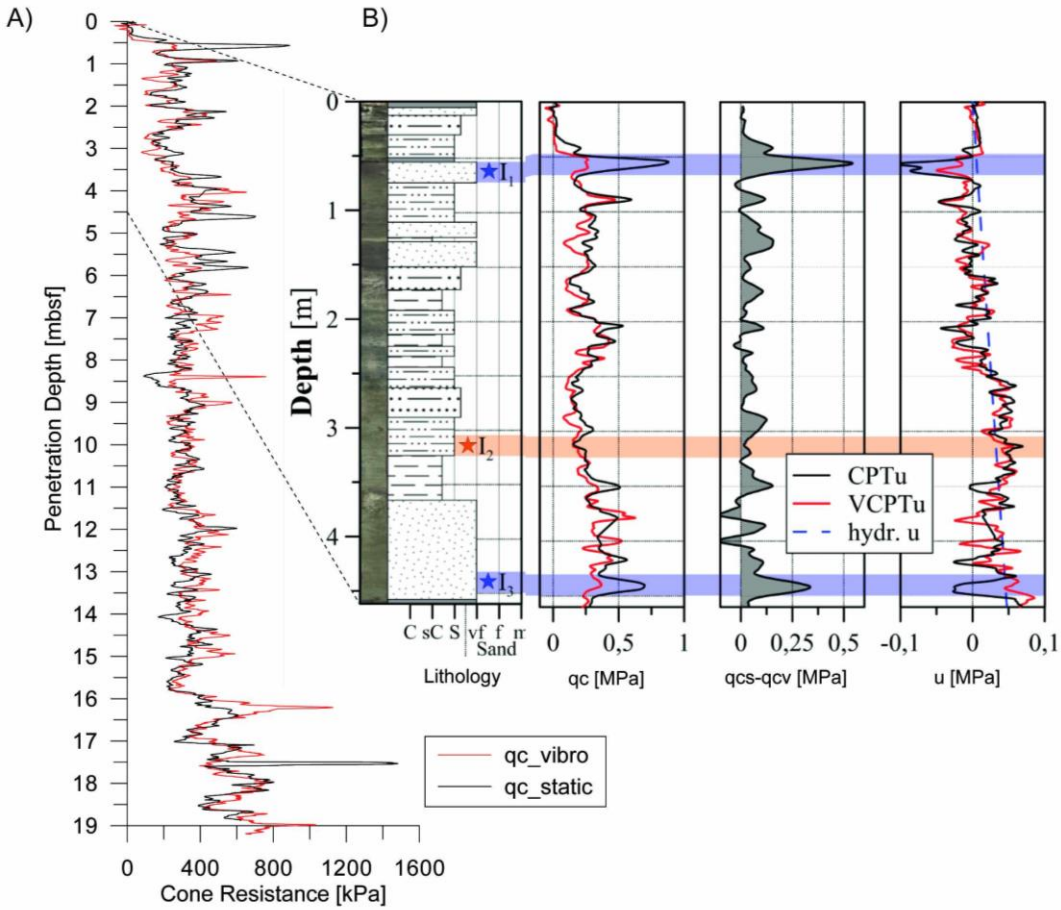

Figure 33 *Initial data from CPTu and VCPTu test using the GOST system: A) Profile of cone resistance over the complete penetration depth. The plot compares the static cone resistance (black line) with the vibro cone resistance (red line). B) In a generic study by Kluger et al. 2014 the in situ data are combined with soil index properties and compared to results of cyclic undrained triaxial tests. In order to relate q_{cs} and q_{cv} , Sasaki et al. (1984) proposed The reduction ratio RR = 1- qc_{vibro}/qc_{static} is used to relate $q_{cstatic}$ and q_{cvibro} (Sasaki et al. 1984). Higher RR values indicate an increase of liquefaction potential.*

VCPTu cone resistance drop ranges between 540 and 340 kPa in layer I_1 and I_3, corresponding to strength reduction of 68 % and 45 % (Kluger et al. 2014). In both silt layers the RR-values are ranging between 0.5 and 0.7 and have therefore medium liquefaction potential (Tokimatsu, 1988). For more details about this geotechnical-generic study please refer to Kluger et al. (2014).

Dynamic CPTu profiles

Three FF-CPTu profiles were taken at OF01, OF02 and OF03 using the SW-FF-CPTu instrument (Figure 29). Penetration depth varied between 0.2 and 1.3 mbsf. Remarkable are the negative pore pressure values over the complete depth in all three profiles. Negative pressure values may relate to the occurrence of free gas, which has been observed in cored sediments (see *"Gravity cores"* below).

Gravity cores

Length of gravity cores varied between 4.5 and 5.4 mbsf. Sediment cored at site OF1, OF2 and OF3 are characterised by fjord-marine deposits consisting on silty clay and clayey silt (see Appendix). The upper portion (0 – 20 cm, 0 – 50 cm) of gravity core GeoB18621 (OF3) and -22 (OF1) are contaminated by industrial waste from the metal factory located at Thamshavn, which is running since 1931 (Figure 34A; L'Heureux et al. 2014). Occurrence of free gas was detected in both cores over the complete length by i) small deformation structures (Figure. 34B), which are related to gas escape after splitting the 1m segments and ii) bending of the end cap of the non-split 1m-segments.

Gravity Core GeoB18623-2 was kept un-split (whole round) to provide material for geotechnical laboratory tests as reference for the dynamic CPTu profile GeoB18623-2 (please refer to Kluger et al. 2014 for more details).

Subsequent to finishing the NORGeotech working program in the coastal setting (Trondheim Bay & Orkdalsfjorden), we took three gravity cores for NGU Trondheim (Dr. J. Faust) on the way to the northern study sites Vesterålen and Lofoten. Coring depth of the cores was up to 4.4 mbsf. The cores were cut in 1m segments without splitting. After the cruise, these core segments were transported directly from Tromsø to Dr. Johan Faust at NGU Trondheim.

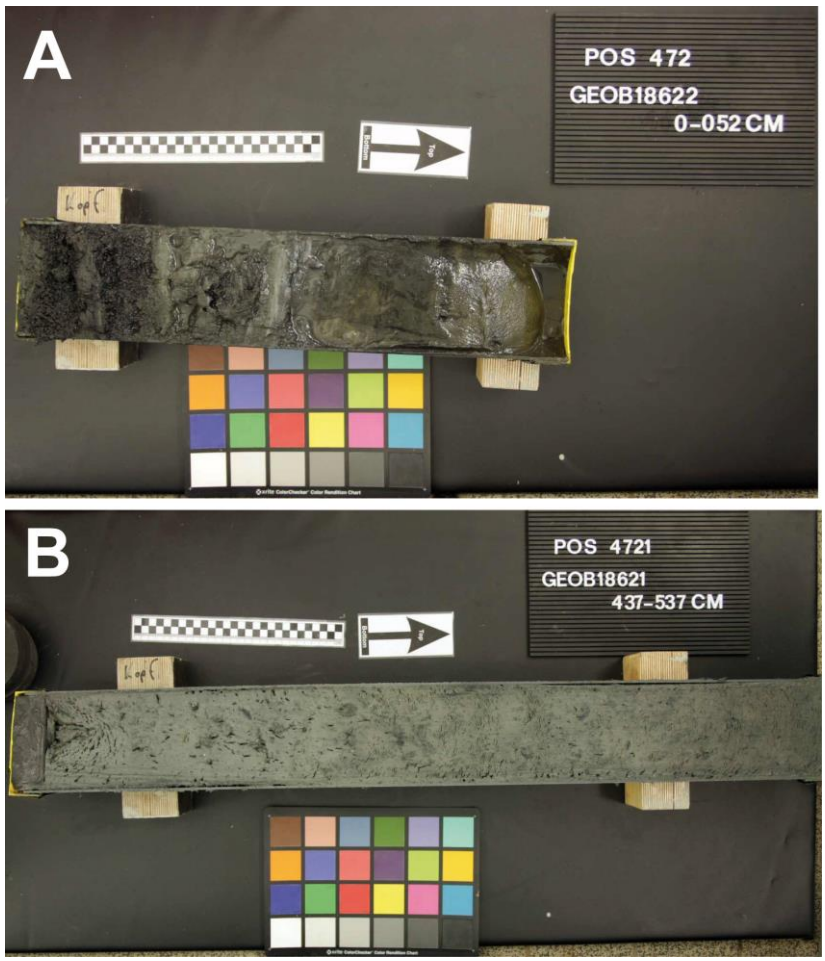

Figure 34 *A) Antrophogenic input from the metal industry at Thamshavn (see L'Heureux et al. 2014); B) Deformation structures related to escape of gas, when the core was split.*

7.2.2 Open Ocean Setting

7.2.2.1 Vesterålen Slope (VS)

Working program along the gently dipping slope off Vesterålen comprises the geotechnical investigation of various deformation features:

i) Main important spot was the structure SL3, which is one of the shallow landslide features lying parallel along the 500 m isobath (see Figure 7).
ii) Corresponding to the morpholoy of a 6km-long deformation structure running along the slope in a water depth of ~600 m this feature was called “Crack”. Due to the lack of geotechnical data the process, which is responsible for this deformation, is not understood.
iii) In addition to the landslide features aligned parallel in ~500 m water depth (Figure 7, SL1-SL4, SLA), the rippled surface of the seafloor as well as the occurrence of little slides imaged by side scan mapping (Figure 7) may indicate on-going surficial deformation of slope sediments.

Figure 35 shows the location of the working program done at the Vesterålen Slope.

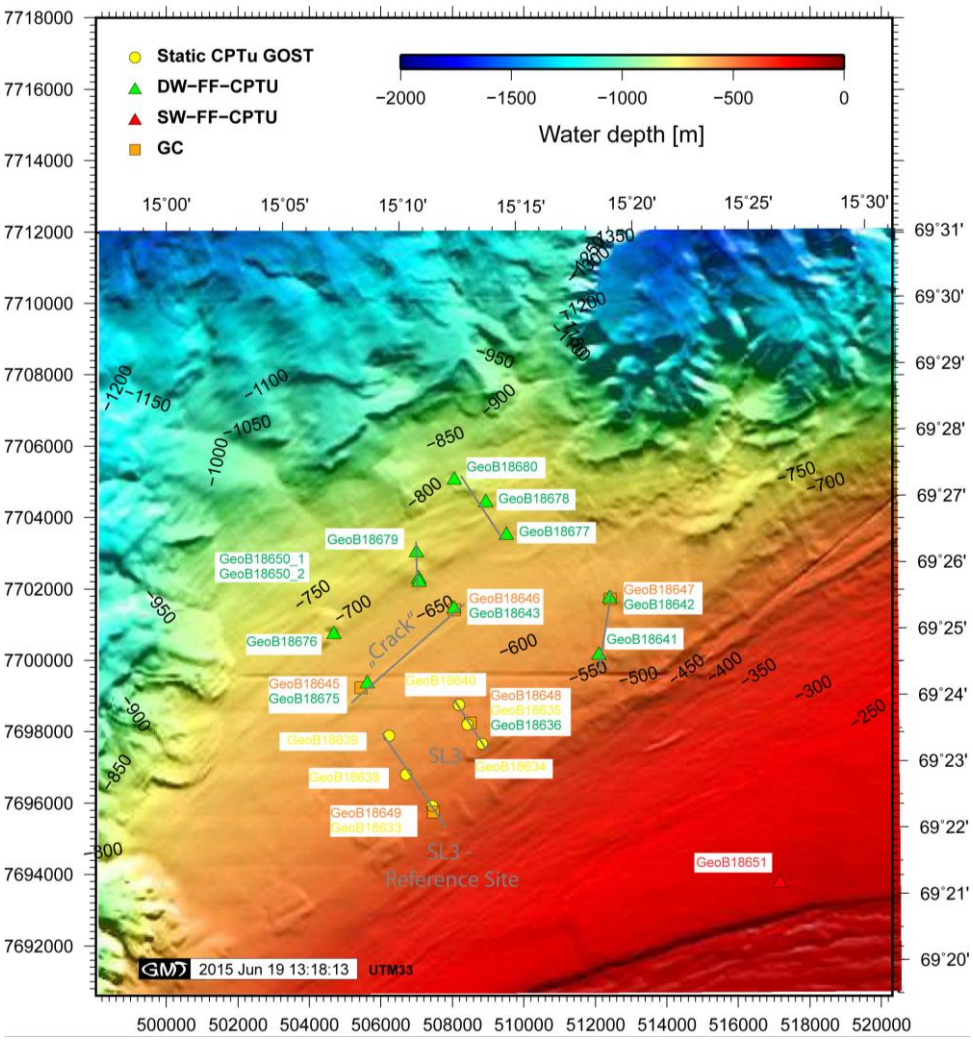

Figure 35 *Location of geotechnical investigation and gravity coring along the continental slope off Vesterålen (Source of bathymetry data: www.mareano.no).*

Static CPTu profiles

Within the landslide feature SL3 six static CPTu measurements were optained profiling i) intact material for reference (GeoB18633, -38, -39) and ii) different morphological parts of SL3 (GeoB18634, -35, -40; Figure 35). Penetration depth ranged between 7 and 19.8 mbsf. The CPTu located upslope (GeoB18633, -34) were stopped at 7 m and 9 m, when q_c reached 20 MPa and 44 MPa, respectively to avoid bending or breaking of the rods. Availability of reliable f_s data is limited as the sleeve friction jacket was blocked during some measurements.

After the CPTu profile GeoB18640 the recovery of the *GOST* system had had to be stopped because of turned and entangled wires. *GOST* was left approximately 10 m under the ship overnight. It was recovered next day during an extensive and tricky operation. In consequence of some damages on the *GOST* system itself and the loss of cable, unfortunately no more CPTu operations were possible during this expedition. Planned *GOST* locations within the “Crack” feature have had to be skipped.

CPTu data related to intact slope sediments reflect clearly the well stratified material, in which the failures occur (Figure 36). Very stiff layers represented by peaks of q_t up to 11.9 MPa maximum are interbedded in soft background sediment, which is characterised by q_t~800 kPa at 19.8 mbsaf penetration depth (Figure 36). In the deeper portion of the profile (8 – 19.8 mbsf) loss of strength indicates the occurrence of mechanically weaker layers (see orange-coloured bars in Figure 36). In situ data provides no evidence for overpressured portions with in the slope sediments (see Appendix). For more details about this study please refer to Stegmann et al. 2014.

Dynamic CPTu profiles

10 DW-FF-CPTu dropes were realised in sediments related to i) the “Crack” and ii) features, where on-going superficial deformation is assumed. Penetration depth varied between 1.30 and 3.5 mbsf. q_c and pore pressure data are reliable. Pore pressure measurements indicated no hints for poorly saturation of the tubing, which has been occurred during profiling in low water depths of the Trondheim Bay (Chapter 7.2.1.1).

Gravity cores

In total 5 gravity cores were recovered in this study area, with a length varying between 3.5 and 5.4 mbsf. Cored material consist on clayey silt and sandy mud (Appendix). Grain size analysis and determination of soil index properties (e.g. plasticity index) will be carried out in the geotechnical laboratories at MARUM. Initial characterisation of deformation behaviour of cored material along the Vesterålen Slope was done during a Bachelor thesis at the University of Bremen. Details about this study are presented in Koopmann, 2016.

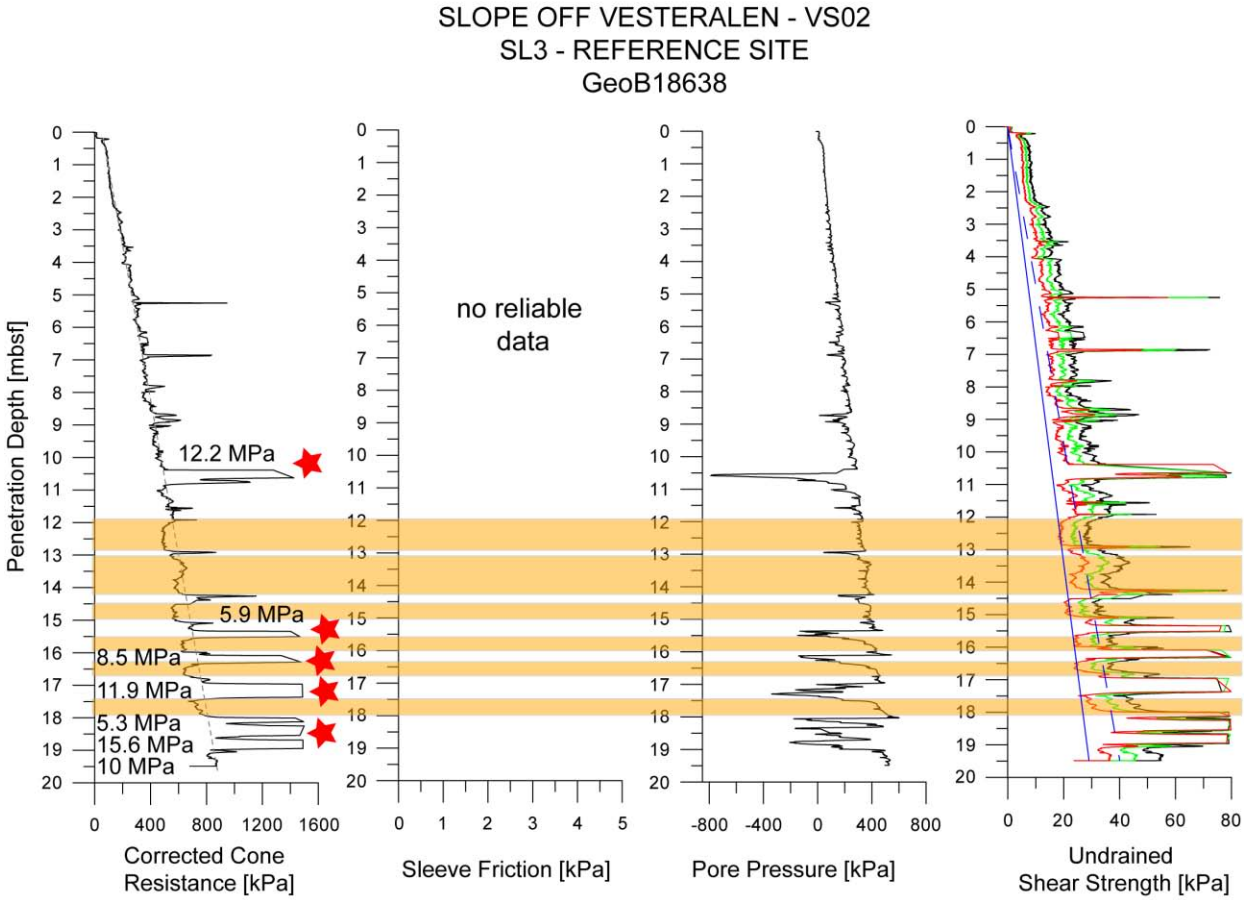

Figure 36 *Data plot of the static CPTu profile GeoB18638. Red-coloured stars mark data peaks, which have been clipped for better illustration. The number specify the value of the peak. Blue lines indicate the ratio of undrained shear strength over the depth of the profile (continuous line: su ratio =0.2; dashed line: su ratio = 0.3, see Chapter 6.1.1))*

7.2.2.2 Lofoten Slope (LS)

Focus of the working program along the slope off Lofoten concentrated on the superficial geotechnical investigation of two deformation features (Figure 37):

i) An elongated, narrow, “Crack”-like structure in water depths around 750 m (similar to the “Crack” along the Vesterålen Slope) is assumed to result from subsidence related to mass wasting processes further downslope (Laberg et al. 2013).

ii) The seafloor morphology of the “Creep Lobe” (*POS472* nomenclature) has been described by Beaten et al. 2013 by linear, along the slope orientated fabric with well-defined lateral margins, which are been interpreted as shear margins (Figures 37 and 38). These downslope-orientated lineations enclose smaller transverse fractures. The “Creep Lobe” represents probably an on-going, retrogressive-multiphase deformation process (Baeten et al. 2013) (Figure 38)

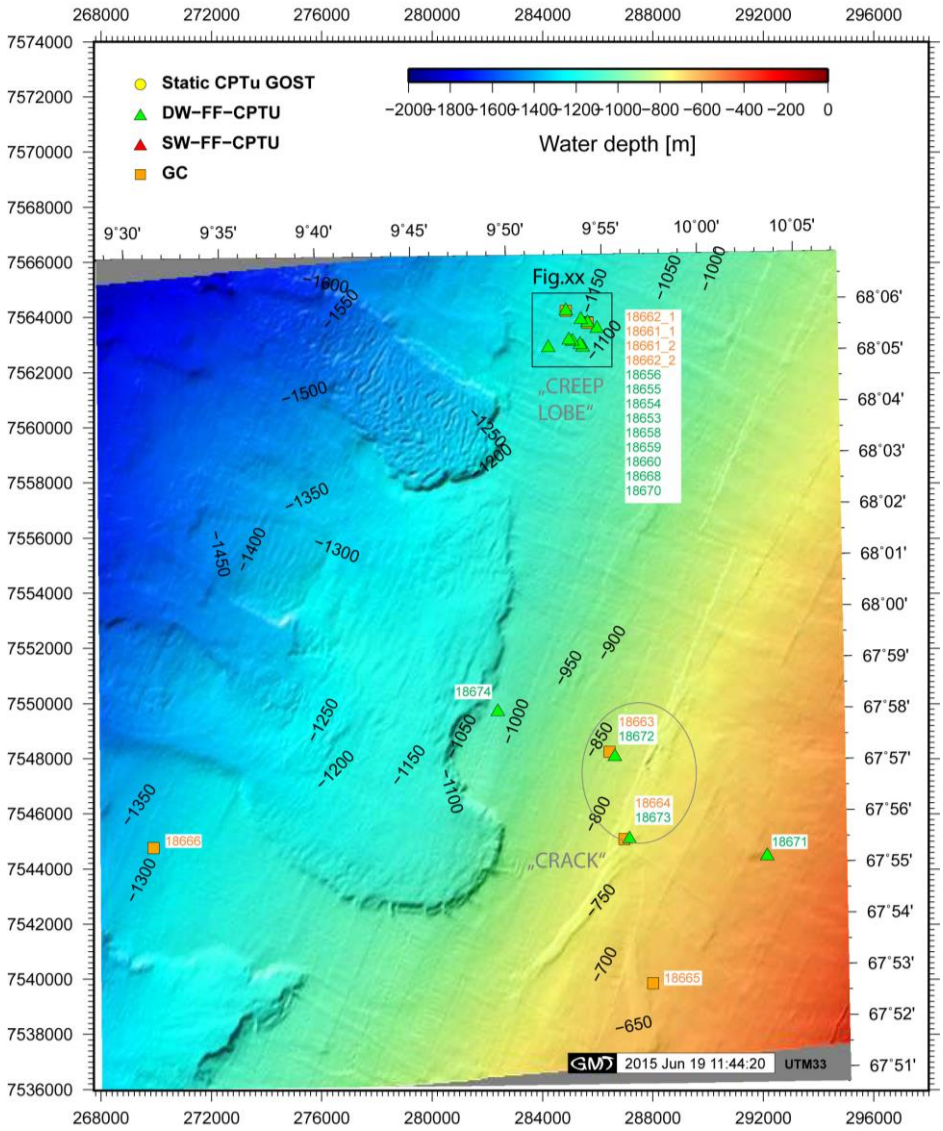

Figure 37 Location of geotechnical investigation and gravity coring along the continental slope off Lofoten (Source of Bathymetry data: University Tromsø, NGU).

Static CPTu profiles

GOST CPTu operations along the Lofoten Slope were not possible as the water depth exceed the length of the power cable.

Dynamic CPTu profiles

13 DW-FF-CPTu deployments were carried out reaching a penetration depth up to 4.1 mbsf. Focus of the dynamic *in situ* testing was profiling of material related to the “Crack”- and the “Creep Lobe”- feature (Figure 37). *In situ* measurements of surficial sediments reveal strength of q_c ~ 200 kPa at depth of 4mbsf (GeoB18653).

Gravity cores

8 gravity core with a maximum length of 5.4 mbsf were recovered. GeoB18661-2 and GeoB18661-2 kept closed for geotechnical laboratory testing including deformation and long-term creeping test as well as standard analysis to obtain grain size analysis and geotechnical soil index parameters.

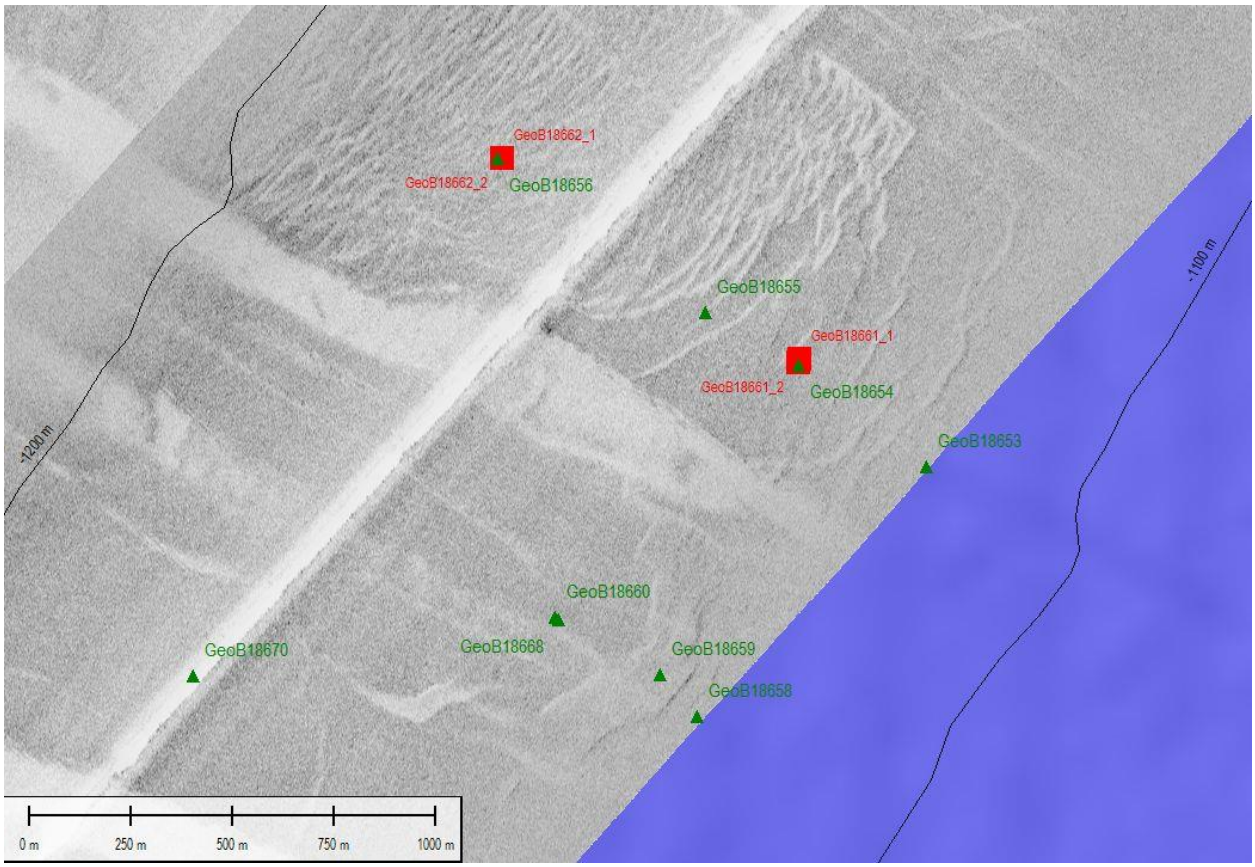

Figure 38 *Position of DW-FF-CPTu measurements and (green-coloured triangles) and gravity cores (red-coloured squares) within the "Creep Lobe" (see Figure 37 for position, reference for the high-resolution side scan sonar data: Baeten et al. 2013).*

8 Station List

GeoB N°		Study Area	Ship's station N°	Gear	Date	Time UTC	Lat °	Lat min dezimal	Lon°	Lon min dezimal	Water Depth [m]	Winch Speed [m/s]	BOKO [m]	Maximum Winch Length at BOKO [m]	Core Length / Penetration Depth [m]	Comment
GeoB186	01-1	TH01	802-1	DW-FF-CPTU	27.07.2014	10:33	63	26,446	10	22,422	67	0,5	67	69	4,5	Stable portion behind the scar of the Western Slide, close to the Calypso core GS08 (L'Heureux et al. 2010)
GeoB186	01-2	TH01	802-1	DW-FF-CPTU	27.07.2014	11:04	63	26,447	10	22,430	67,4	0,5	67	70	4,5	Stable portion behind the scar of the Western Slide, close to the Calypso core GS08 (L'Heureux et al. 2010)
GeoB186	02-1	TH02	804-1	DW-FF-CPTU	27.07.2014	11:54	63	26,700	10	23,799	34	0,5	34	36	0,85	Banana at 70 cm core length
GeoB186	02-2	TH02	804-1	SW-FF-CPTU	27.07.2014	13:22	63	26,696	10	23,783	33,5	0,5	33	36	0,53	
GeoB186	03	TH03	804-1	SW-FF-CPTU	27.07.2014	13:56	63	26,865	10	24,879	25,8	0,5	26	29	0,41-0,6	1990 Landslide
GeoB186	04	TH04	805-1	SW-FF-CPTU	27.07.2014	14:44	63	27,140	10	24,816	53,7	0,5	51	57	2,5	1990 Landslide
GeoB186	05-1	TH05	806-1	SW-FF-CPTU	27.07.2014	15:34	63	26,152	10	23,042	30,4	0,5	31	40	0,56	Intact ridge of the 1888 landslide
GeoB186	05-2	TH05	806-1	SW-FF-CPTU	27.07.2014	15:41	63	26,153	10	23,037	30,8	0,5	31	37	0,32	Intact ridge of the 1888 landslide
GeoB186	06	TH04	807-1	DW-FF-CPTU	27.07.2014	17:47	63	27,137	10	24,811	50,3	0,5	54	59	3,5	1990 Landslide
GeoB186	07	TH Survey	807-2	Multibeam Start	27.07.2014	19:24	63	26,510	10	21,740	122					
GeoB186	07	TH Survey	807-2	Multibeam End	27.07.2014	23:21	63	27,820	10	26,680	47					
GeoB186	08	TH01	808-1	GOST CPTU	28.07.2014	11:13	63	26,461	10	22,402	70,1		210 (70)	216 (72)	18,7	Stable portion behind the scar of the Western Slide, close to the Calypso core GS08 (L'Heureux et al. 2010), Data cable broken, 2nd Test successful
GeoB186	09	TH04	809/1	GOST CPTU	28.07.2014	15:07	63	27,149	10	24,781	52,9		164 (55)	169 (56)	10	1990 Landslide
GeoB186	10	TH03	810/1	GOST CPTU	29.07.2014	11:40	63	27,008	10	24,811	48		141 (47)	143 (48)	18,5	1990 Landslide
GeoB186	11	TH06	812/1	GOST CPTU	29.07.2014		63	27,130	10	22,46	65,8		187 (62)	190 (63)	18,6	Western Slope of Munkholmen
GeoB186	12-1	TH Survey	813/2	Multibeam Start	29.07.2014	19:22	63	21,690	10	21,690	68					
GeoB186	12-1	TH Survey	813/2	Multibeam End	30.07.2014	02:23	63	22,750	10	22,750	78,3					
GeoB186	12-2	TH Survey	814/1	Multibeam Start	30.07.2014	02:50	63	27,900	10	21,460	73,9					
GeoB186	12-2	TH Survey	814/1	Multibeam End	30.07.2014	05:40	63	27,840	10	21,360	96,6					
GeoB186	13	TH03	815/1	DW-FF-CPT	30.07.2014	06:50	63	27,008	10	24,835	43	0,5	43	45		1990 Landslide
GeoB186	14	TH06	816/1	DW-FF-CPT	30.07.2014	07:57	63	27,122	10	22,479	62	0,5	63	65		Western slope of Munkholmen

GeoB N°		Study Area	Ship's station N°	Gear	Date	Time UTC	Lat °	Lat min dezimal	Lon°	Lon min dezimal	Water Depth [m]	Winch Speed [m/s]	BOKO [m]	Maximum Winch Length at BOKO [m]	Core Length / Penetration Depth [m]	Comment
GeoB186	15-1	TH01	817/1	SW-FF-CPT / CPT winch	30.07.2014	09:24	63	26,466	10	22,401	70,1	0,5;1;2;3;4;5;6			0,9 - 3,7	Rate-dependent FF-CPT-Test in the intact portion behind the scar of the W' Slide, close to Calypso Core GS08 and FF-CPTU 8, FF-CPTU 9, FF-CPTU 10 for reference (Steiner et al., 2013)
GeoB186	16	TH01	817/2	Gravity Core	30.07.2014	11:42	63	26,465	10	22,426	69	0,8	72	69	5	Stable portion behind the scar of the Western Slide, close to the Calypso core GS08 (L'Heureux et al. 2010)
GeoB186	17	TH06	818/1	Gravity Core	30.07.2014	12:39	63	27,117	10	22,474	67	0,8	65	67	4,96	Western slope of Munkholmen
GeoB186	18	TH04	819/1	Gravity Core	30.07.2014	13:27	63	27,151	10	24,821	55	0,8	55	60	1,49	1990 Slide, Banana
GeoB186	19	TH03	820/1	Gravity Core	30.07.2014	14:57	63	27,011	10	24,820	44,7	0,8	42	45	2,34	1990 Slide
GeoB186	20	OF Survey	821/1-822/1	Multibeam Start	30.07.2014	14:57	63	27,011	10	24,820	41,5					
GeoB186	20	OF Survey	821/1-822/1	Multibeam End	31.07.2014	02:30	63	22,753	9	58,162	423					
GeoB186	21	OF03	823/1	Gravity Core	31.07.2014	06:18	63	19,547	9	53,082	62,9	1	59	63	5,37	1930 Slide, area of the initial failure, characterisation of deeper strata
GeoB186	22	OF01	824/1	Gravity Core	31.07.2014	07:04	63	19,496	9	52,651	67,7	1	63	67	4,52	1930 Slide, "Stable Nose" along the headwall of the retrogressive failure
GeoB186	23-1	OF02	825/1	Gravity Core	31.07.2014	07:38	63	19,323	9	52,330	38	1	35	40	4,46	1930 Slide above the escarpement
GeoB186	23-2	OF02	825/2	Gravity Core	31.07.2014	08:04	63	19,318	9	52,339	36,4	1	35	36,4	4,6	1930 Slide above the escarpement, geotechnical core (not opened)
GeoB186	24-1	OF02	826/1	GOST CPTU	31.07.2014	11:20	63	19,310	9	52,270	43,2		135 (45)	137 (46)	18,9	1930 Slide above the escarpement
GeoB186	24-2	OF02	826/2	GOST CPTU vibro mode	31.07.2014	12:45	63	19,321	9	52,271	41,8		129 (43)	132 (44)	18,9	1930 Slide above the escarpement
GeoB186	25	OF03	827/1	GOST CPTU	31.07.2014	14:53	63	19,543	9	53,041	68		202 (67)	205 (68)	18,3	1930 Slide, area of the initial failure, characterisation of deeper strata
GeoB186	26	OF Survey	828/1	Multibeam Start	31.07.2014	17:20	63	19,202	9	51,480	150					
GeoB186	26	OF Survey	828/1	Multibeam End	31.07.2014	21:30	63	23,050	9	59,450	350					
GeoB186	27-1	OF01	829/1	GOST CPTU	01.08.2014	07:20	63	19,491	9	52,647	63,4		201 (67)	204 (68)	18,9	1930 Slide, "Stable Nose" along the headwall of the retrogressive failure
GeoB186	27-2	OF01	829/2	SW-FF-CPTU	01.08.2014	10:17	63	19,504	9	52,636	64,7	0,5	63	65		1930 Slide, "Stable Nose" along the headwall of the retrogressive failure
GeoB186	28	OF03	830/1	SW-FF-CPTU	01.08.2014	10:46	63	19,547	9	53,084	63,8	0,5	64	66	1,3	1930 Slide, "Stable Nose" along the headwall of the retrogressive failure
GeoB186	29	OF02	831/1	SW-FF-CPTU	01.08.2014	11:08	63	19,325	9	52,298	42,4	0,5	40	42,4	0,9	1930 Slide above the escarpement

GeoB N°		Study Area	Ship's station N°	Gear	Date	Time UTC	Lat °	Lat min dezimal	Lon°	Lon min dezimal	Water Depth [m]	Winch Speed [m/s]	BOKO [m]	Maximum Winch Length at BOKO [m]	Core Length / Penetration Depth [m]	Comment
GeoB186	30	T	833/1	Gravity Core	01.08.2014	13:17	63	28,630	9	11,630	503,2	1	513	517	3,7	Gravity Core taken for NGU
GeoB186	31	T	834/1	Gravity Core	01.08.2014	16:48	63	42,610	9	51,720	223,5	1	223	229	4,44	Gravity Core taken for NGU
GeoB186	32	TF	835/1	Gravity Core	01.08.2014	17:34	63	42,480	9	51,280	221,5	1	224	230	4,37	Gravity Core taken for NGU
Transit to the Vesteralen					02.08.2014											
Transit to the Vesteralen					03.08.2014											
GeoB186	33	VS03	836/1	GOST CPTU	04.08.2014	06:11	69	22,355	15	11,351	494		1524 (508)	1531 (510)	9,8	Intact sediment beside SL3, reference site
GeoB186	34	VS04	837/1	GOST CPTU	04.08.2014	11:08	69	23,291	15	13,473	539		1654 (551)	1665 (555)	7,8	Headscar of SL3
GeoB186	35	VS05	838/1	GOST CPTU	04.08.2014	12:42	69	23,582	15	12,863	560		1713 (571)	1724 (575)	18,9	Deposits of SL3
GeoB186	36	VS	839/1	DW-FF-CPTU	04.08.2014	17:27	69	23,408	15	11,970	560	0,5	560	564	2	
GeoB186	37	VS Survey	840/1	Multibeam Start	04.08.2014	19:42	69	24,140	15	13,790	576					
GeoB186	37	VS Survey	840/1	Multibeam End	05.08.2014	05:36	69	21,520	15	5,760	542					
GeoB186	38	VS02	841/1	GOST CPTU	05.08.2014	08:04	69	22,833	15	10,238	546,5		1680 (560)	1702 (567)	19,5	Intact sediment beside SL3, reference site
GeoB186	39	VS01	842/1	GOST CPTU	05.08.2014	10:46	69	23,411	15	9,516	586		1795 (598)	1818 (606)	19,5	Intact sediment beside SL3, reference site
GeoB186	40	VS06	843/1	GOST CPTU	05.08.2014	14:50	69	28,878	15	12,503	575		1763 (588)	1784 (595)	19,6	Distal deposits of SL3, TOPAS13, line 3
GeoB186	41	VS	844/1	DW-FF-CPTU	06.08.2014	14:28	69	24,618	15	18,496	570	0,5	573	578	2,11	Small-scale failure feature
GeoB186	42	VS	845/1	DW-FF-CPTU	06.08.2014	16:01	69	25,470	15	18,966	611	0,5	610	615	1,32	Small-scale failure feature
GeoB186	43	VS	846/1	DW-FF-CPTU	06.08.2014	17:41	69	25,325	15	12,301	646	0,5	643	648	2,54	Reference site beneath the "crack" feature
GeoB186	44	VS Survey	847/1	Multibeam Start	06.08.2014	18:56	69	22,430	15	16,460	365					
GeoB186	44	VS Survey	847/1	Multibeam End	07.08.2014	03:33	69	22,700	15	17,923	361					
GeoB186	45	VS	848	Gravity Core	07.08.2014	06:22	69	24,130	15	8,324	629	1	639	642	4,53	"Crack" feature
GeoB186	46	VS	849	Gravity Core	07.08.2014	07:30	69	25,309	15	12,317	644	1	653	658	5,39	Reference site beneath the crack feature
GeoB186	47	VS	850/1	Gravity Core	07.08.2014	08:49	69	25,464	15	18,988	612	1	618	623	4,38	Small-scale failure feature
GeoB186	48	VS05	851/1	Gravity Core	07.08.2014	10:10	69	23,603	15	12,999	560	1	566	571	3,89	Deposits of SL3

GeoB N°		Study Area	Ship's station N°	Gear	Date	Time UTC	Lat °	Lat min dezimal	Lon°	Lon min dezimal	Water Depth [m]	Winch Speed [m/s]	BOKO [m]	Maximum Winch Length at BOKO [m]	Core Length / Penetration Depth [m]	Comment
GeoB186	49	VS03	852/1	Gravity Core	07.08.2014	11:15	69	22,360	15	11,430	493	1	503	508	5,12	Intact sediments beside SL3, reference site, Incident with GOST
GeoB186	50	VS	853/2	DW-FF-CPTU	07.08.2014	14:24	69	25,786	15	10,790	690	0,5	688	692	3,5	Morphological steps,
GeoB186	51	VS	854/1	SW-FF-CPTU with FF-CPTU-Winch	07.08.2014	16:17	6	21,165	15	26,175	175	0,5				CPT-Winch test below the shelf break
GeoB186	52	VS Survey	855/1	Multibeam Start	07.08.2014	18:09	69	22,470	15	22,210	269					
GeoB186	52	VS Survey	855/1	Multibeam End	07.08.2014	20:26	69	21,510	15	5,130	555					
GeoB186	53	LS	856/1	DW-FF-CPTU	08.08.2014	14:56	68	5,460	9	54,725	1120	0,5	1125	1128	4,09	"Creep Lobe"
GeoB186	54	LS	857/1	DW-FF-CPTU	08.08.2014	16:15	68	5,580	9	54,246	1149	0,5	1140	1146	3,33	"Creep Lobe"
GeoB186	55	LS	858/1	DW-FF-CPTU	08.08.2014	17:41	68	5,639	9	53,901	1165,6	0,5	1152	1158	3,07	"Creep Lobe"
GeoB186	56	LS	859/1	DW-FF-CPTU	08.08.2014	18:41	68	5,819	9	53,124	1127	0,5	1180	1185	4,38	"Creep Lobe"
GeoB186	57	LS Survey	860/1	Multibeam Start	08.08.2014	20:14	68	0,570	9	52,800	1230					
GeoB186	57	LS Survey	860/1	Multibeam End	08.08.2014	23:43	68	5,000	9	54,100	1260					
GeoB186	58	LS	861/1	DW-FF-CPTU	09.08.2014	00:20	68	5,107	9	53,990	1140	0,5	1130	1133	2,9	"Creep Lobe"
GeoB186	59	LS	862/1	DW-FF-CPTU	09.08.2014	01:04	68	5,158	9	53,849	1147	0,5	1139	1144	2,9	"Creep Lobe"
GeoB186	60	LS	863/1	DW-FF-CPTU	09.08.2014	01:42	68	5,222	9	53,461	1167	0,5			3,44	"Creep Lobe", Test failed, electronical problems
GeoB186	61-1	LS	863/1	Gravity Core	09.08.2014	06:40	68	5,588	9	54,249	1150	1	1155	1161	5,01	"Creep Lobe"
GeoB186	61-2	LS	863/2	Gravity Core	09.08.2014	07:57	68	5,582	9	54,245	1150	1	1155	1161		"Creep Lobe" - Geotechnical Core (not opened)
GeoB186	62-1	LS	864/1	Gravity Core	09.08.2014	09:14	68	5,820	9	53,141	1197	1	1197	1205		"Creep Lobe" - Geotechnical Core (not opened)
GeoB186	62-2	LS	864/2	Gravity Core	09.08.2014	10:40	68	5,820	9	53,141	1197	1	1199	1206	3,77	"Creep Lobe"
GeoB186	63	LS	865/1	Gravity Core	09.08.2014	12:43	67	57,259	9	54,878	837	1	847	853	4,56	"Crack" feature
GeoB186	64	LS	866/1	Gravity Core	09.08.2014	13:42	67	55,488	9	55,767	760	1	774	780	5,02	"Crack" feature
GeoB186	65	LS	867/1	Gravity Core	09.08.2014	14:59	67	52,677	9	57,154	645	1	654	660	4,4	Reference Site along the stable portion of the slope
GeoB186	66	LS	868/1	Gravity Core	09.08.2014	17:02	67	55,453	9	31,373	1319	1	1334	1342	5,42	Reference Site along the stable portion of the slope
GeoB186	67	LS Survey	869/1	Multibeam Start	09.08.2014	18:04	67	55,630	9	30,520	1340					
GeoB186	67	LS Survey	869/1	Multibeam End	10.08.2014	03:41	68	56,170	9	56,170	1340					
GeoB186	68	LS	870/1	DW-FF-CPTU	10.08.2014	04:56	68	5,219	9	53,473	1160	0,5	1151	1159	3,57	"Creep Lobe"
GeoB186	69	LS	871/1	DW-FF-CPTU	10.08.2014	06:19	68	4,909	9	52,910	987,5	0,5	1152	1158	4,11	

GeoB N°		Study Area	Ship's station N°	Gear	Date	Time UTC	Lat °	Lat min dezimal	Lon°	Lon min dezimal	Water Depth [m]	Winch Speed [m/s]	BOKO [m]	Maximum Winch Length at BOKO [m]	Core Length / Penetration Depth [m]	Comment
GeoB186	70	LS	872/1	DW-FF-CPTU	10.08.2014	07:25	68	5,105	9	52,203	1188		1179	1184	3,56	Reference site to "Creep Lobe"
GeoB186	71	LS	873/1	DW-FF-CPTU	10.08.2014	10:10	67	55,124	10	3,166	600	0,5	599	604	3,61	In the stable portion of the slope beside a small-scale failure feature
GeoB186	72	LS	874/1	DW-FF-CPTU	10.08.2014	11:33	67	57,250	9	54,810	838	0,5	838	844	3,07	Reference site to "Crack" Feature
GeoB186	73	LS	875/1	DW-FF-CPTU	10.08.2014	12:39	67	55,500	9	55,830	761		762	767	3,73	
GeoB186	74	LS	876/1	DW-FF-CPTU	10.08.2014	13:53	67	58,010	9	49,310	1040	0,5	1040	1045	3,14	Behind the escarpment of the large failure
GeoB186	75	VS	877/1	DW-FF-CPTU	11.08.2014	08:12	69	24,140	15	8,320	628		628	644	5,4	"Crack" Feature
GeoB186	76	VS	878/1	DW-FF-CPTU	11.08.2014	09:16	69	24,940	15	7,160	688	0,5	688	708	3,78	Behind the escarpement of the small-scale failure feature
GeoB186	77	VS	879/1	DW-FF-CPTU	11.08.2014	10:39	69	26,430	15	14,560	687	0,5	688	697	3,17	Superficial Deformation Feature
GeoB186	78	VS	880/1	DW-FF-CPTU	11.08.2014	11:34	69	26,930	15	13,680	744	0,5	744	750	2,26	Superficial Deformation Feature
GeoB186	79	VS	881/1	DW-FF-CPTU	11.08.2014	12:48	69	26,170	15	10,710	731	0,5	731	739	2,15	Superficial Deformation Feature
GeoB186	80	VS	882/1	DW-FF-CPTU	11.08.2014	13:54	69	27,270	15	12,340	807	0,5	807	814	7,24	Failed portion of a small-scale feature
GeoB186	81	VS Survey	883/1	Multibeam Start	11.08.2014	15:25	69	28,840	15	11,680	1068					
GeoB186	81	VS Survey	883/1	Multibeam End	11.08.2014	17:25	69	27,240	15	27,280	721					
Transit to Tromsö (Port of Destination)					12.08.2014											

List of abbreviations:

TH	Trondheim Harbour
OF	Orkdalsfjorden
TF	Trondheimfjorden
VS	Vesterålen Slope
LS	Lofoten Slope
DW-FF-CPTU	Deep water free-fall cone penetration testing unit
SW-FF-CPTU	Shallow water free-fall cone penetration testing unit
GOST CPTU	Geotechnical Offshore Seabed Tool cone penetration testing unit

9 Acknowledgements

We thank Master Matthias Günther and his officers on the bridge for his expert manoeuvring in the study area, his cooperation, and outstanding support during complex operations.

Special thanks go to the entire crew of R/V *POSEIDON* for their friendly support and patience and virtuous technical assistance with the various devices used.

Colleagues at MARUM Bremen (Goetz Ruhland, Volker Diekamp) as well as at GEOMAR (Klas Lackschewitz) have also provided crucial help with expedition planning, logistical decisions, and post-cruise demobilisation.

Klaus Bohn is thanked for his outstanding professional logistical assistance.

We acknowledge the funding of the German Science Foundation (DFG) to realise the *POS472* cruise within the frame of MARUM research area SD (Seafloor Dynamics, project SD3).

The planning and preparation to realise this expedition benefits from stimulating and trustful exchanges with our Norwegian colleagues. THANKS TO THE NORTH – we appreciate your enthusiasm and co-operation!

10 References

Becker, J.J., Sandwell, D.T., Smith, W.H.F., Braud, J., Binder, B., Depner, J., Fabre, D., Factor, J., Ingalls, S., Kim, S.H., Ladner, R., Marks, K., Nelson, S., Pharaoh, A., Trimmer, R., Von Rosenberg, J., Wallace, G., Weatherall, P., 2009. Global Bathymetry and Elevation Data at 30 Arc Seconds Resolution: SRTM30_PLUS. Marine Geodesy 32, 355-371, doi: 10.1080/01490410903297766.

Baeten, N. J., Laberg, J. S., Forwick, M., Vorren, T. O., Vanneste, M., Forsberg, C. F. & Ivanov, M., 2013. Morphology and origin of smaller-scale mass movements on the continental slope off northern Norway. Geomorphology *187*, 122-134.

Best, A.I., Clayton, C.R.I., Longva, O., Szuman, M., 2003. The role of free gas in the activation of submarine slides in Finneidfjord. In, Locat, J. and Mienert, J. (eds.) Submarine mass movements and their consequences: 1st International Symposium. 1st International Symposium on Submarine Mass Movements and their Consequences Dordrecht, Netherlands, Kluwer Academic, 491-498.

Bjerrum, L., 1967. Progressive failure in slopes of overconsolidated plastic clay and clay shales. Journal of the Soil Mechanics and Foundation Division of the American Society of Civil Engineers 93, 1-49.

Bjerrum, L., 1971. Subaqueous slope failures in Norwegian fjords. Norwegian Geotechnical Institute, Publ. 88.

Boulanger R.W., Idriss I.M., 2006. Liquefaction susceptibility criteria for silts and clays. Journal of Geotechechnics and Geoenvironmental Engineering 132, 11, 1413-1426.

Boulanger R.W., Idriss I.M., 2007. Evaluation of cyclic softening in silts and clays. Journal of Geotechnical and Geoenvironmental Engineering 133, 6, 641-652.

Bryn, P., Berg, K., Forsberg, C. F., Solheim, A., & Kvalstad, T. J., 2005. Explaining the Storegga slide. Marine and Petroleum Geology 22,1, 11-19.

Caress, D.W., Chayes, D.N., 1996. Improved processing of Hydrosweep DS multibeam data on the R/V Maurice Ewing. Marine Geophysical Researches 18, 631-650.

Corner, G.D., 2006. A transgressive-regressive model of fjord-valley fill: Stratigraphy, facies and depositional controls. In Dalrymple, R.W., Leckie, D.A. & Tillman, R.W. (eds.): Incised Valleys in Time and Space. Society of Sedimentary Geology (SEPM), Special Publication 85, 161-178.

Dayal, U., Allen, J.H., 1975. The effect of penetration rate on the strength of remolded clay and sand samples. *Canadian Geotechnical. Journal* 12, 336–348.

Emdal, A., Janbu, N., Sand, K., 1996. The shoreline slide at Lade. In: Senneset, K. (ed.): Landslides. Proceedings of the 7th International symposium on Landslides,Trondheim, Norway, vol. 1, 533-538.

Hampton, M.A., Lee, H.J. & Locat, J., 1996. Submarine landslides. Review of Geophysics 34, 33–59.

Jorat, M.E., Kreiter, S., Mörz, T., Moon, V., de Lange, W., 2014. Utilizing cone penetration tests for landslide evaluation. In: Krastel S et al (eds) Submarine Mass Movements and Their Consequences. Springer, Heidelberg, 55-71.

Laberg, J.S., Vorren, T.O., 2000. The Trænadjupet Slide, offshore Norway—morphology, evacuation and triggering mechanisms. Marine Geology *171*, 1, 95-114.

Laberg, J.S., Vorren, T.O., 2004. Weichselian and Holocene Growth of the northern high-latitude Lofoten Contourite Drift on the continental slope of Norway. Sedimentary Geology 164 (1-2), 1-17.

Laberg, J.S. et al., 2005. Cenozoic alongslope processes and sedimentation on the NW European Atl. Margin. Marine Petroleum Geology 22 (9-10), 1069-1088.

Laberg, J.S., Guidard, S., Mienert, J., Vorren, T.O. Haflidasson, H., Nygard, A., 2007. Morphology and morphogenesis of a high-latitude canyon; the Andoya Canyon, Norwegian Sea. Marine Geology 246 (2-4), 68-85.

Laberg, J. S., et al., 2006. Frequency and triggering mechanisms of submarine landslides of the North Norwegian continental margin. Norwegian Geological Journal 86. 155 -161.

Lee, H.J., 2009. Timing of occurrence of large submarine landslides on the Atlantic Ocean margin. Marine Geology 264, 53-64.

Kluger, M.O, Kreiter, S, L'Heureux, J.S, Stegmann, S., Moon, V. and Mörz, T., 2016 In Situ Cyclic Softening of Marine Silts by Vibratory CPTU at Orkdalsfjord Test Site, Mid Norway. In: Lamarche, G, Mountjoy, J, Bull, S, Hubble, T, Krastel, S, Lane, E, Micallef, A, Moscardelli, L, Mueller, C, Pecher, I and Woelz, S (eds.) Submarine Mass Movements and their Consequences. Advances in Natural and Technological Hazards Research, 41. Springer International Publishing, 201-209. doi:10.1007/978-3-319-20979-1_20

Lecomte, I., et al., 2008. Submarine Slides at Finneidfjord (Norway): Geophysical Investigations. Symposium on the Application of Geophysics to Engineering and Environmental Problems 21 (1) 376.

Leroueil, S., 2001. Natural slopes and cuts: movement and failure mechanisms. Geotechnique 51, 197-243.

Locat, J., 2001. Instabilities along ocean margins: a geomorphological and geotechnical perspective. Marine and Petroleum Geology 18 (4), 503-512.

Locat, J., Lee, H. J., 2002. Submarine landslides: Advances and challenges. Canadian Geotechnical Journal 39, 193.

Longva, O., Janbu, N., Blikra, L.H. & Boe, R, 2003. The 1996 Finneidfjord slide: seafloor failure and slide dynamics. In: Locat, J. & Mienert, J. (eds.): Submarine Mass Movements and Their Consequences, 531-538. Dordrecht, Netherlands: Kluwer academic Publishers.

Lunne, T., Robertson, P.K., Powell, J.J.M., 1997: Cone Penetration Testing in Geotechnical Practice; Spon Press (Taylor and Francis Group), pp. 312.

L'Heureux, J.-S., Longva, O., Hansen, L., Vingerhagen, G., 2007. The 1990 submarine slide outside the Nidelva River mouth, Trondheim, Norway. In V. Lykousis, D. Sakellariou & J. Locat, (eds.): Submarine Mass Movements and Their Consequences, Kluwer Series on Advances in Natural and Technological Hazards Research, vol. 27, 259-267.

L'Heureux, J.-S., Hansen, L. & Longva, O. 2009: Development of the submarine channel at the mouth of the Nidelva River, Trondheimsfjorden, Norway, Marine Geology 260, 30-44. doi:10.1016/j.margeo.2009.01.005

L'Heureux, J. S., Hansen. L., Longva, O., Emdal, A., Grande, L.O., 2010. A multidisciplinary study of submarine landslides at the Nidelva fjord delta, Central Norway, - Implications for the assessment of geohazards. Norwegian Journal of Geology, Vol 90, pp. 1-20. Trondheim 2010, ISSN 029-196X.

L'Heureux, J.-S., Glimsdal, S., Longva, O., Hansen, L. & C. B. Harbitz. 2011. The 1888 shoreline landslide and tsunami in Trondheimsfjorden, central Norway. Marine Geophysical Research, 32:313–329, DOI 10.1007/s11001-010-9103-z.

L'Heureux, J.-S., Longva, O., Steiner, A., Hansen, L., Vardy, Mark E., Vanneste, M., Haflidason, H., Brendryen, J., Kvalstad, T.J., Forsberg, C.F., Chand, S. & A., Kopf, 2012. Identification of Weak Layers and Their Role for the Stability of Slopes at Finneidfjord, Northern Norway. In: Submarine Mass Movements and Their Consequences. Y. Yamada, Kawamura, K., Ikehara, K., Ogawa, Y., Urgeles, R., Mosher, D., Chaytor, J. and Strasser, M. Heidelberg, Springer: 321-330.

L'Heureux, J. S., Longva, O., Hansen, L., & Vanneste, M., 2014. The 1930 landslide in Orkdalsfjorden: morphology and failure mechanism. In Krastel, S., Behrmann, J.H.; Völker, D., Stipp, M., Berndt, C. Urgeles, R., Chaytor, J.,Huhn, K., Strasser, M. Submarine Mass Movements and Their Consequences, Springer International Publishing, 239-247, doi: 10.1007/978-3-319-00972-8_21..

Longva, O., Janbu, N., Blikra, L.H. & Boe, R., 2003: The 1996 Finneidfjord slide: seafloor failure and slide dynamics. In: Locat, J. & Mienert, J. (eds.): Submarine Mass Movements and Their Consequences, 531-538. Dordrecht, Netherlands: Kluwer academic Publishers.

Lunne, T., Robertson, P.K. & Powell, J.J.M. 1997: Cone Penetration Testing in Geotechnical Practice; Spon Press (Taylor and Francis Group), pp. 312.

Maltman, A. (Ed.), 1994. The Geological Deformation of Sediments. Chapman & Hall, London, pp. 363.

Maslin, M., Owen, M., Day, S., Long, D., 2004. Linking continental-slope failures and climate change: testing the clathrate gun hypothesis. Geology 32: 53–56.

Mienert, J. (ed), 2004. COSTA—continental slope stability: major aims and topics. Marine Geology, 217, 1-7.

Moore, C.J. & science party, 1995. Abnormal fluid pressures and fault-zone dilation in the Barbados accretionary prism: Evidence from logging while drilling. Geology, 23, 7, 605-608.

Owen, M., Day, S., & M. Maslin, 2007. Late Pleistocene submarine mass movements: occurrence and causes. Quaternary Science Reviews, 26, 958–978.

Petley, N.D., Higuchi, T., Petlet, D., Bulmer, H.M., Carey, J., 2005. Development of progressive landslide failure in cohesive materials. Geology 33: 201-204.

Pfender, M., H.W. Villinger, 2002. Miniaturized data logger for deep sea sediment temperature measurements, Marine. Geology 186: 557-570

Rise, L., et al. 2009. The Lofoten-Vesterålen continental margin, North Norway: Canyons and mass-movement activity. In: 1st international Conference. on seafloor mapping for geohazard assessment, Ischia.

Rise, L., Chand, S., Haflidason, H., L'Heureux, J. S., Hjelstuen, B. O., Bellec, V., & Bøe, R. (2012). Investigations of slides at the upper continental slope off Vesterålen, North Norway. In *Submarine mass movements and their consequences* (pp. 167-176). Springer Netherlands.

Rygg, N. & Oset, F. 1996: The Balsfjord landslide. In Senneset, K. (ed.): Landslides . Proceedings of the 7th International symposium on Landslides, Trondheim, Norway, vol. 1, 573-577

Sasaki Y, Itoh Y, Shimazu T (1984) A Study of the relationship between the results of vibratory cone penetration tests and earthquake induced settlement of embankments. Proceedings of the 19th Annual Meeting of JSSMFE.

Skaven-Haug, S. 1955: Undervannsskred i Trondheim havneomraade. Teknisk Ukeblad Vol. 102 (7) Norwegian Geotechnical Institute, Oslo, Norway,133-144.

Stegmann, S., Moerz, T., Kopf, A., 2006. Initial Results of a new Free Fall-Cone Penetrometer (FF-CPT) for geotechnical *in situ* characterisation of soft marine sediments. Norwegian Journal of Geology 86/3: 199-208.

Stegmann, S., Kopf, A. 2007. Marine deep-water Free-fall CPT measurements for landslide characterisation off Crete, Greece (Eastern Mediterranean Sea). Part 1: A new 4000m cone penetrometer. In: Lykousis, V, Sakellariou, D and Locat, J (eds.) Submarine Mass Movements and Their Consequences. 3 International Symposium. Advances in Natural and Technological Hazards Series, 27. Springer Netherlands, 171-177. doi:10.1007/978-1-4020-6512-5.

Stegmann, S, Kreiter, S, L'Heureux, JS, Vanneste, M, Völker, D, Baeten, NJ, Knudsen, S, Rise, L, Longva, O, Brendryen, J, Haflidason, H, Chand, S, Mörz, T and Kopf, AJ (2016) First Results of the Geotechnical In Situ Investigation for Soil Characterisation Along the Upper Slope Off Vesterålen: Northern Norway. In: Lamarche, G, Mountjoy, J, Bull, S, Hubble, T, Krastel, S, Lane, E, Micallef, A, Moscardelli, L, Mueller, C, Pecher, I and Woelz, S (eds.) Submarine Mass Movements and their Consequences. Advances in Natural and Technological Hazards Research, 41. Springer International Publishing, 211-219. doi:10.1007/978-3-319-20979-1_21

Steiner, A., Kopf, A. J., L'Heureux, J. S., Kreiter, S., Stegmann, S., Haflidason, H., & Moerz, T., 2013. In situ dynamic piezocone penetrometer tests in natural clayey soils—a reappraisal of strain-rate corrections. Canadian Geotechnical Journal 51(3), 272-288.

Sultan, N., Cochonat, P., Canals, M., Cattaneo, A., Dennielou, B., Haflidason, H., Laberg, J.S., Long, D., Mienert, J., Trincardi, F., Urgeles, R.,Vorrene, T.O.,Wilson, C., 2004. Triggering mechanisms of slope instability processes and sediment failures on continental margins: a geotechnical approach. Marine Geology, 213, 291–321.

Terzaghi, K., 1925. Erdbaumechanik auf bodenphysikalischer Grundlage, Franz Deuticke, Leipzig, Germany, pp. 399.

Tokimatsu K (1988) Penetration tests for dynamic problems. Proceedings of the ISOPT-1, 1, 117-136.Vanneste, M., L'Heureuc, J-S., Beaten, N., Brendryen, J., Vardy, M.E., Steiner, S., Forsberg, C.F., Kvalstad, T.J., Laberg, J.S., Chand, S., Longva, O., Rise, L., Haflidason, H., Hjulstuen, B.O., Forwick, M., Morgan, E., Lecomte, I., Kopf, A., Vorren, T.O., and Reichel, T., 2012. Shallow Landslides and Their Dynamicsin Coastal and Deepwater Environments. In: Yamada, Y. et al. (Eds.), Submarine Mass Movements and Their Consequences, Advances in Natural and Technological Hazards Research 32, Springer, doi: 10.1007/978-94-007-2162-3_3.

Wessel, P., Smith, W.H.F., 1998. New, improved version of the Generic Mapping Tools released. EOS Trans. AGU 79, 579.

Vardy, Mark E., et al. 2012. Multidisciplinary investigation of a shallow near-shore landslide, Finneidfjord, Norway. Near Surface Geophysics 10.4, 267-277.

Wentworth C.K., 1922. A scale of grade and class terms for clastic sediments. The Journal of Geology 30, 377-392

Wood, D. M., 1985. Some fall cone tests. Geotechnique 35.1.

Youd T.L., Idriss I.M., Andrus R.D. et al., 2001. Liquefaction resistance of soils: summary report from the 1996 NCEER and 1998 NCEER/NSF workshops on evaluation of liquefaction resistance of soils. Journal of Geotechnical and Geoenvironmental Engineering 127(10), 817-833.

11 Appendix

11.1 Core Logs

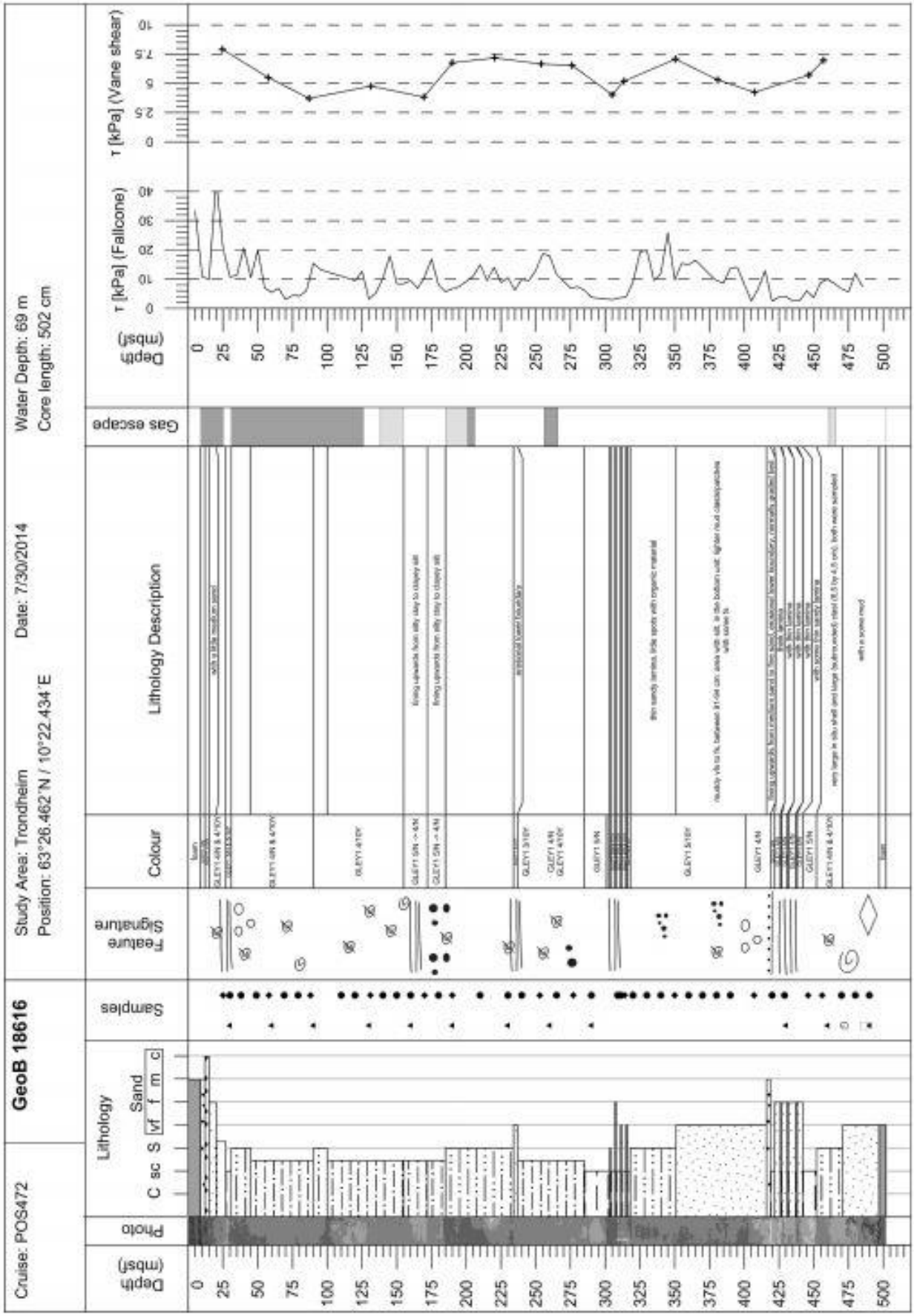
Cruise: POS472
GeoB 18616
Study Area: Trondheim
Position: 63°26.462'N / 10°22.434'E
Date: 7/30/2014
Water Depth: 69 m
Core length: 502 cm
Depth (mbsf)
Photo
Lithology
Sand
C sc S vf f m c
Samples
Feature Signature
Colour
Lithology Description
Gas escape
τ [kPa] (Falcone)
τ [kPa] (Vane shear)

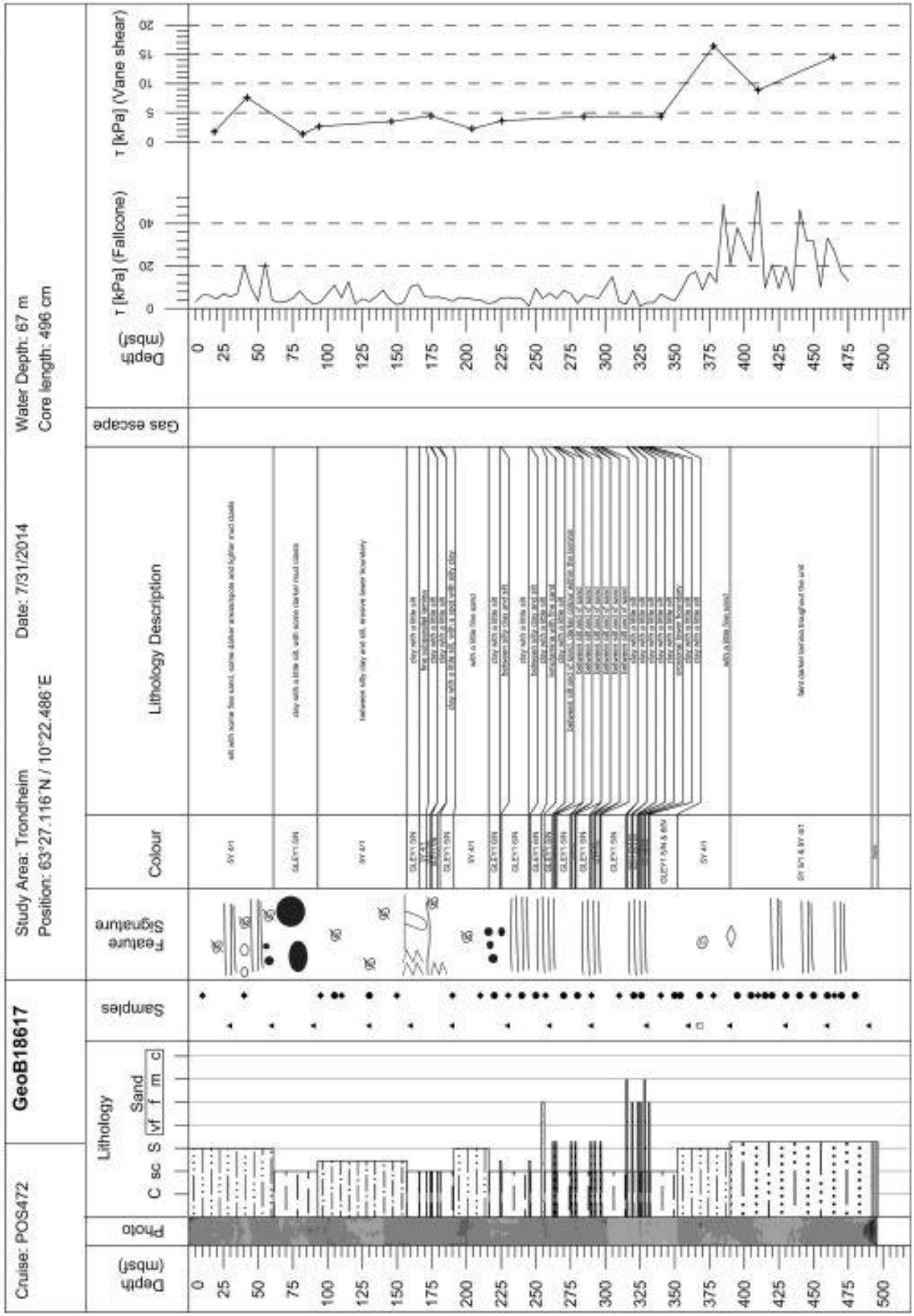
Cruise: POS472
GeoB18617
Study Area: Trondheim
Position: 63°27.116'N / 10°22.486'E
Date: 7/31/2014
Water Depth: 67 m
Core length: 496 cm
Depth (mbsf)
Photo
Lithology
C sc S
Sand
vf f m c
Samples
Feature Signature
Colour
Lithology Description
Gas escape
τ [kPa] (Fallcone)
τ [kPa] (Vane shear)

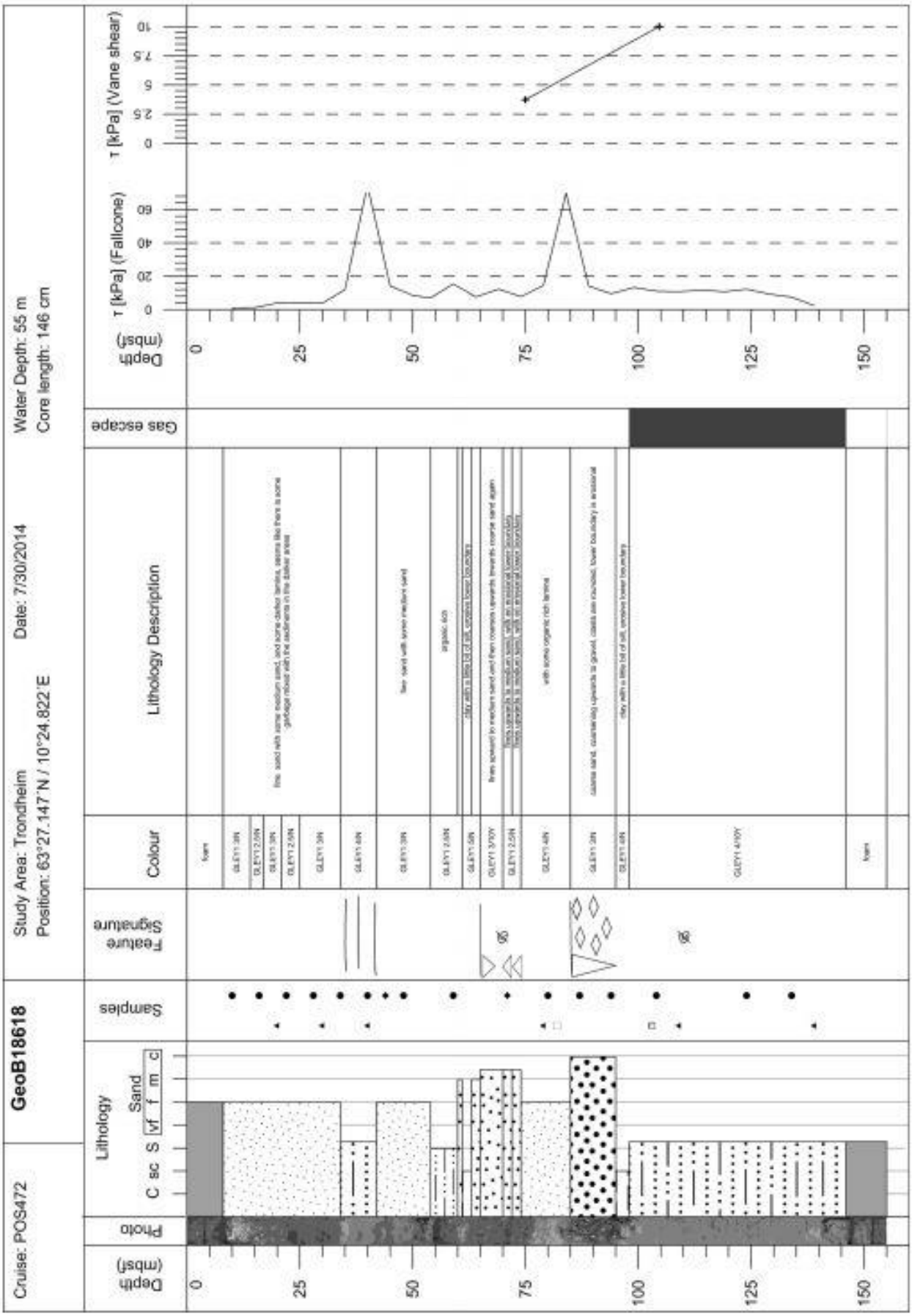
Cruise: POS472
GeoB18618
Study Area: Trondheim
Position: 63°27.147'N / 10°24.822'E
Date: 7/30/2014
Water Depth: 55 m
Core length: 146 cm
Depth (mbsf)
Photo
Lithology
Sand
C sc S vf f m c
Samples
Feature Signature
Colour
Lithology Description
Gas escape
τ [kPa] (Fallcone)
τ [kPa] (Vane shear)

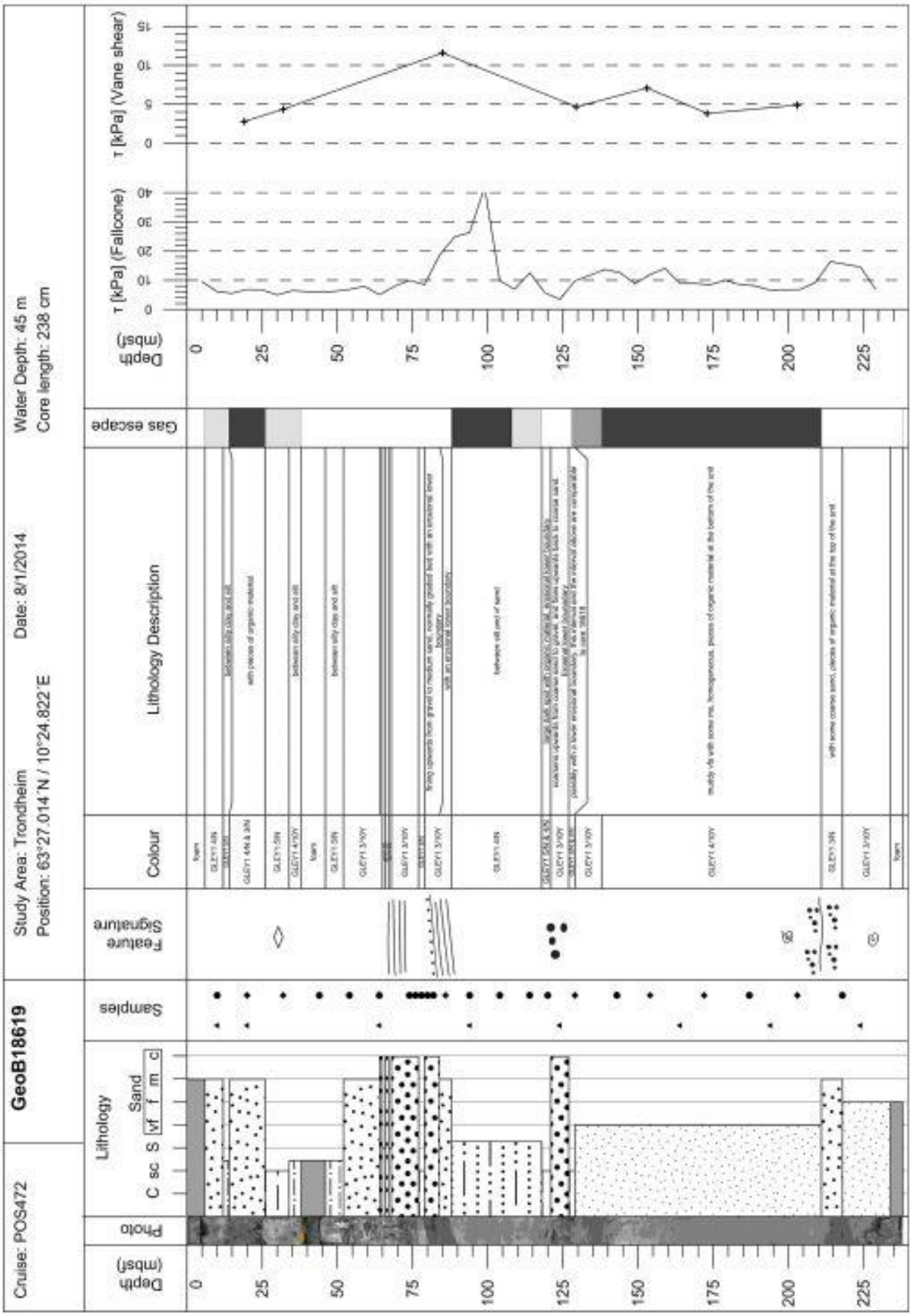
Cruise: POS472
GeoB18619
Study Area: Trondheim
Position: 63°27.014'N / 10°24.822'E
Date: 8/1/2014
Water Depth: 45 m
Core length: 238 cm
Depth (mbsf)
Photo
Lithology
C sc S
Sand
vf f m c
Samples
Feature Signature
Colour
Lithology Description
Gas escape
τ [kPa] (Falcone)
τ [kPa] (Vane shear)
0
25
50
75
100
125
150
175
200
225

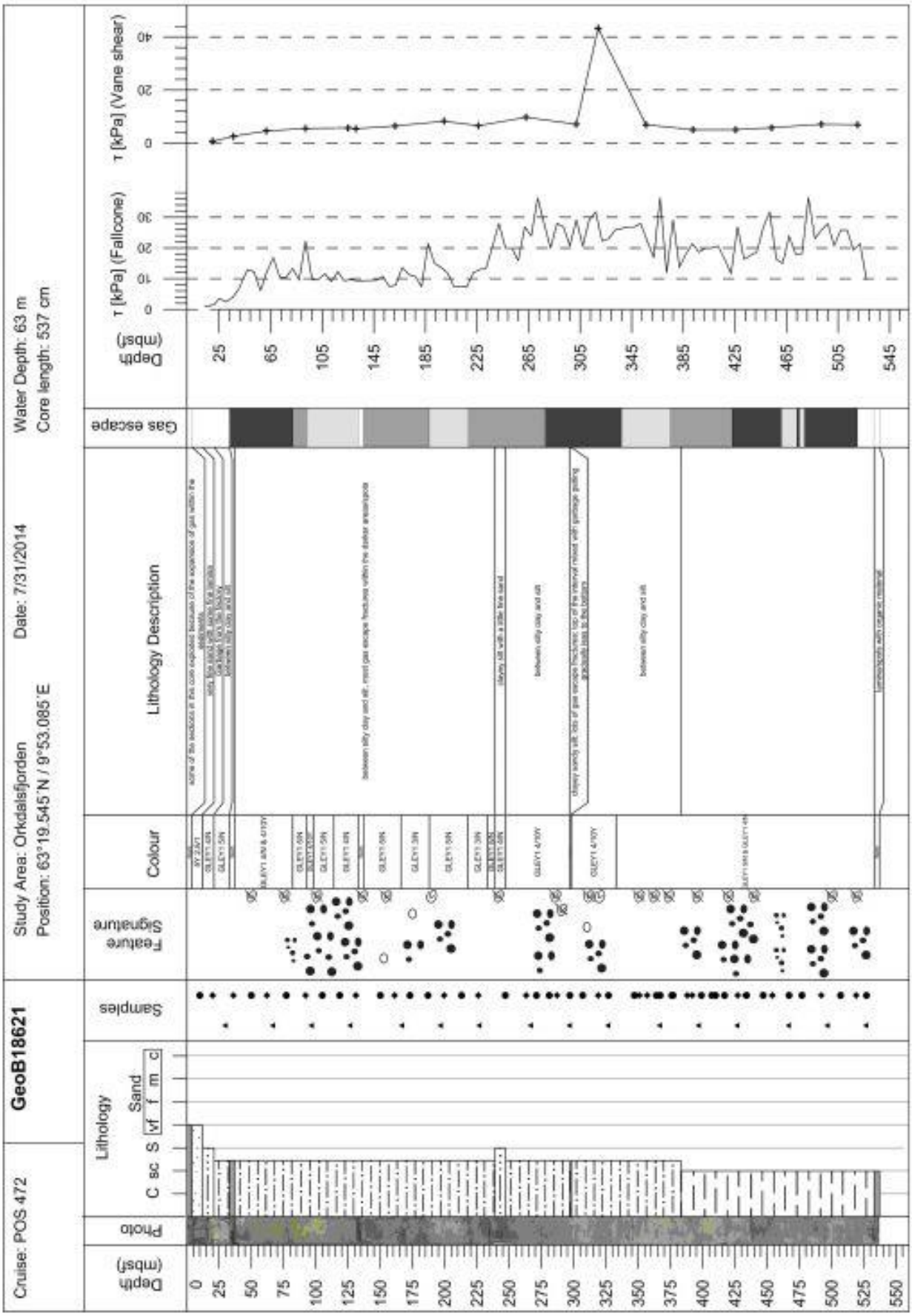
Cruise: POS 472
GeoB18621
Study Area: Orkdalsfjorden
Position: 63°19.545'N / 9°53.085'E
Date: 7/31/2014
Water Depth: 63 m
Core length: 537 cm
Depth (mbsf)
Photo
Lithology
C sc S Sand vf f m c
Samples
Feature Signature
Colour
Lithology Description
Gas escape
Depth (mbsf)
τ [kPa] (Fallcone)
τ [kPa] (Vane shear)

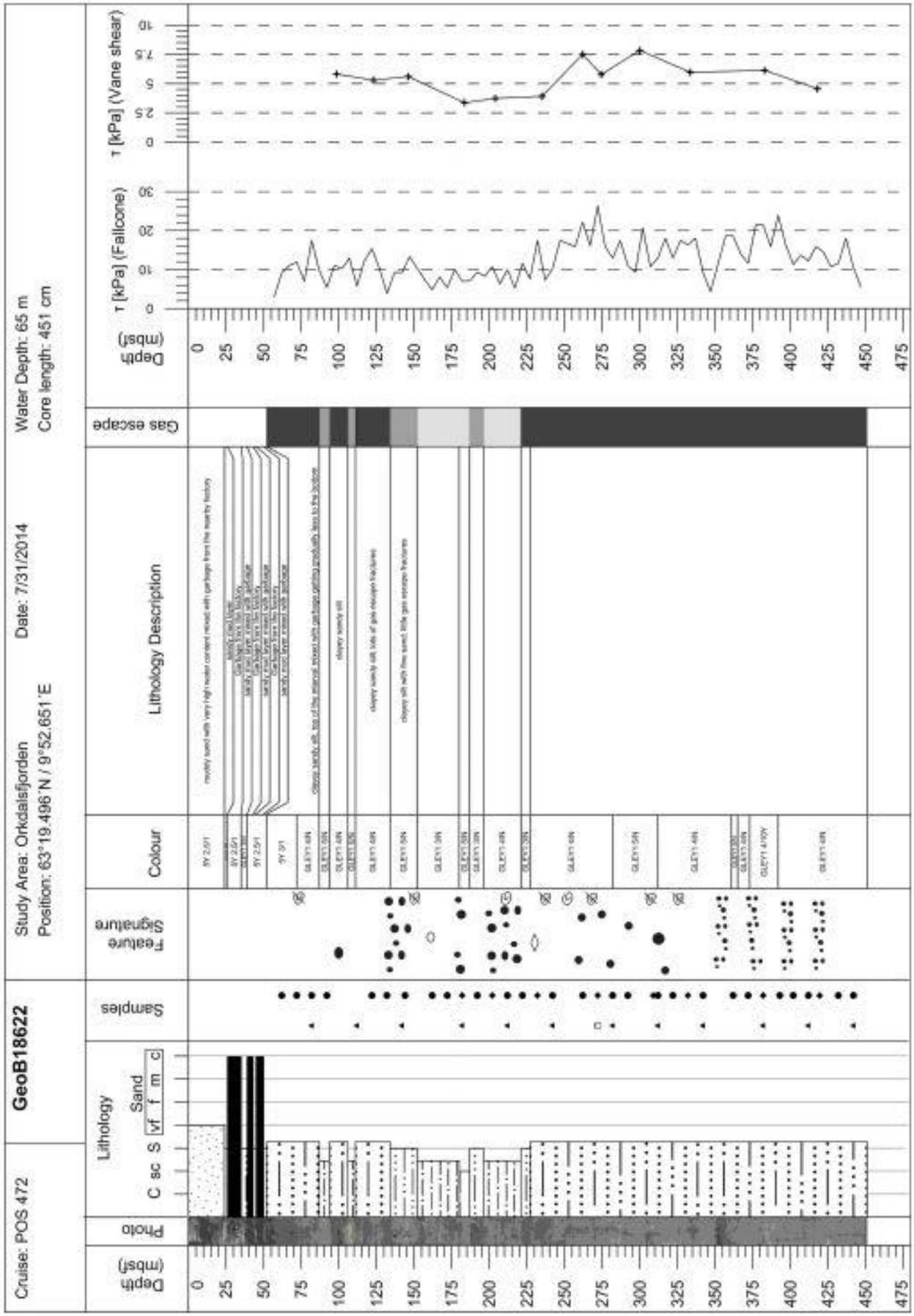
Cruise: POS 472
GeoB18622
Study Area: Orkdalsfjorden
Position: 63°19.496´N / 9°52.651´E
Date: 7/31/2014
Water Depth: 65 m
Core length: 451 cm
Depth (mbsf)
Photo
Lithology
Sand
C sc S vf f m c
Samples
Feature Signature
Colour
Lithology Description
Gas escape
τ [kPa] (Falllcone)
τ [kPa] (Vane shear)

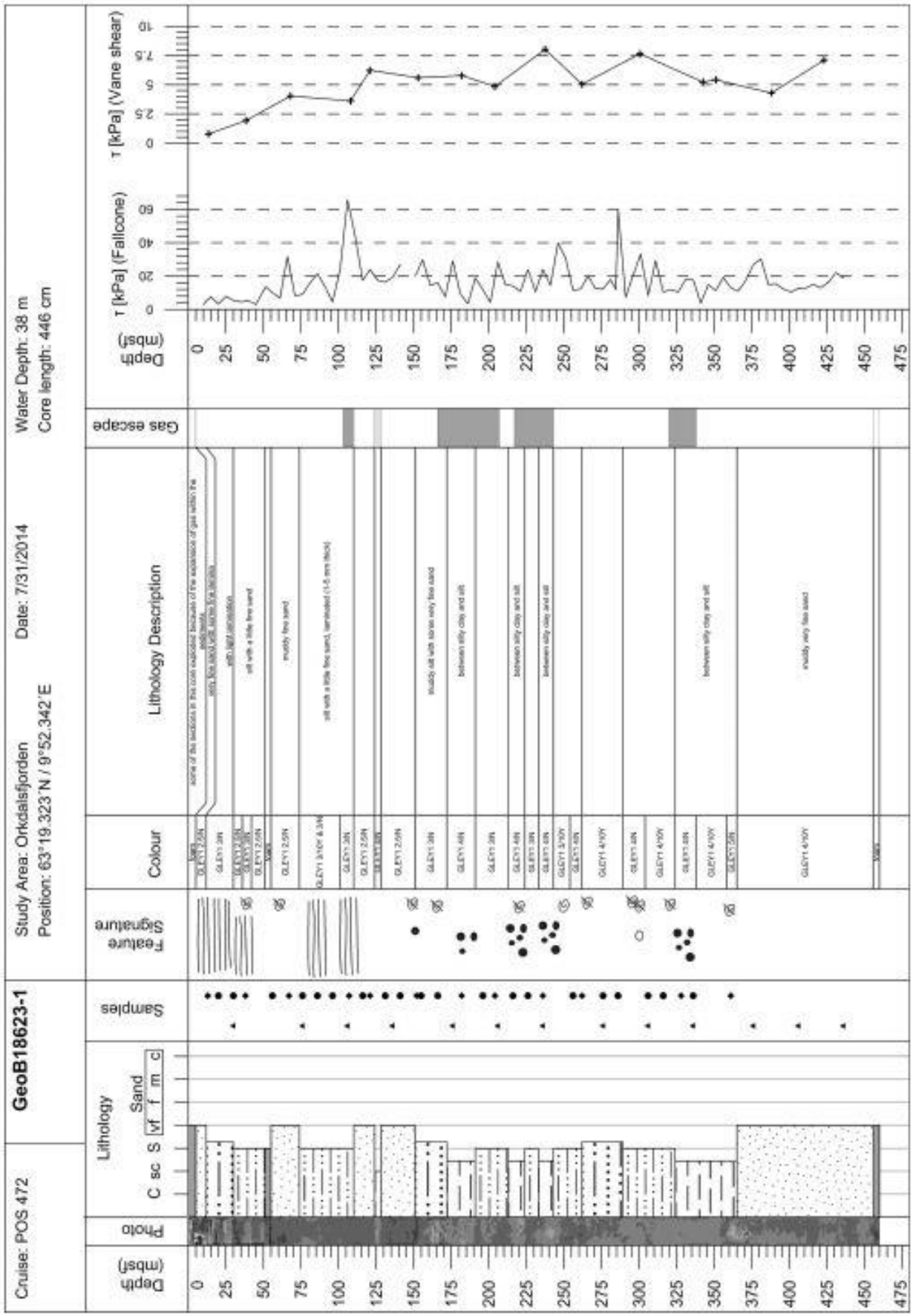
Cruise: POS 472
GeoB18623-1
Study Area: Orkdalsfjorden
Position: 63°19.323'N / 9°52.342'E
Date: 7/31/2014
Water Depth: 38 m
Core length: 446 cm
Depth (mbsf)
Photo
Lithology
C sc S Sand vf f m c
Samples
Feature Signature
Colour
Lithology Description
Gas escape
τ [kPa] (Falcone)
τ [kPa] (Vane shear)

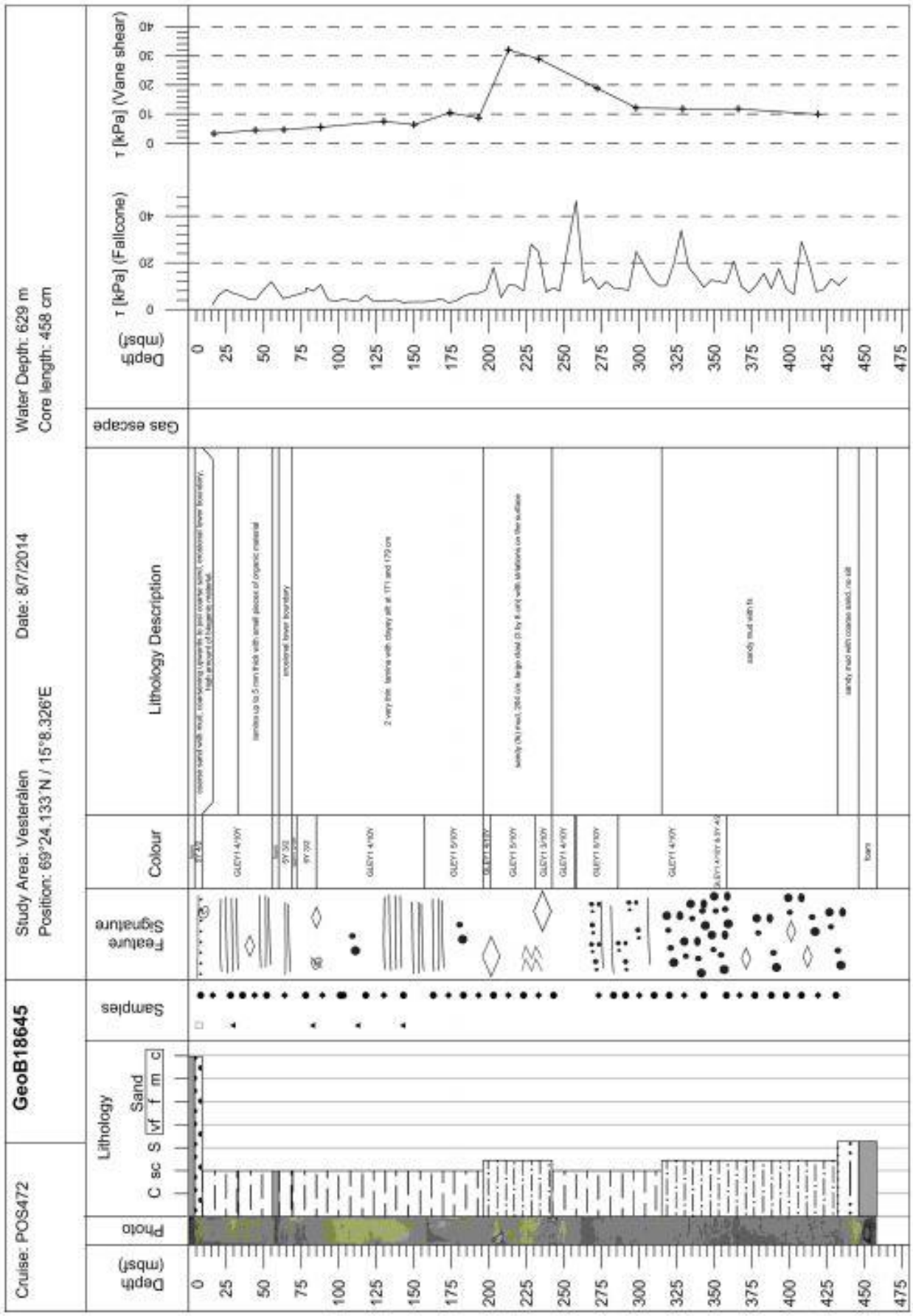
Cruise: POS472
GeoB18645
Study Area: Vesterålen
Position: 69°24.133'N / 15°8.326'E
Date: 8/7/2014
Water Depth: 629 m
Core length: 458 cm
Depth (mbsf)
Photo
Lithology
C sc S
Sand
vf f m c
Samples
Texture Signature
Colour
Lithology Description
Gas escape
τ [kPa] (Fallcone)
τ [kPa] (Vane shear)

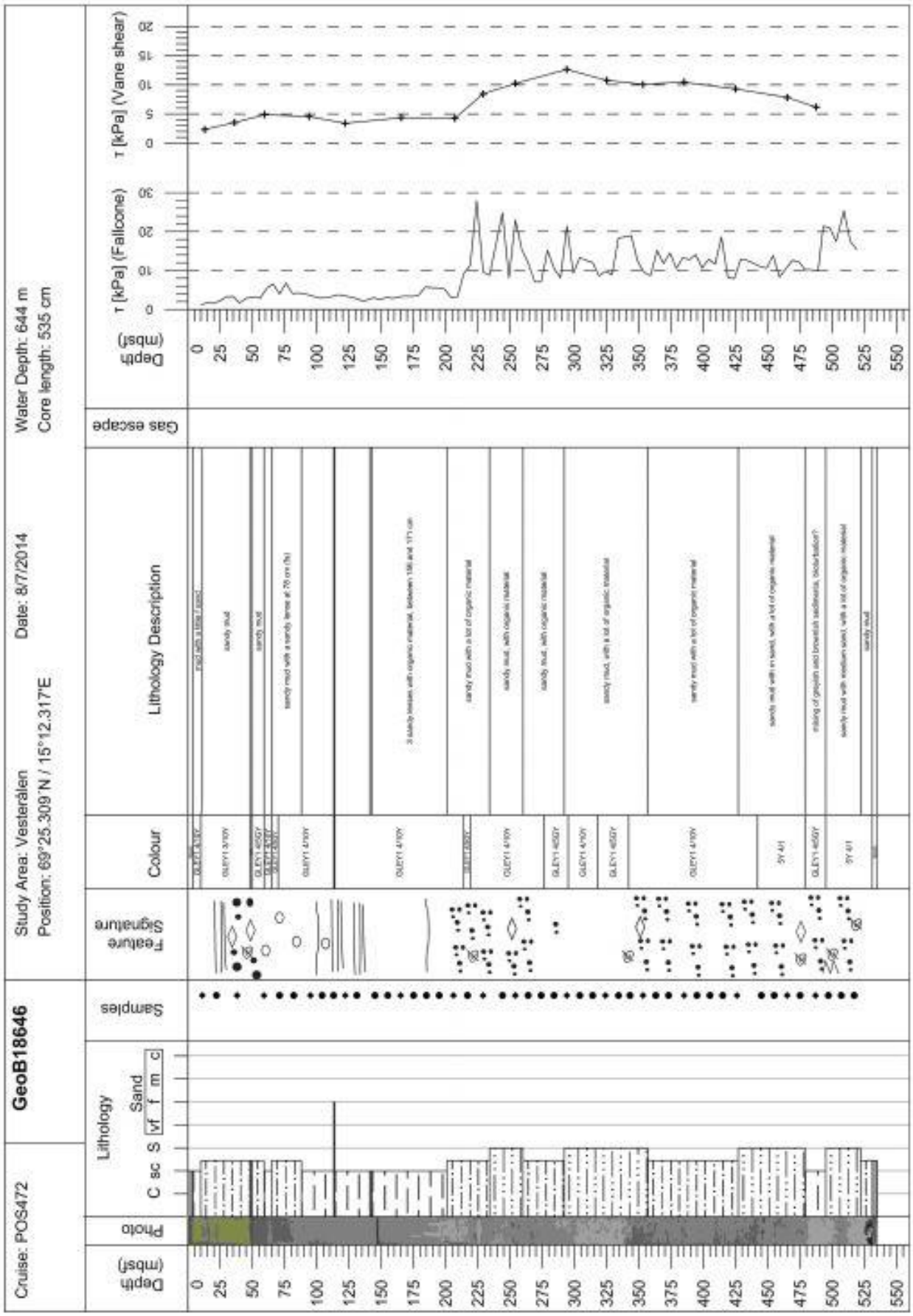
Cruise: POS472
GeoB18646
Study Area: Vesterålen
Position: 69°25.309'N / 15°12.317'E
Date: 8/7/2014
Water Depth: 644 m
Core length: 535 cm
Depth (mbsf)
Photo
Lithology
C sc S
Sand
vf f m c
Samples
Feature Signature
Colour
Lithology Description
Gas escape
τ [kPa] (Falkone)
τ [kPa] (Vane shear)

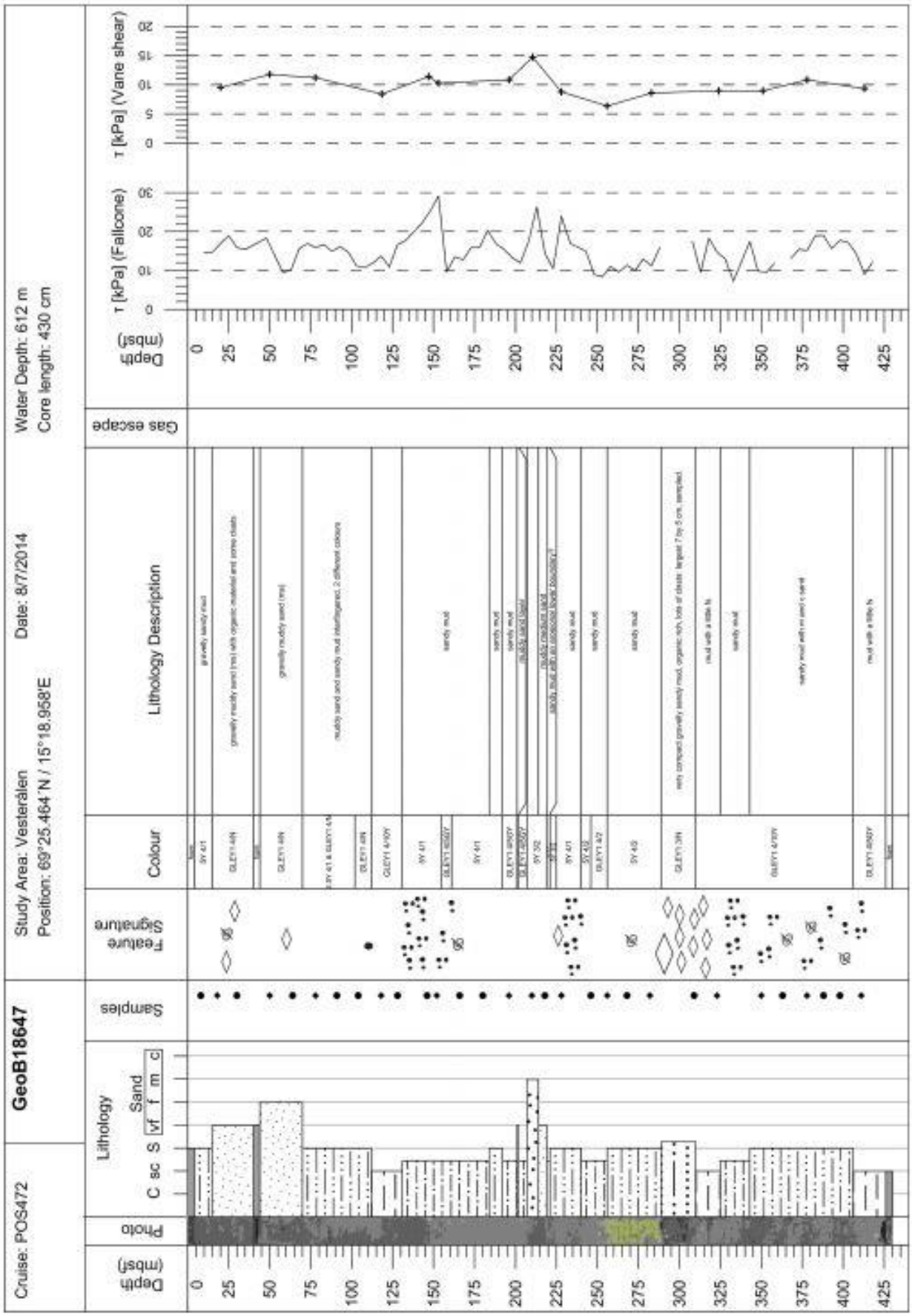
Cruise: POS472
GeoB18647
Study Area: Vesterålen
Position: 69°25.464'N / 15°18.958'E
Date: 8/7/2014
Water Depth: 612 m
Core length: 430 cm
Depth (mbsf)
Photo
Lithology
Sand
C sc S vf f m c
Samples
Feature Signature
Colour
Lithology Description
Gas escape
τ [kPa] (Falcone)
τ [kPa] (Vane shear)

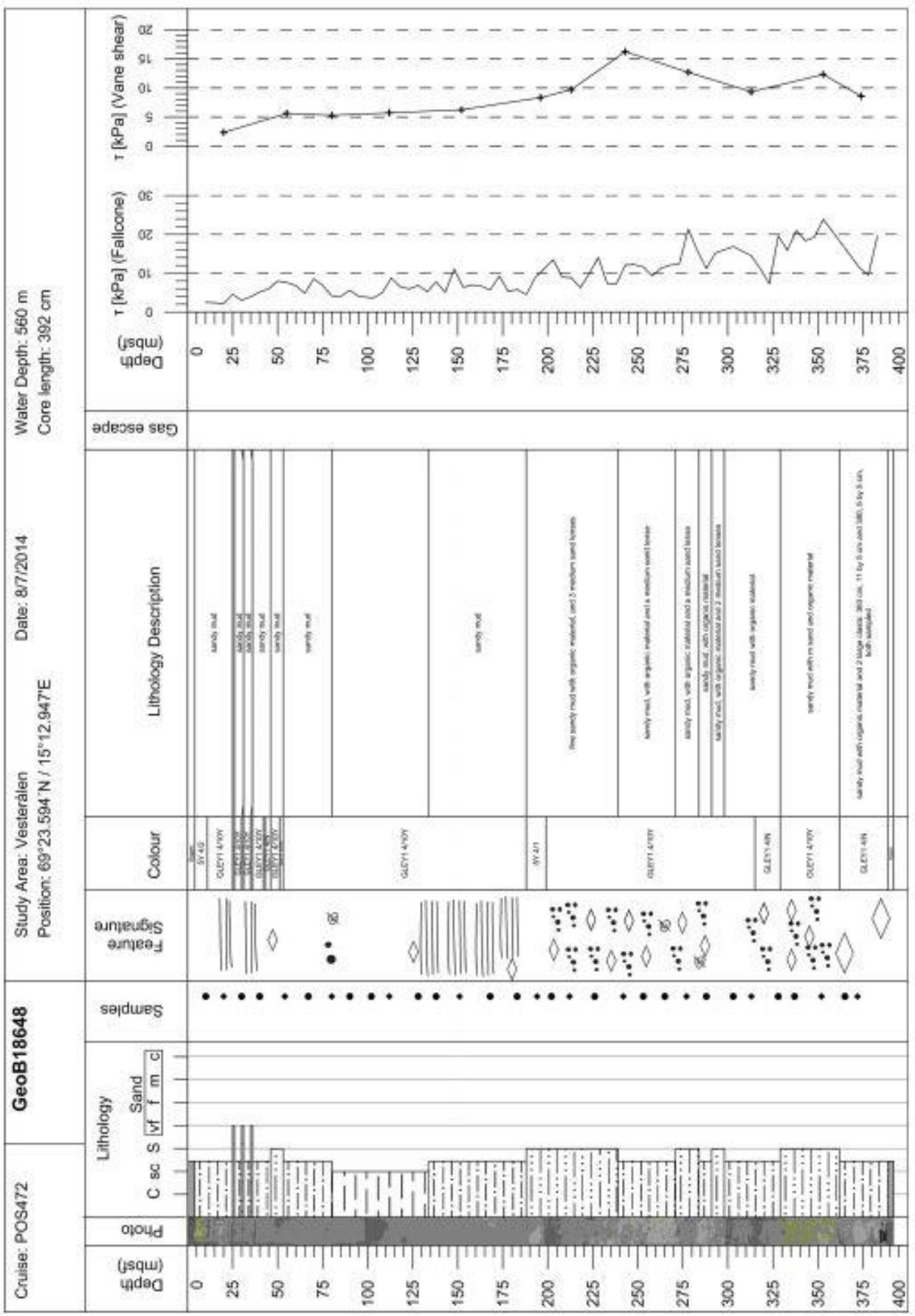
Cruise: POS472
GeoB18648
Study Area: Vesterålen
Position: 69°23.594'N / 15°12.947'E
Date: 8/7/2014
Water Depth: 560 m
Core length: 392 cm
Depth (mbsf)
Photo
Lithology
Sand
vf f m c
C sc S
Samples
Feature Signature
Colour
Lithology Description
Gas escape
τ [kPa] (Fallcone)
τ [kPa] (Vane shear)

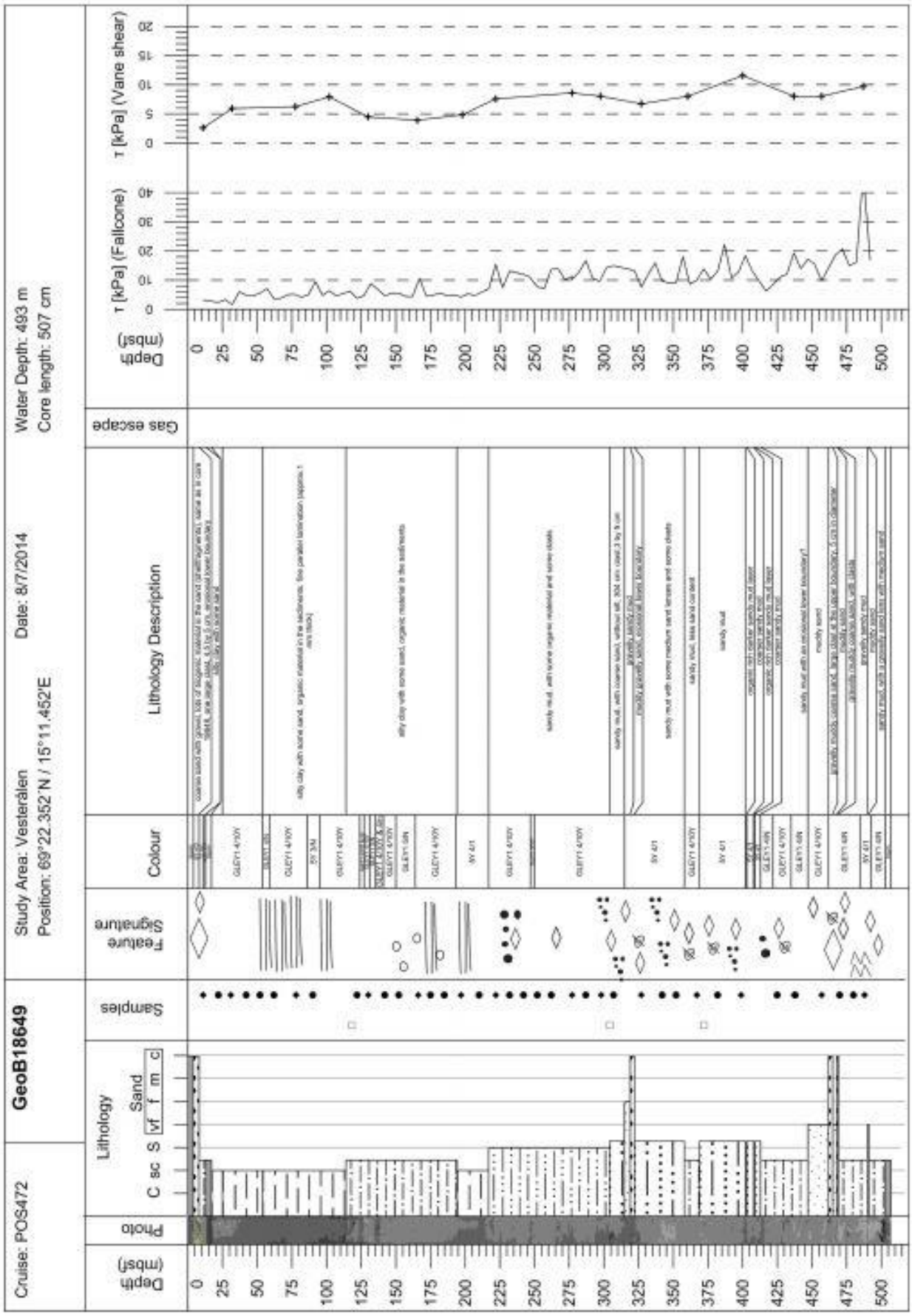
Cruise: POS472
GeoB18649
Study Area: Vesterålen
Position: 69°22.352'N / 15°11.452'E
Date: 8/7/2014
Water Depth: 493 m
Core length: 507 cm
Depth (mbsf)
Photo
Lithology
Sand
C sc S vf f m c
Samples
Feature Signature
Colour
Lithology Description
Gas escape
τ [kPa] (Fallcone)
τ [kPa] (Vane shear)

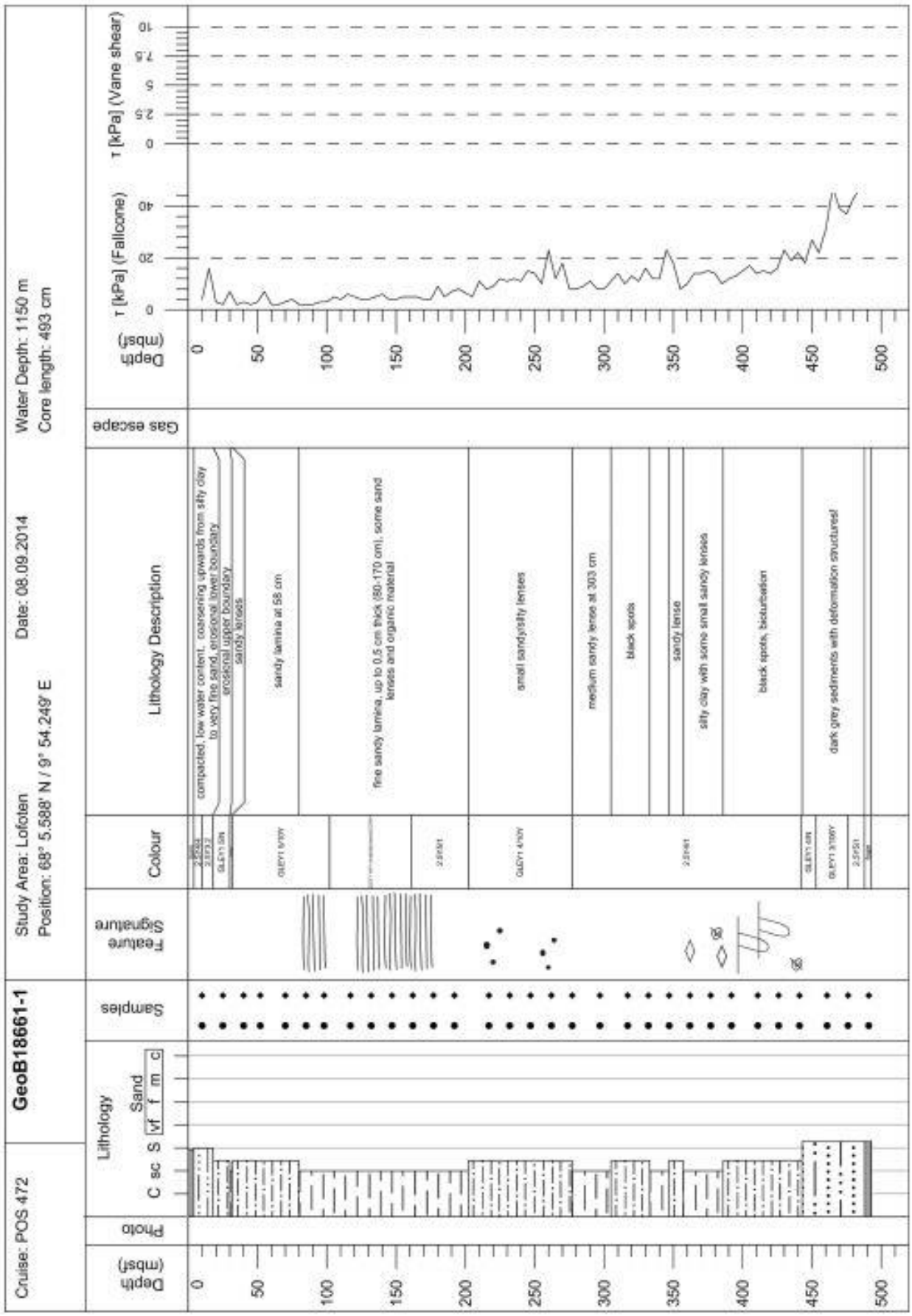
Cruise: POS 472
GeoB18661-1
Study Area: Lofoten
Position: 68° 5.588' N / 9° 54.249' E
Date: 08.09.2014
Water Depth: 1150 m
Core length: 493 cm
Depth (mbsf)
Photo
Lithology
C sc S
Sand
vf f m c
Samples
Feature Signature
Colour
Lithology Description
Gas escape
τ [kPa] (Fallcone)
τ [kPa] (Vane shear)
compacted, low water content, coarsening upwards from silty clay to very fine sand, erosional lower boundary
erosional upper boundary
sandy lenses
sandy lamina at 58 cm
fine sandy lamina, up to 0.5 cm thick (80-170 cm), some sand lenses and organic material
small sandy/silty lenses
medium sandy lense at 303 cm
black spots
sandy lense
silty clay with some small sandy lenses
black spots, bioturbation
dark grey sediments with deformation structures!

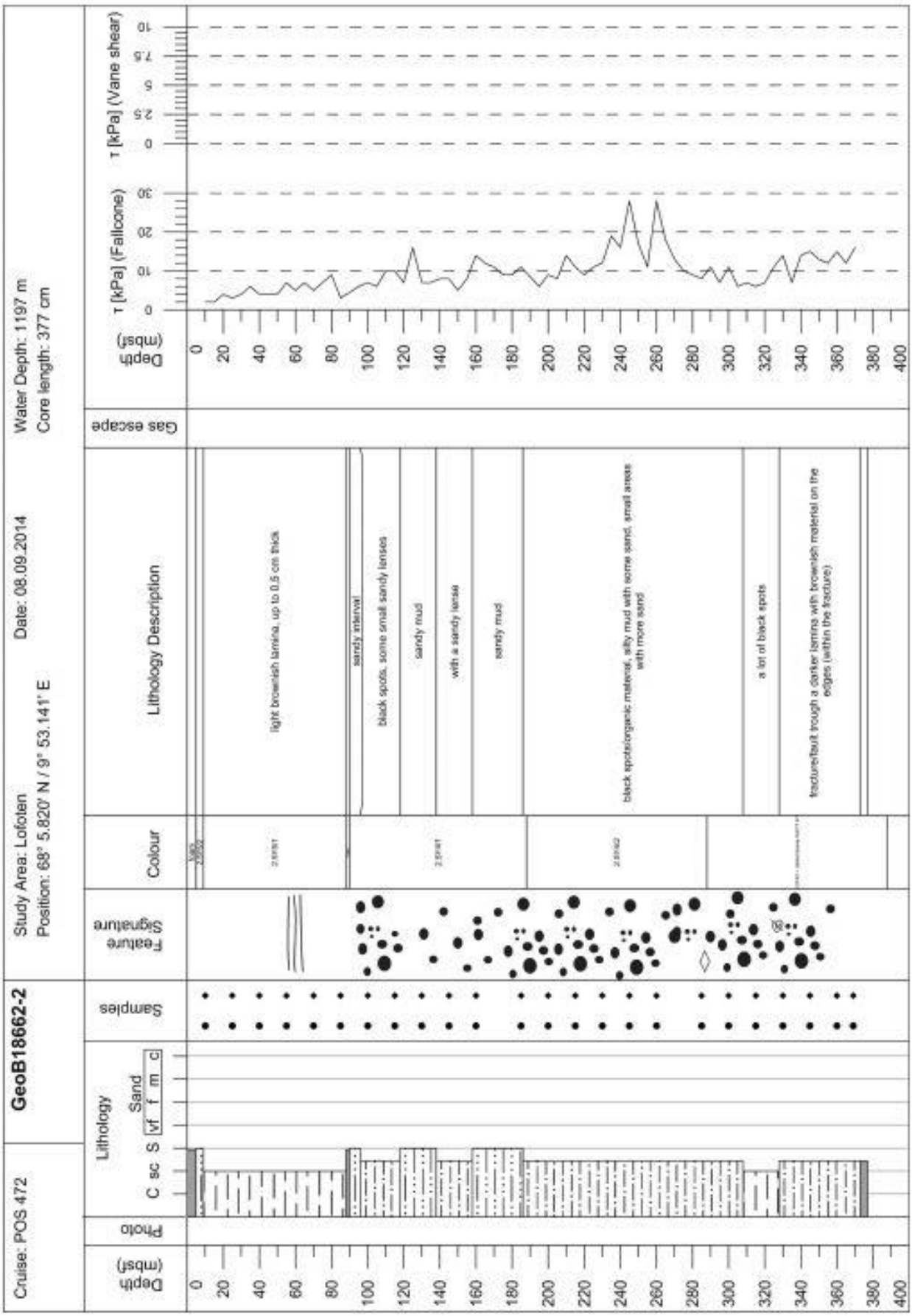
Cruise: POS 472
GeoB18662-2
Study Area: Lofoten
Position: 68° 5.820' N / 9° 53.141' E
Date: 08.09.2014
Water Depth: 1197 m
Core length: 377 cm
Depth (mbsf)
Photo
Lithology
C sc S
Sand
vf f m c
Samples
Feature Signature
Colour
Lithology Description
light brownish lamina, up to 0.5 cm thick
sandy interval
black spots, some small sandy lenses
sandy mud
with a sandy lense
sandy mud
black spots/organic material, silty mud with some sand, small areas with more sand
a lot of black spots
fracture/fault trough a darker laming with brownish material on the edges (within the fracture)
Gas escape
τ [kPa] (Fallcone)
τ [kPa] (Vane shear)

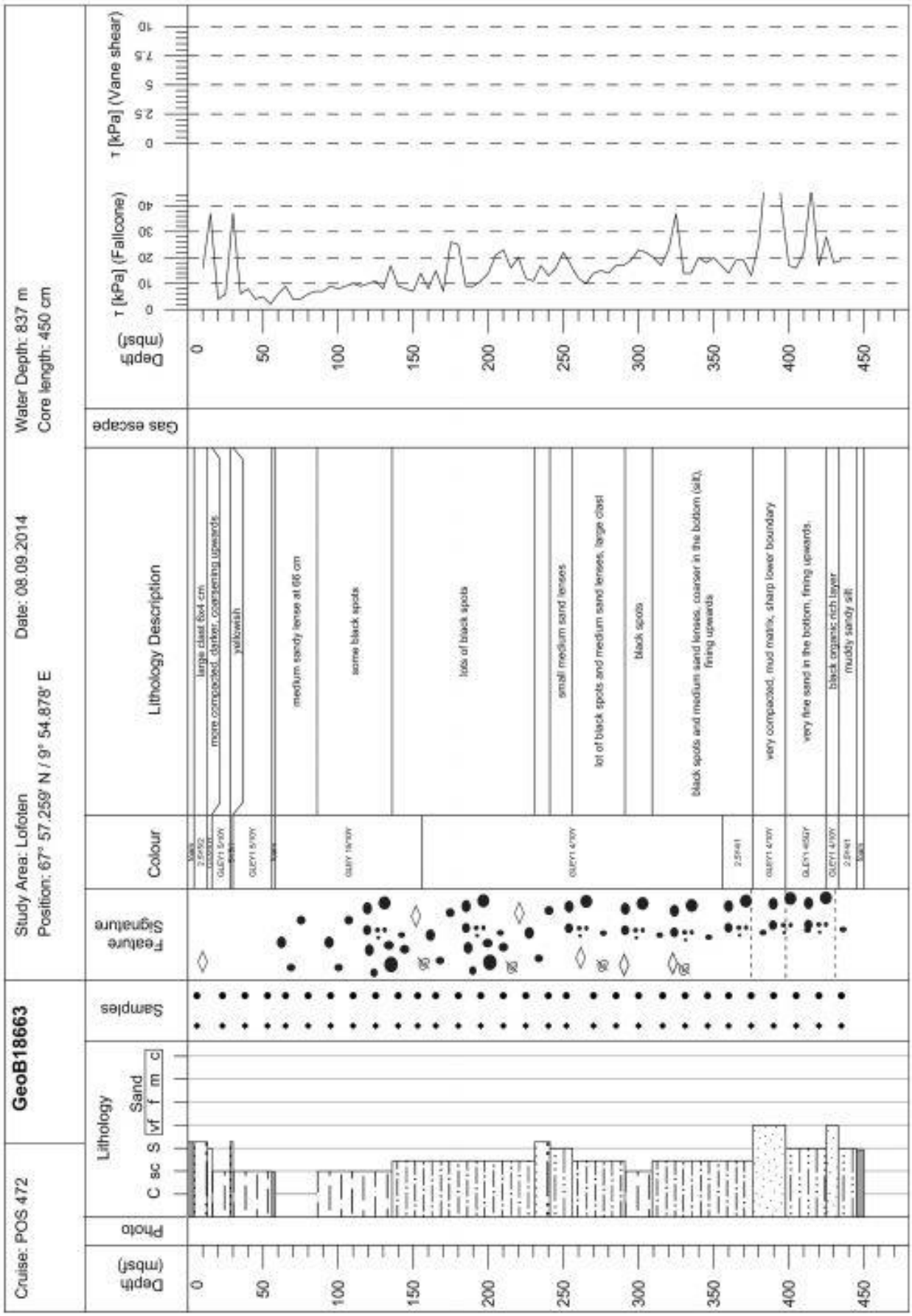
Cruise: POS 472
GeoB18663
Study Area: Lofoten
Position: 67° 57.259' N / 9° 54.878' E
Date: 08.09.2014
Water Depth: 837 m
Core length: 450 cm
Depth (mbsf)
Photo
Lithology
C sc S
Sand
vf f m c
Samples
Feature Signature
Colour
Lithology Description
large clast 6x4 cm
more compacted, darker, coarsening upwards
yellowish
medium sandy lense at 66 cm
some black spots
lots of black spots
small medium sand lenses
lot of black spots and medium sand lenses, large clast
black spots
black spots and medium sand lenses, coarser in the bottom (silt), fining upwards
very compacted, mud matrix, sharp lower boundary
very fine sand in the bottom, fining upwards.
black organic rich layer
muddy sandy silt
Gas escape
τ [kPa] (Falcone)
τ [kPa] (Vane shear)

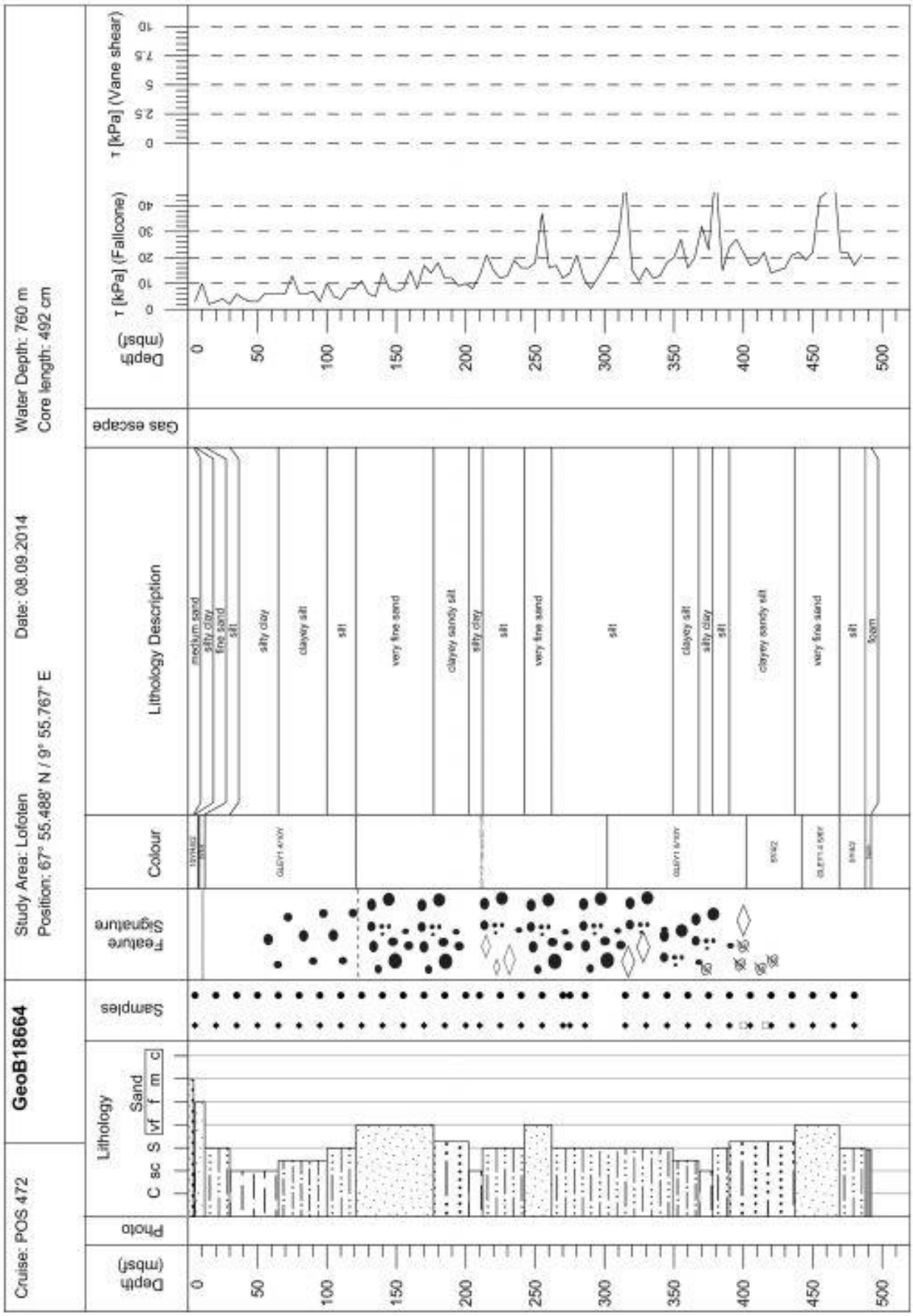
Cruise: POS 472
GeoB18664
Study Area: Lofoten
Position: 67° 55.488' N / 9° 55.767' E
Date: 08.09.2014
Water Depth: 760 m
Core length: 492 cm
Depth (mbsf)
Photo
Lithology
C sc S
Sand
vf f m c
Samples
Feature Signature
Colour
Lithology Description
medium sand
silty clay
fine sand
silt
silty clay
clayey silt
silt
very fine sand
clayey sandy silt
silty clay
silt
very fine sand
silt
clayey silt
silty clay
silt
clayey sandy silt
very fine sand
silt
foam
Gas escape
τ [kPa] (Fallcone)
τ [kPa] (Vane shear)

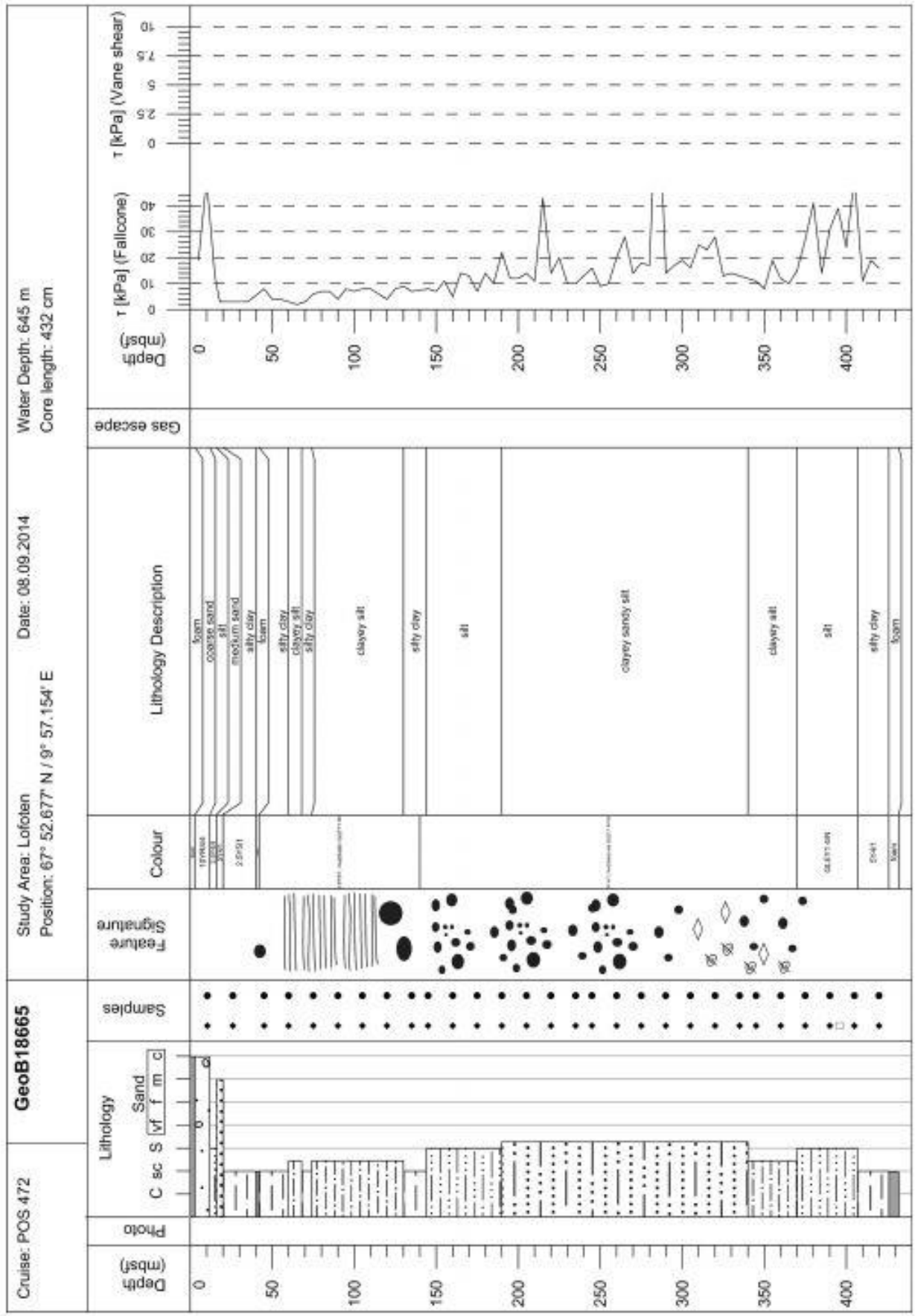
Cruise: POS 472
GeoB18665
Study Area: Lofoten
Position: 67° 52.677' N / 9° 57.154' E
Date: 08.09.2014
Water Depth: 645 m
Core length: 432 cm
Depth (mbsf)
Photo
Lithology
Sand
C sc S vf f m c
Samples
Feature Signature
Colour
Lithology Description
foam
coarse sand
silt
medium sand
silty clay
foam
silty clay
clayey silt
silty clay
clayey silt
silt
clayey sandy silt
clayey silt
silt
silty clay
foam
Gas escape
τ [kPa] (Fallcone)
τ [kPa] (Vane shear)

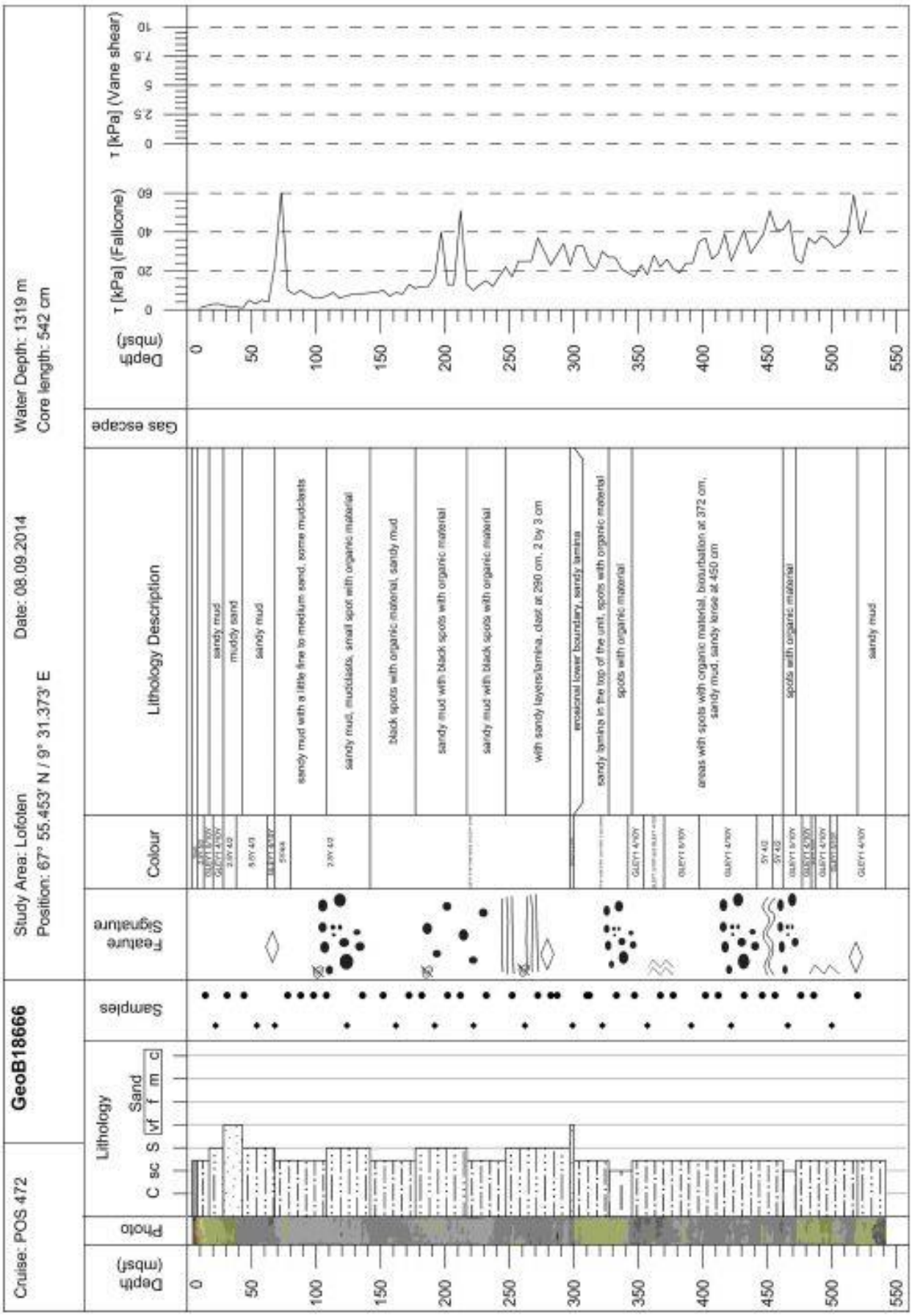
Cruise: POS 472
GeoB18666
Study Area: Lofoten
Position: 67° 55.453' N / 9° 31.373' E
Date: 08.09.2014
Water Depth: 1319 m
Core length: 542 cm
Depth (mbsf)
Photo
Lithology
Sand
C sc S vf f m c
Samples
Feature Signature
Colour
Lithology Description
Gas escape
τ [kPa] (Fallcone)
τ [kPa] (Vane shear)
sandy mud with a little fine to medium sand, some mudclasts
sandy mud, mudclasts, small spot with organic material
black spots with organic material, sandy mud
sandy mud with black spots with organic material
sandy mud with black spots with organic material
with sandy layers/lamina, clast at 290 cm, 2 by 3 cm
erosional lower boundary, sandy lamina
sandy lamina in the top of the unit, spots with organic material
spots with organic material
areas with spots with organic material, bioturbation at 372 cm, sandy mud, sandy lense at 450 cm
spots with organic material
sandy mud
sandy mud
muddy sand
sandy mud

11.2 Initial MSCL Logging Data

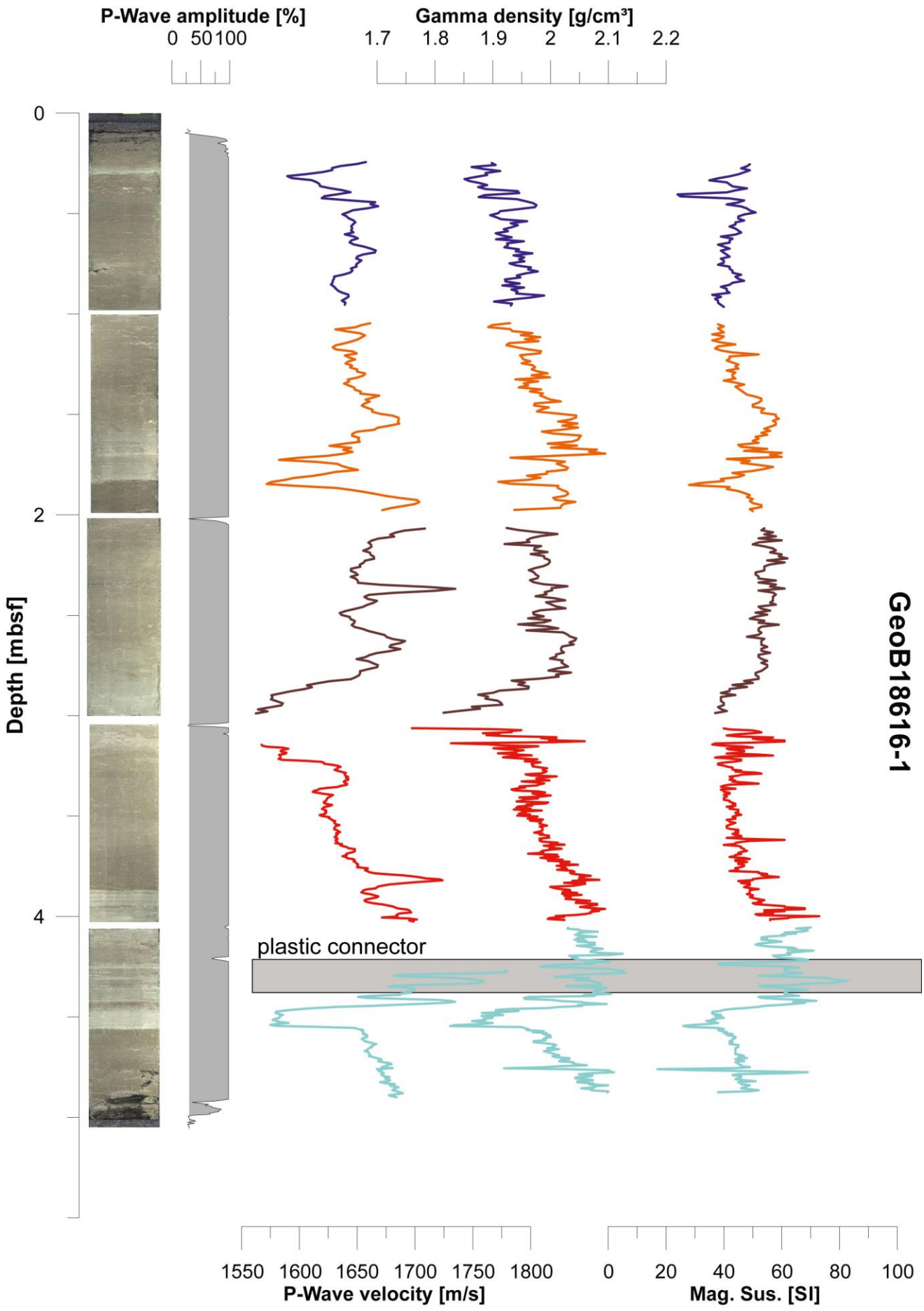
P-Wave amplitude [%]
0 50 100
Gamma density [g/cm³]
1.7 1.8 1.9 2 2.1 2.2
0
2
4
Depth [mbsf]
GeoB18616-1
plastic connector
1550 1600 1650 1700 1750 1800
P-Wave velocity [m/s]
0 20 40 60 80 100
Mag. Sus. [SI]

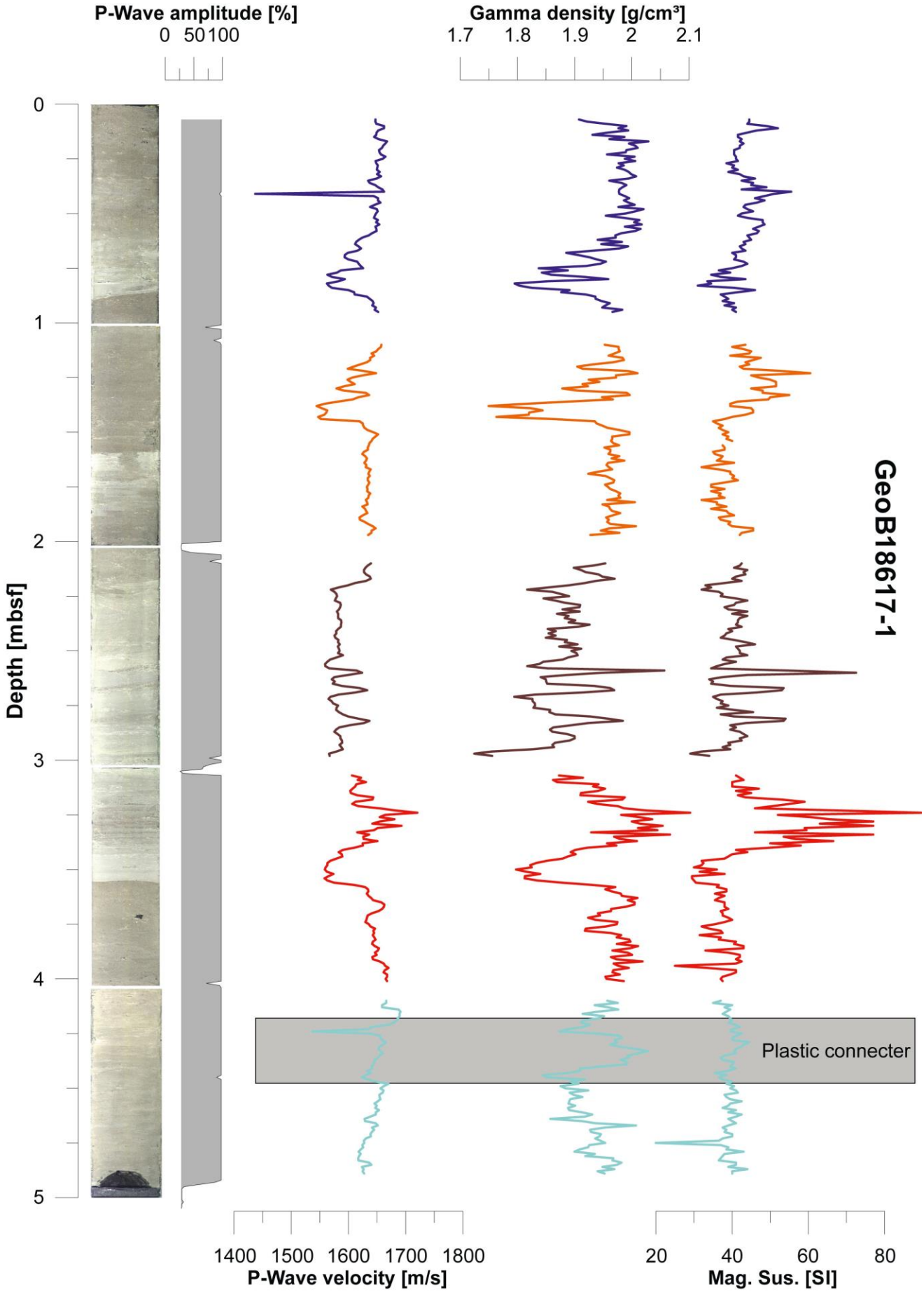
P-Wave amplitude [%]
0 50 100
Gamma density [g/cm³]
1.7 1.8 1.9 2 2.1
Depth [mbsf]
0
1
2
3
4
5
GeoB18617-1
Plastic connecter
1400 1500 1600 1700 1800
P-Wave velocity [m/s]
20 40 60 80
Mag. Sus. [SI]

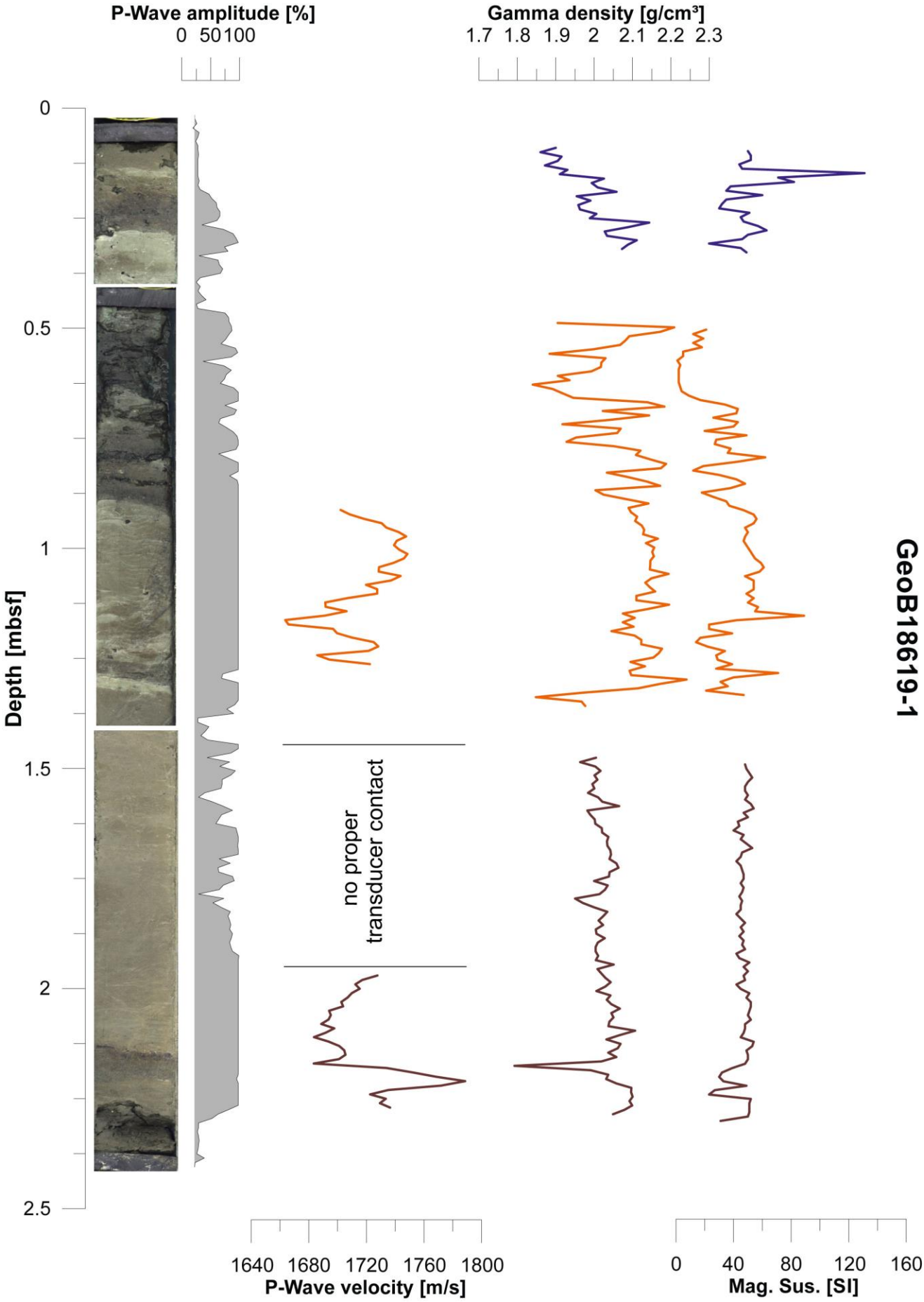
P-Wave amplitude [%]
0 50100
Gamma density [g/cm³]
1.7 1.8 1.9 2 2.1 2.2 2.3
Depth [mbsf]
0
0.5
1
1.5
2
2.5
no proper transducer contact
GeoB18619-1
1640 1680 1720 1760 1800
P-Wave velocity [m/s]
0 40 80 120 160
Mag. Sus. [SI]

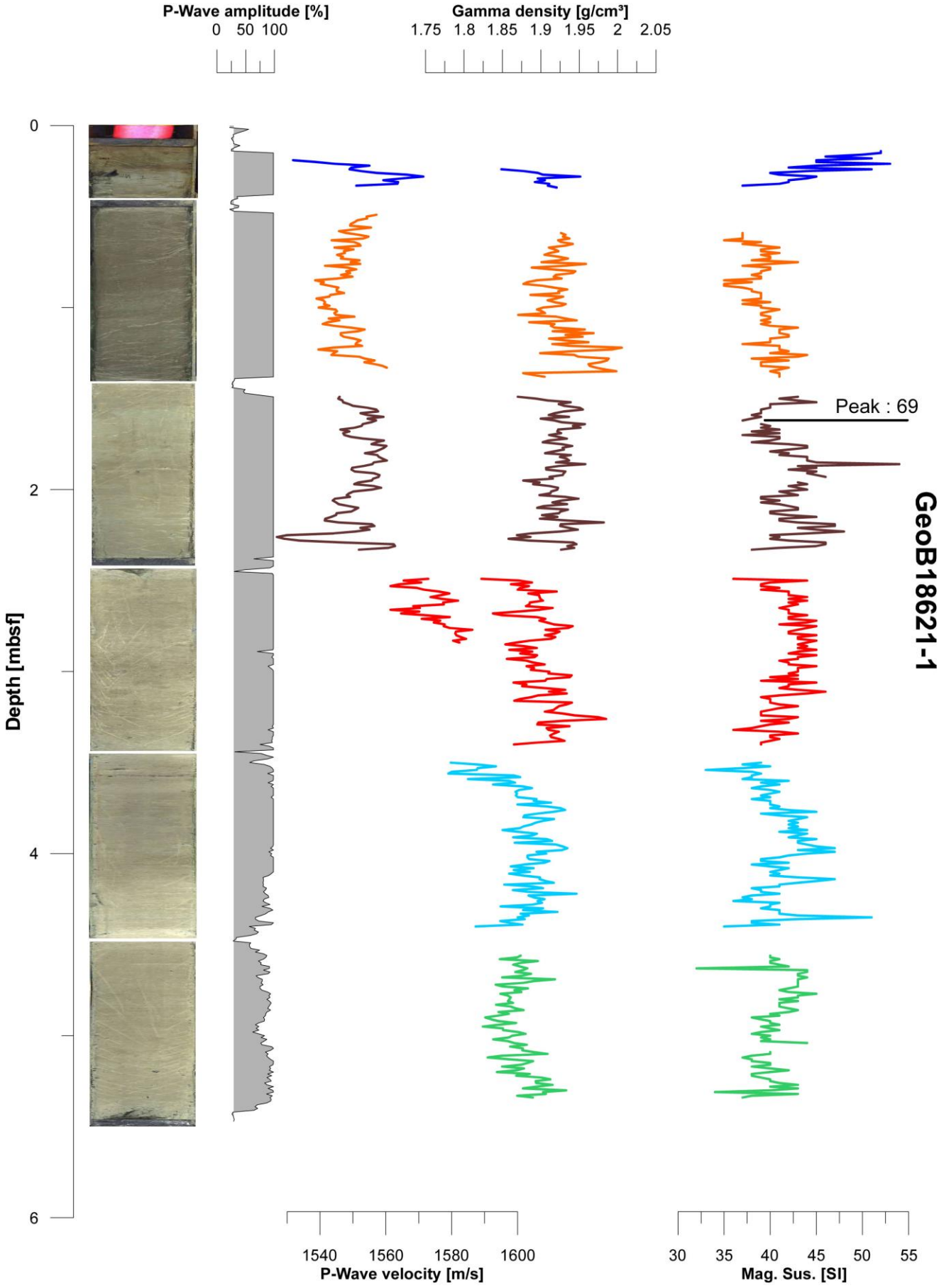
P-Wave amplitude [%]
0 50 100
Gamma density [g/cm³]
1.75 1.8 1.85 1.9 1.95 2 2.05
Peak : 69
GeoB18621-1
Depth [mbsf]
0
2
4
6
1540 1560 1580 1600
P-Wave velocity [m/s]
30 35 40 45 50 55
Mag. Sus. [SI]

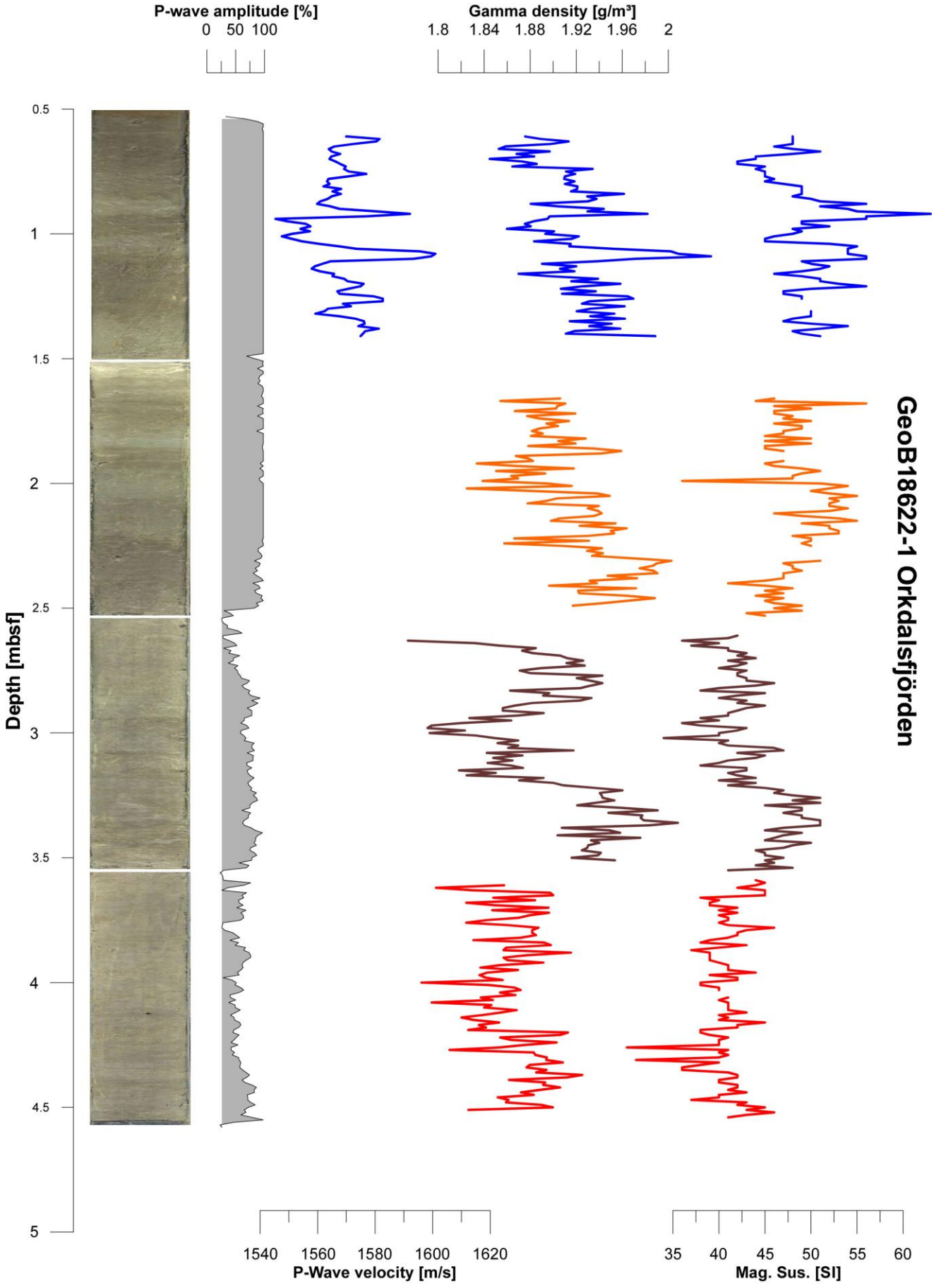
P-wave amplitude [%]
0 50 100
Gamma density [g/m³]
1.8 1.84 1.88 1.92 1.96 2
Depth [mbsf]
0.5
1
1.5
2
2.5
3
3.5
4
4.5
5
GeoB18622-1 Orkdalsfjörden
1540 1560 1580 1600 1620
P-Wave velocity [m/s]
35 40 45 50 55 60
Mag. Sus. [SI]

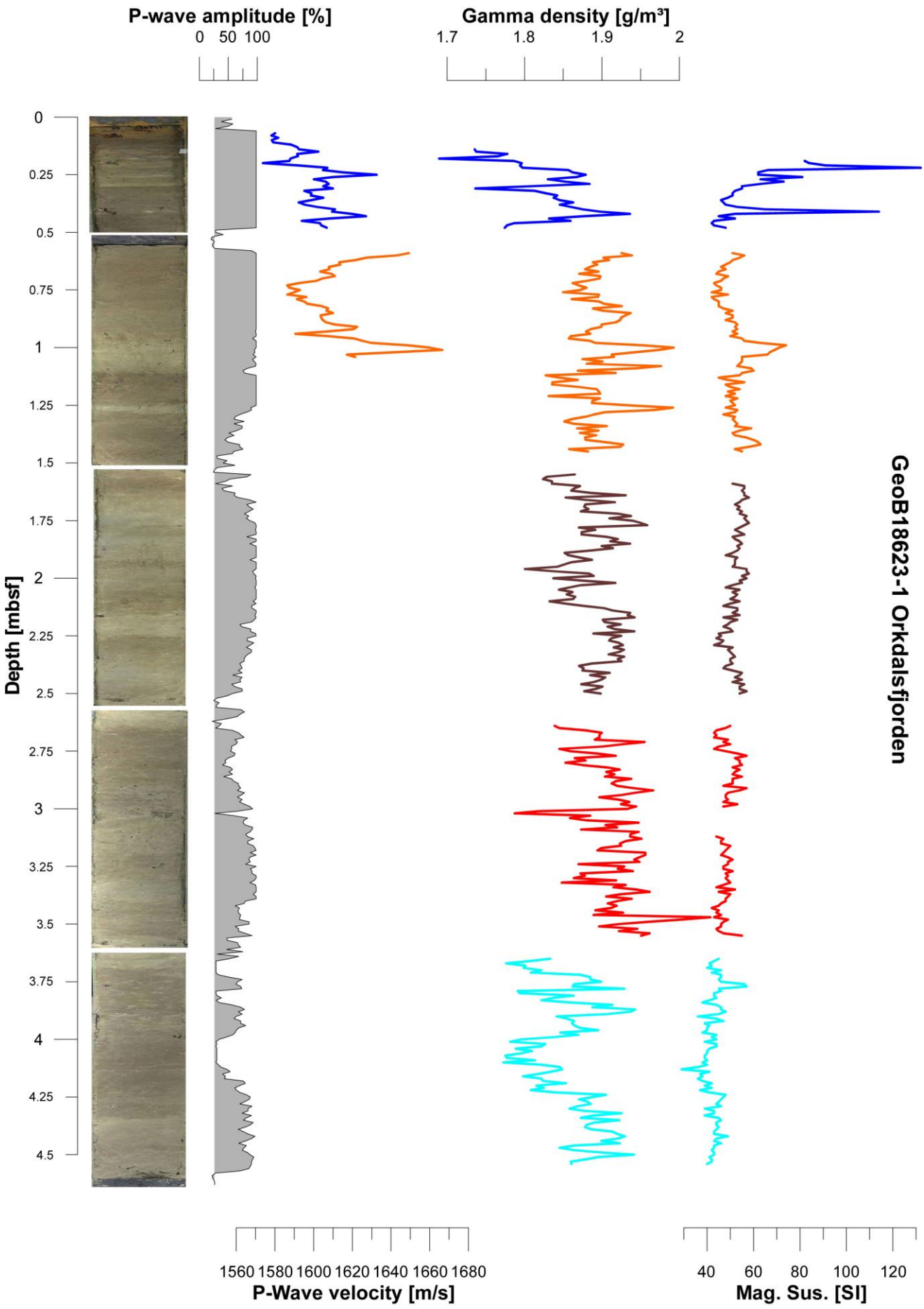
P-wave amplitude [%]
0 50 100
Gamma density [g/m³]
1.7 1.8 1.9 2
Depth [mbsf]
0 0.25 0.5 0.75 1 1.25 1.5 1.75 2 2.25 2.5 2.75 3 3.25 3.5 3.75 4 4.25 4.5
GeoB18623-1 Orkdalsfjorden
1560 1580 1600 1620 1640 1660 1680
P-Wave velocity [m/s]
40 60 80 100 120
Mag. Sus. [SI]

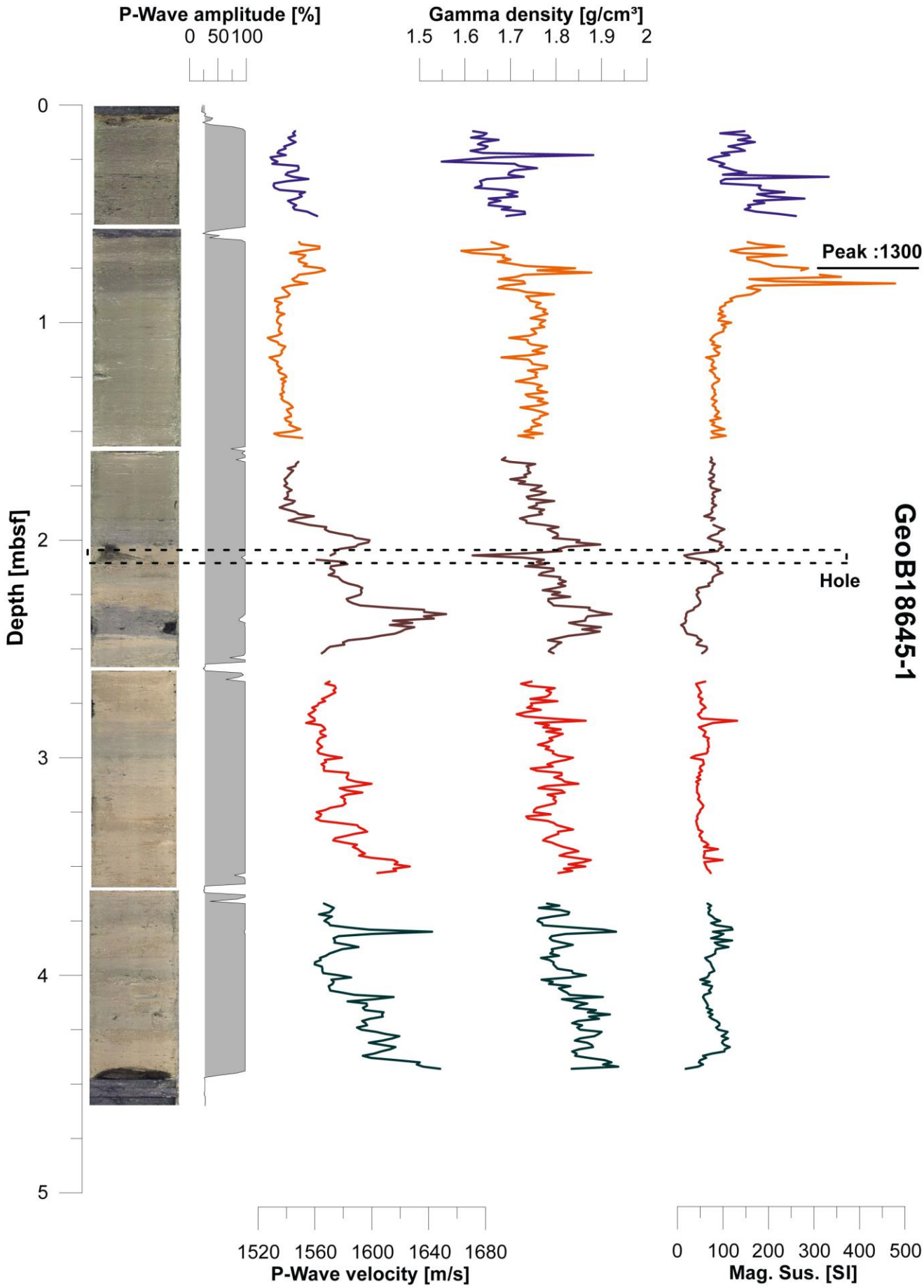
P-Wave amplitude [%]
0 50 100
Gamma density [g/cm³]
1.5 1.6 1.7 1.8 1.9 2
Peak :1300
Hole
GeoB18645-1
Depth [mbsf]
0
1
2
3
4
5
1520 1560 1600 1640 1680
P-Wave velocity [m/s]
0 100 200 300 400 500
Mag. Sus. [SI]

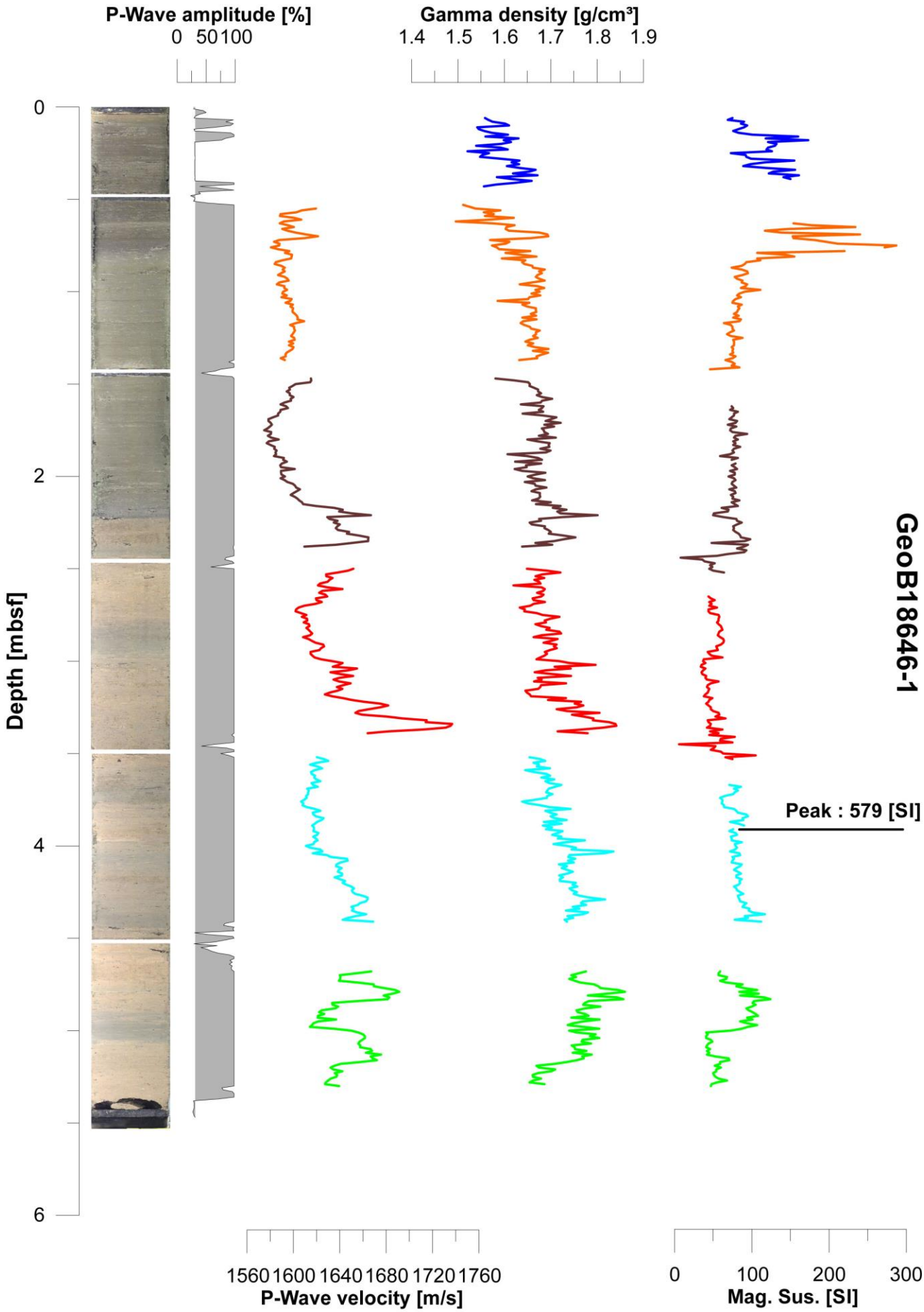
P-Wave amplitude [%]
0 50 100
Gamma density [g/cm³]
1.4 1.5 1.6 1.7 1.8 1.9
0
2
4
6
Depth [mbsf]
GeoB18646-1
Peak : 579 [SI]
1560 1600 1640 1680 1720 1760
P-Wave velocity [m/s]
0 100 200 300
Mag. Sus. [SI]

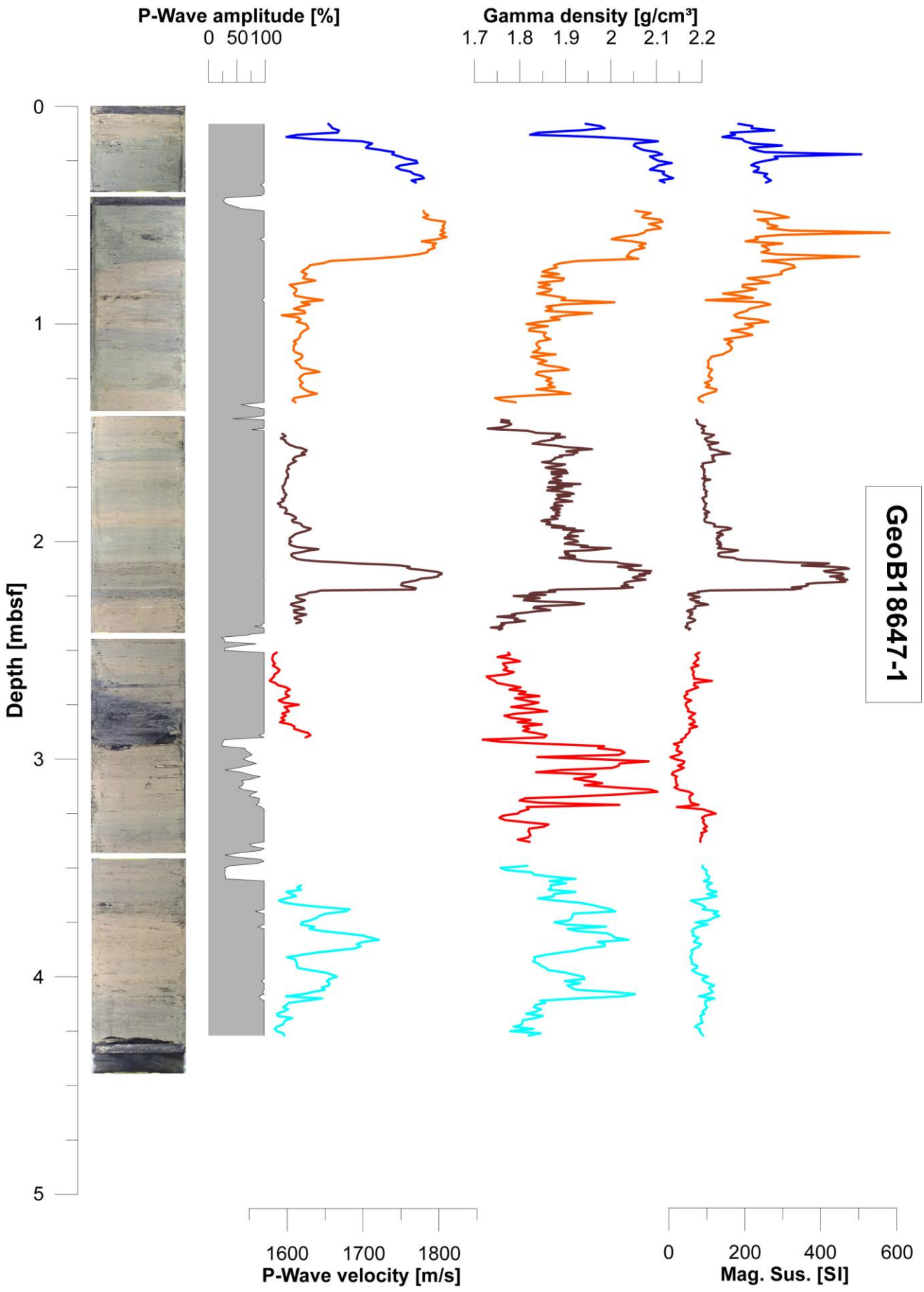
P-Wave amplitude [%]
0 50 100
Gamma density [g/cm³]
1.7 1.8 1.9 2 2.1 2.2
Depth [mbsf]
0
1
2
3
4
5
GeoB18647-1
1600 1700 1800
P-Wave velocity [m/s]
0 200 400 600
Mag. Sus. [SI]

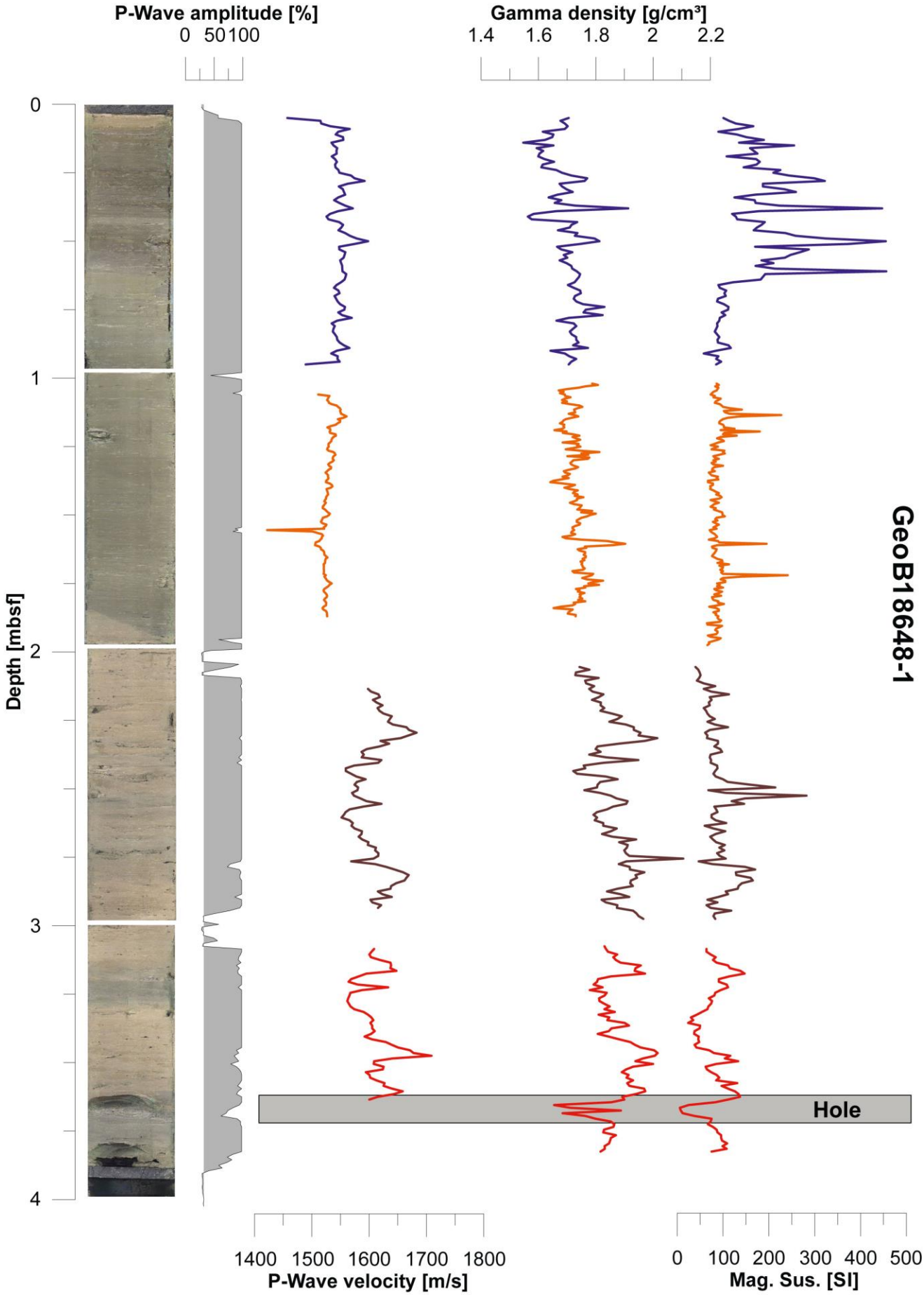
P-Wave amplitude [%]
0 50 100
Gamma density [g/cm³]
1.4 1.6 1.8 2 2.2
Depth [mbsf]
0
1
2
3
4
GeoB18648-1
Hole
1400 1500 1600 1700 1800
P-Wave velocity [m/s]
0 100 200 300 400 500
Mag. Sus. [SI]

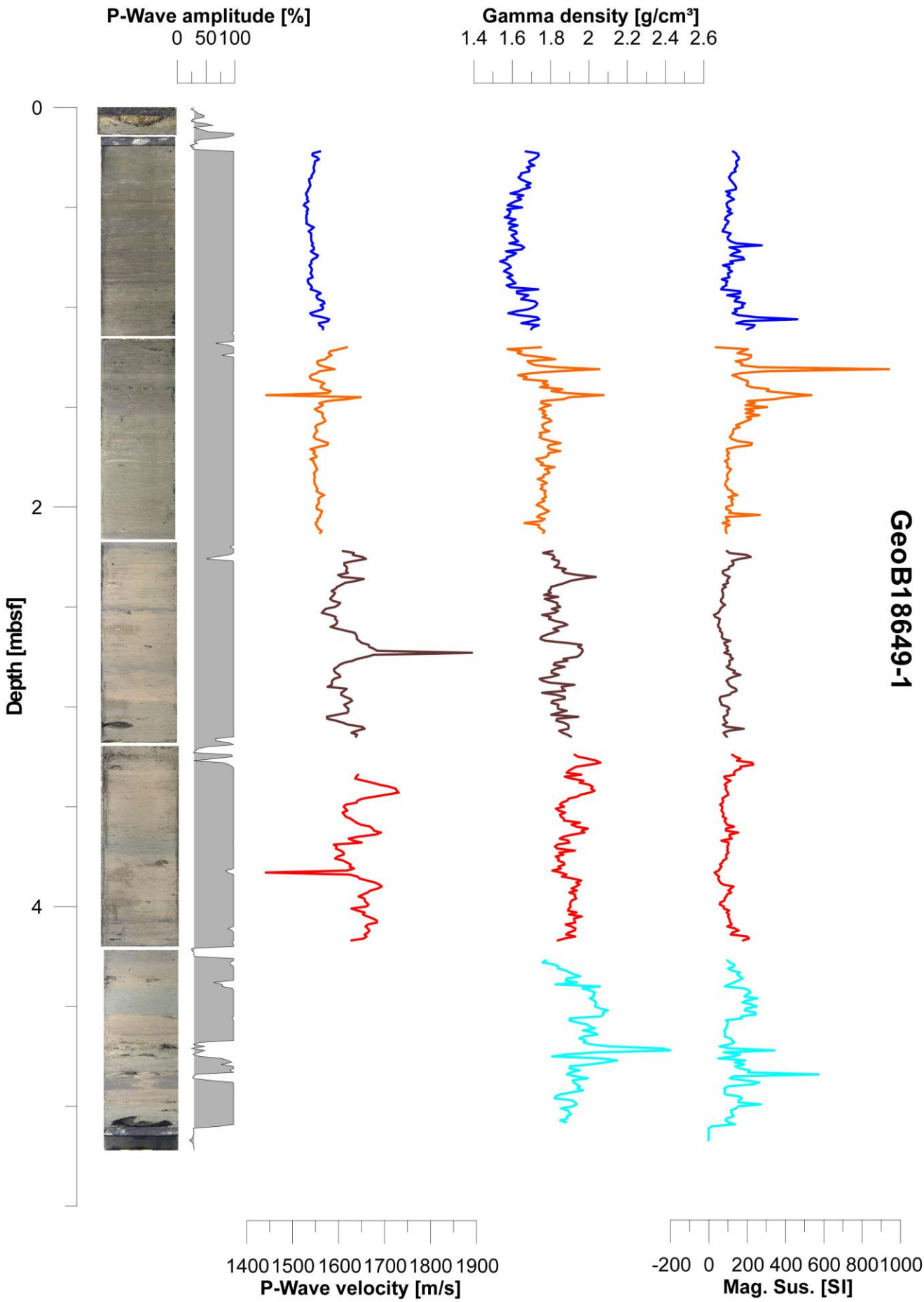
P-Wave amplitude [%]
0 50 100
Gamma density [g/cm³]
1.4 1.6 1.8 2 2.2 2.4 2.6
0
2
4
Depth [mbsf]
GeoB18649-1
1400 1500 1600 1700 1800 1900
P-Wave velocity [m/s]
-200 0 200 400 600 800 1000
Mag. Sus. [SI]

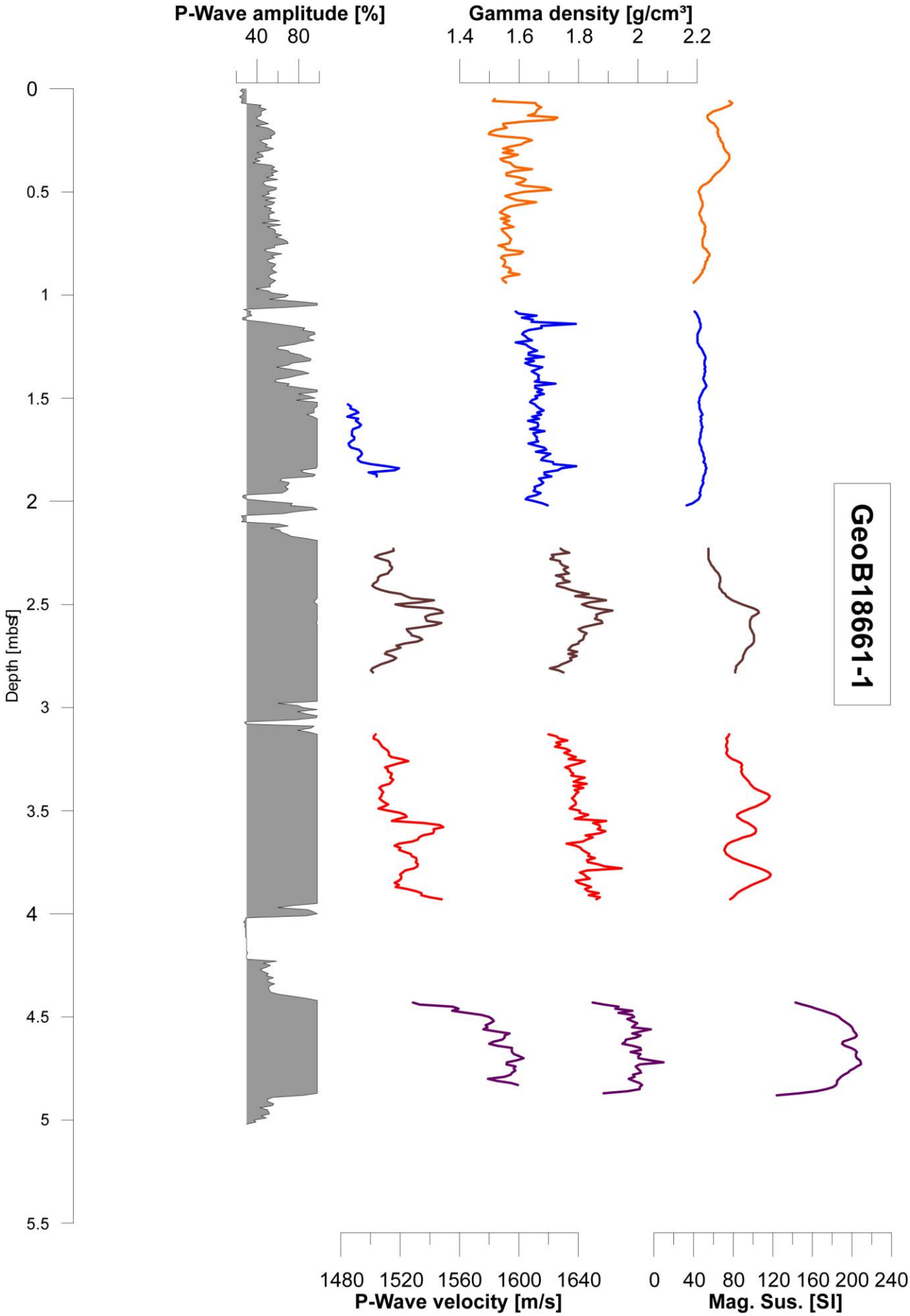
P-Wave amplitude [%]
40 80
Gamma density [g/cm³]
1.4 1.6 1.8 2 2.2
Depth [mbsf]
0 0.5 1 1.5 2 2.5 3 3.5 4 4.5 5 5.5
GeoB18661-1
1480 1520 1560 1600 1640
P-Wave velocity [m/s]
0 40 80 120 160 200 240
Mag. Sus. [SI]

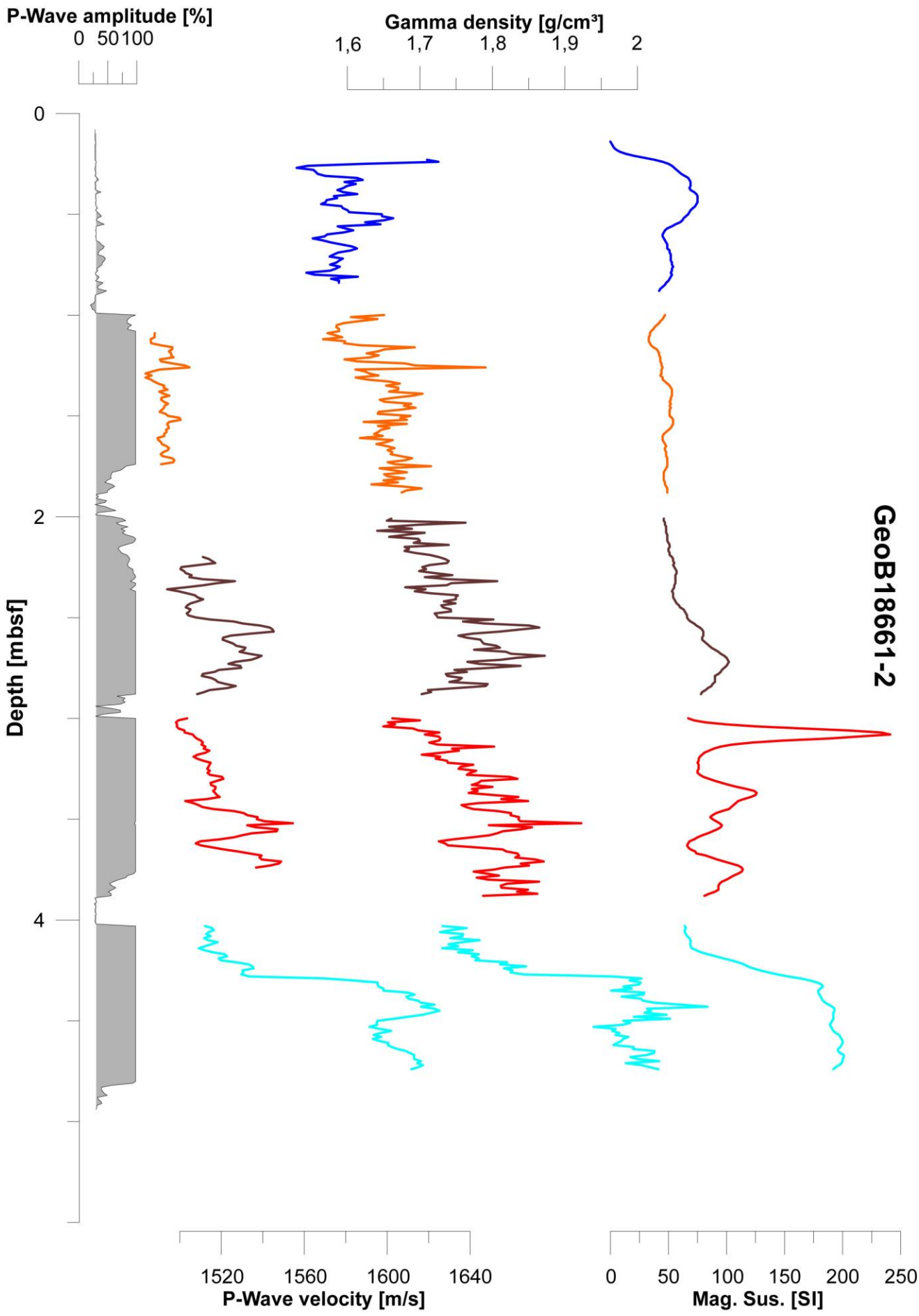
P-Wave amplitude [%]
0 50 100
Gamma density [g/cm³]
1,6 1,7 1,8 1,9 2
0
2
4
Depth [mbsf]
GeoB18661-2
1520 1560 1600 1640
P-Wave velocity [m/s]
0 50 100 150 200 250
Mag. Sus. [SI]

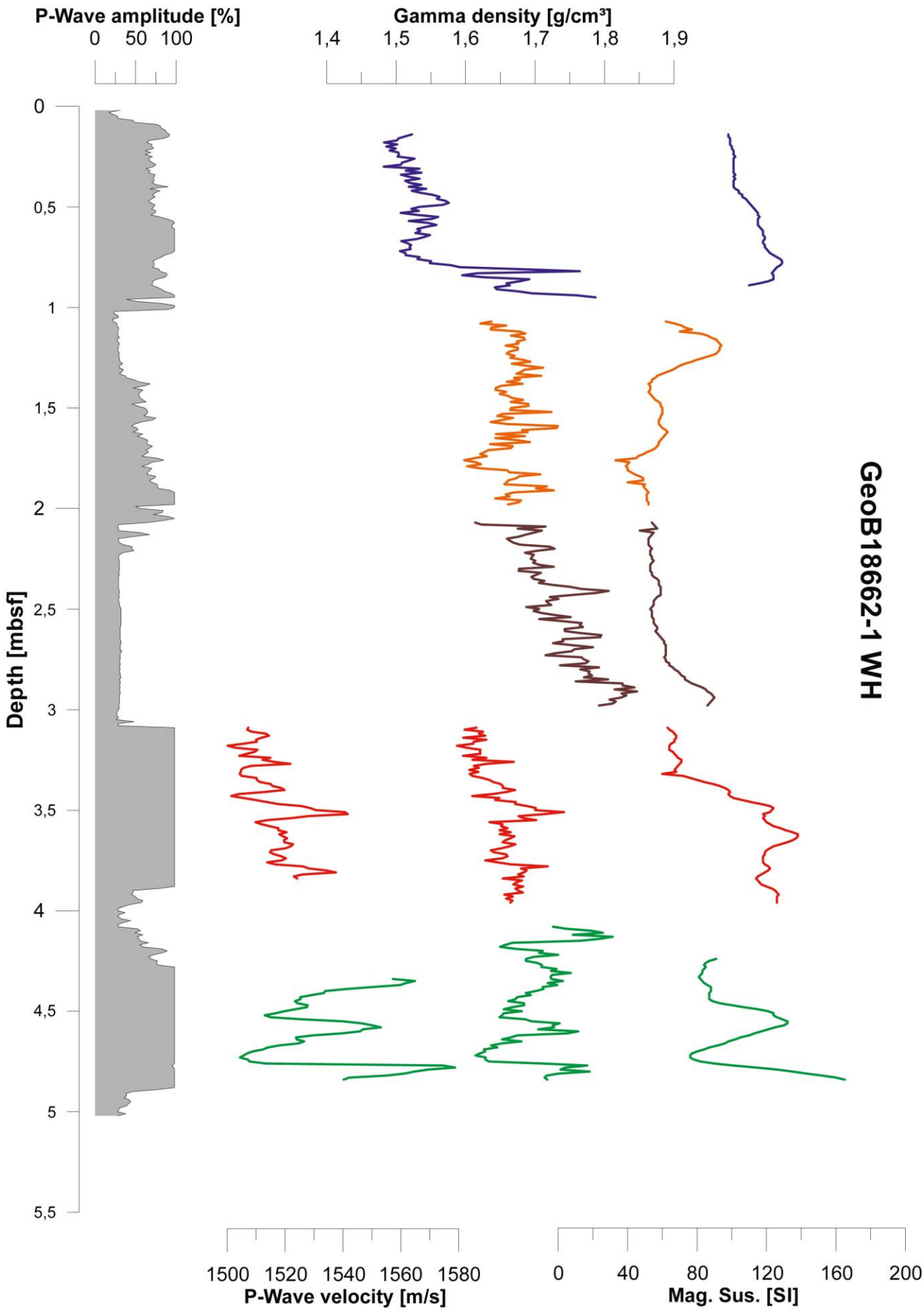
P-Wave amplitude [%]
0 50 100
Gamma density [g/cm³]
1,4 1,5 1,6 1,7 1,8 1,9
Depth [mbsf]
0
0,5
1
1,5
2
2,5
3
3,5
4
4,5
5
5,5
GeoB18662-1 WH
1500 1520 1540 1560 1580
P-Wave velocity [m/s]
0 40 80 120 160 200
Mag. Sus. [SI]

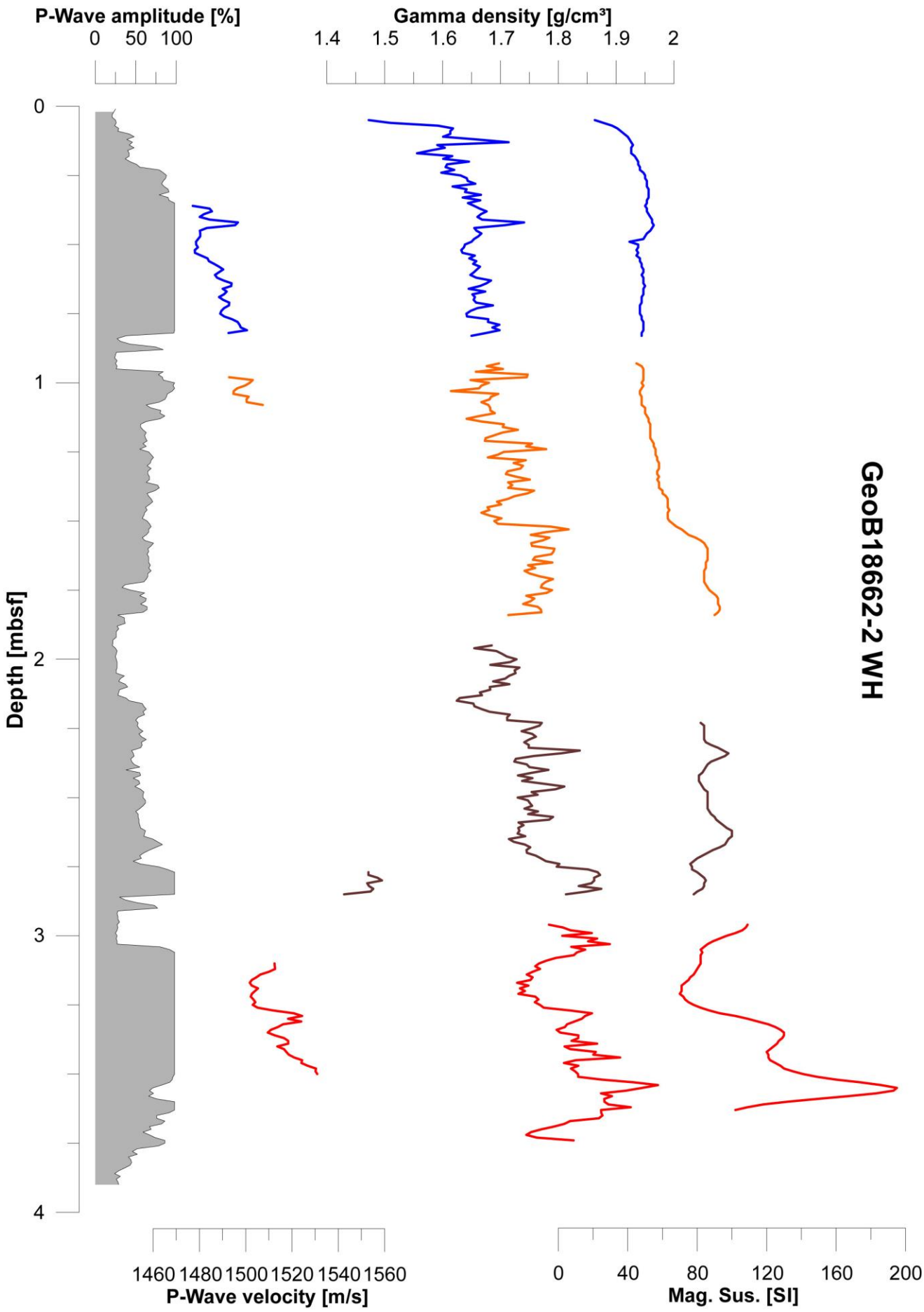
P-Wave amplitude [%]
0 50 100
Gamma density [g/cm³]
1.4 1.5 1.6 1.7 1.8 1.9 2
Depth [mbsf]
0
1
2
3
4
GeoB18662-2 WH
1460 1480 1500 1520 1540 1560
P-Wave velocity [m/s]
0 40 80 120 160 200
Mag. Sus. [SI]

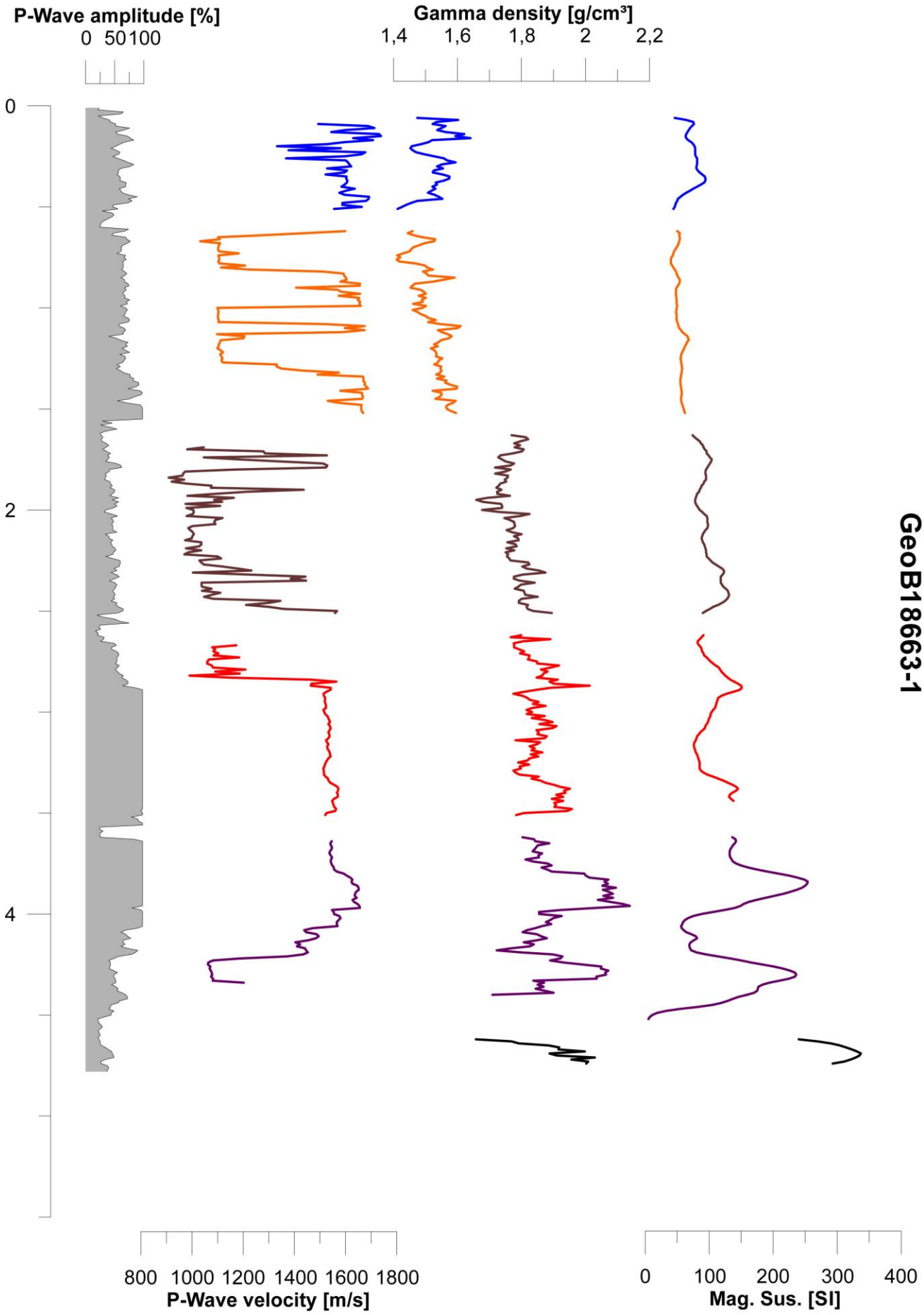
P-Wave amplitude [%]
0 50 100
Gamma density [g/cm³]
1,4 1,6 1,8 2 2,2
0
2
4
GeoB18663-1
800 1000 1200 1400 1600 1800
P-Wave velocity [m/s]
0 100 200 300 400
Mag. Sus. [SI]

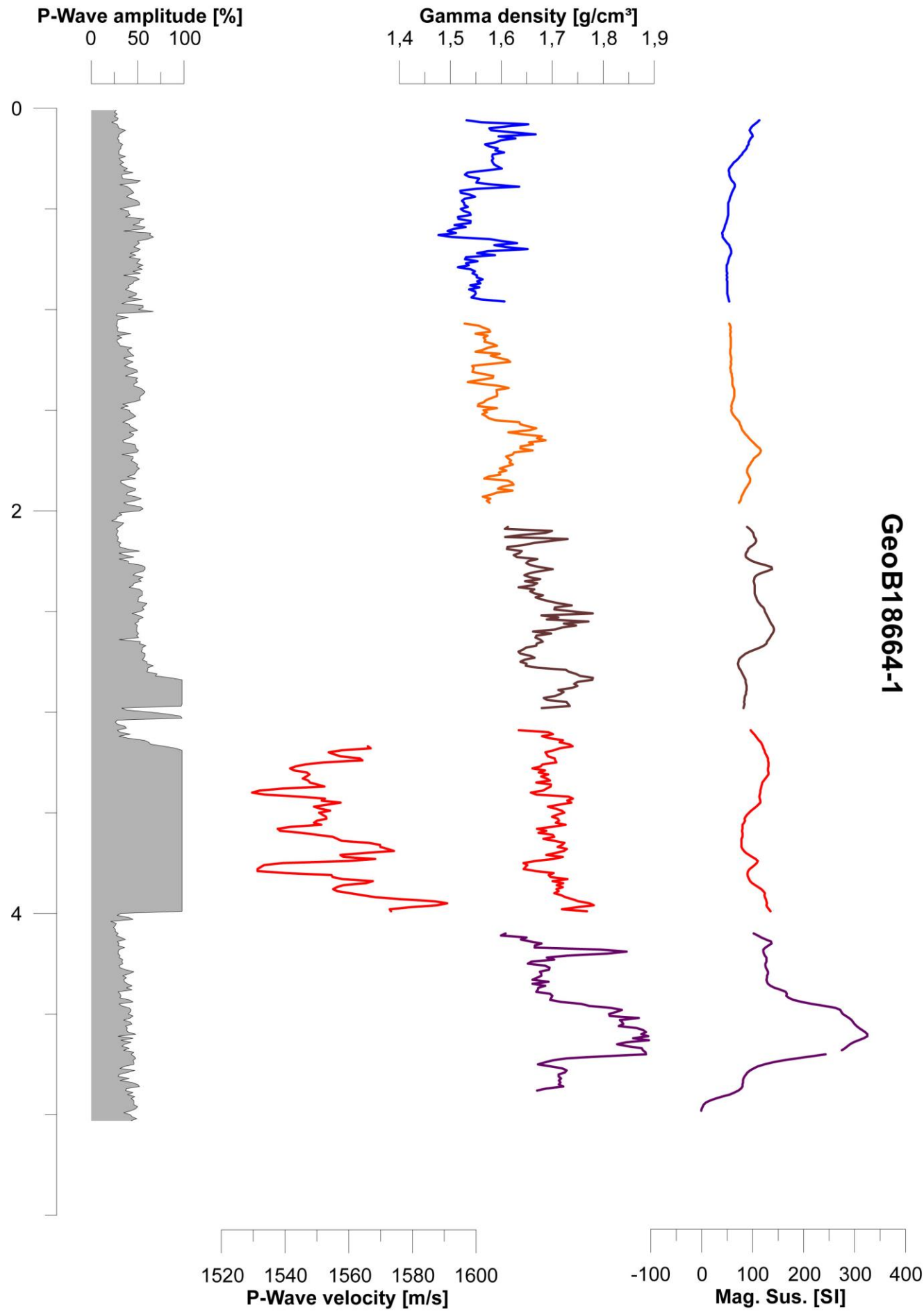
P-Wave amplitude [%]
0 50 100
Gamma density [g/cm³]
1,4 1,5 1,6 1,7 1,8 1,9
0
2
4
GeoB18664-1
1520 1540 1560 1580 1600
P-Wave velocity [m/s]
-100 0 100 200 300 400
Mag. Sus. [SI]

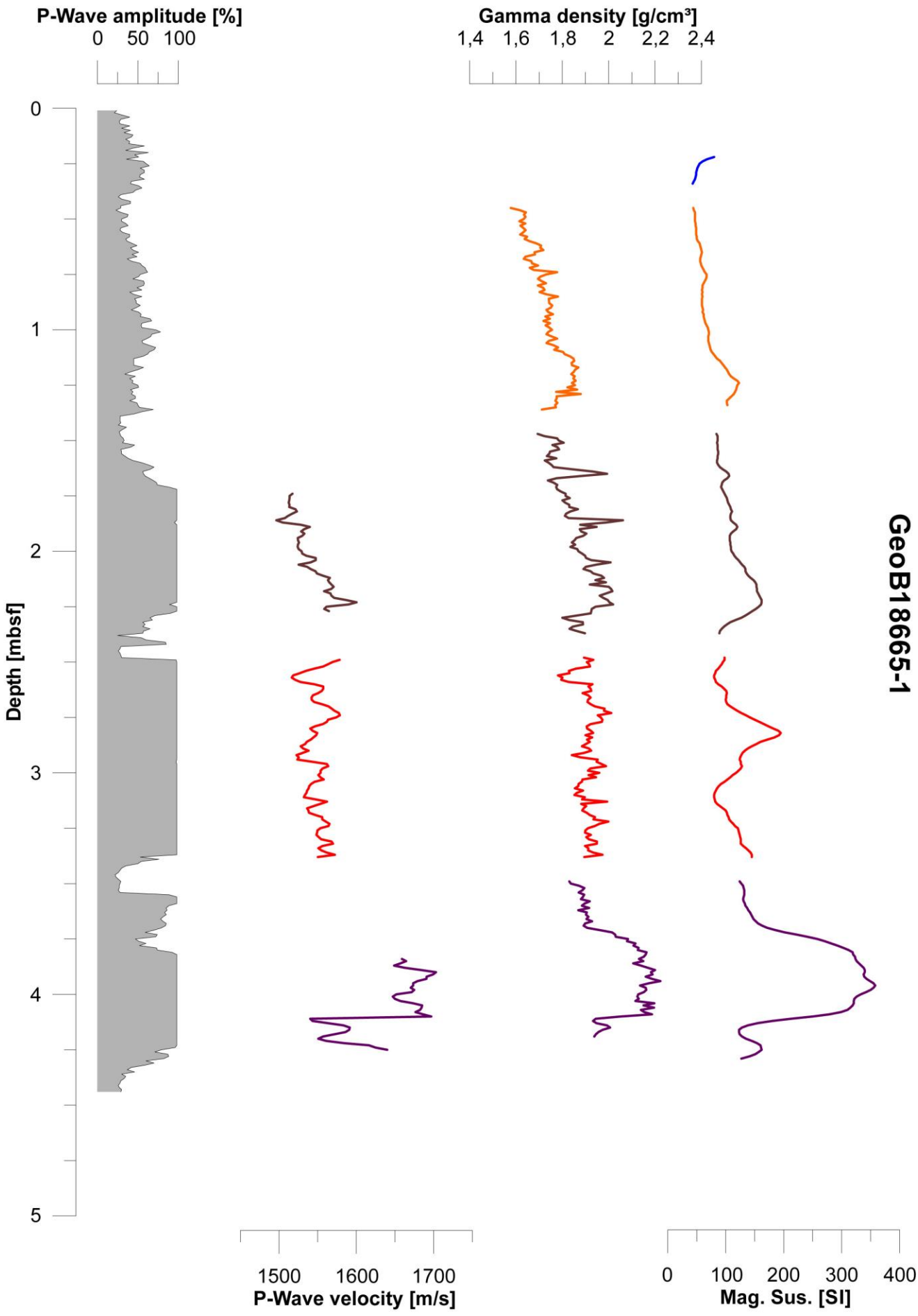
P-Wave amplitude [%]
0 50 100
Gamma density [g/cm³]
1,4 1,6 1,8 2 2,2 2,4
Depth [mbsf]
0
1
2
3
4
5
GeoB18665-1
1500 1600 1700
P-Wave velocity [m/s]
0 100 200 300 400
Mag. Sus. [SI]

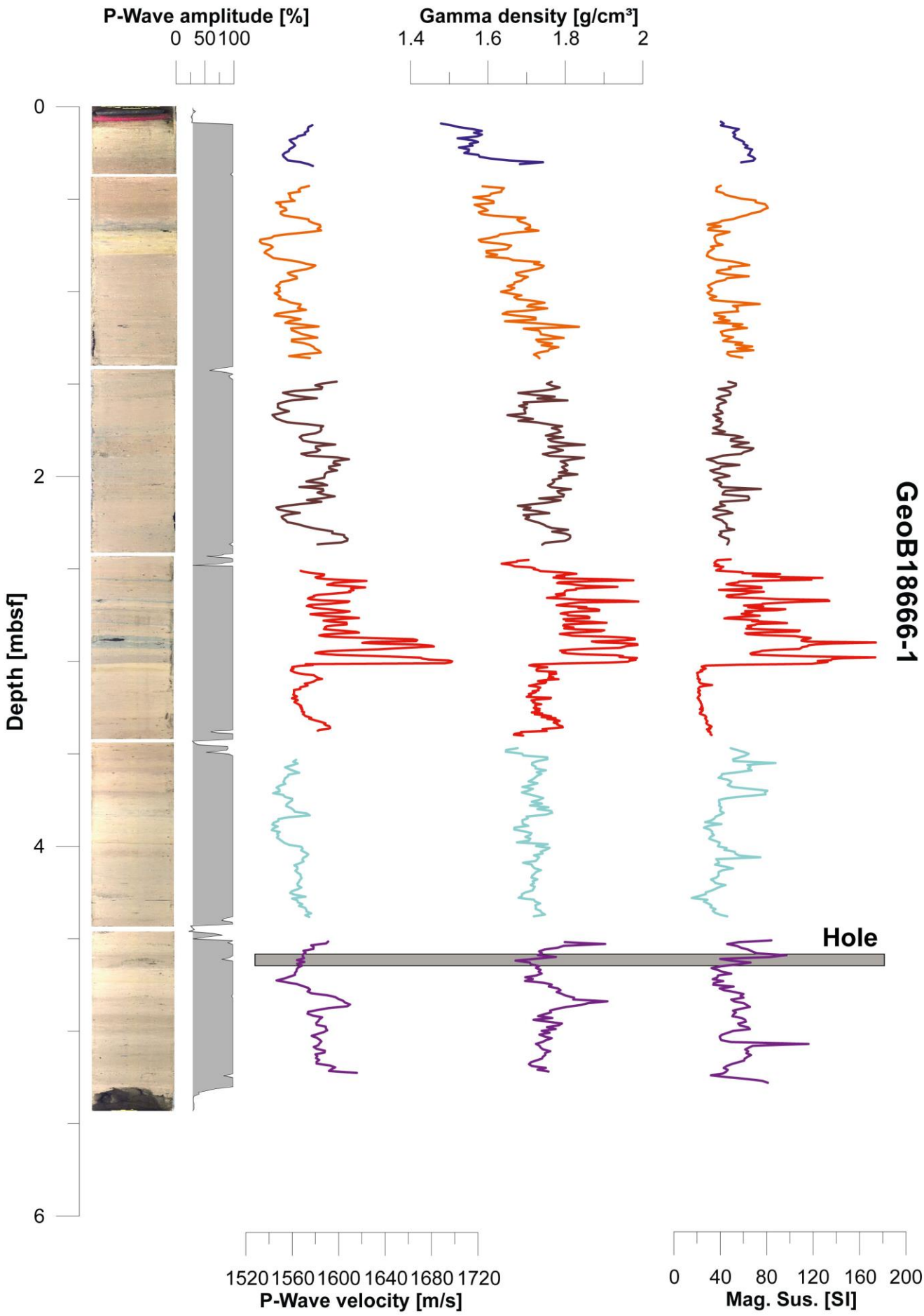
P-Wave amplitude [%]
0 50 100
Gamma density [g/cm³]
1.4 1.6 1.8 2
0
2
4
6
Depth [mbsf]
GeoB18666-1
Hole
1520 1560 1600 1640 1680 1720
P-Wave velocity [m/s]
0 40 80 120 160 200
Mag. Sus. [SI]

11.3 Bathymetry Maps (including track line)

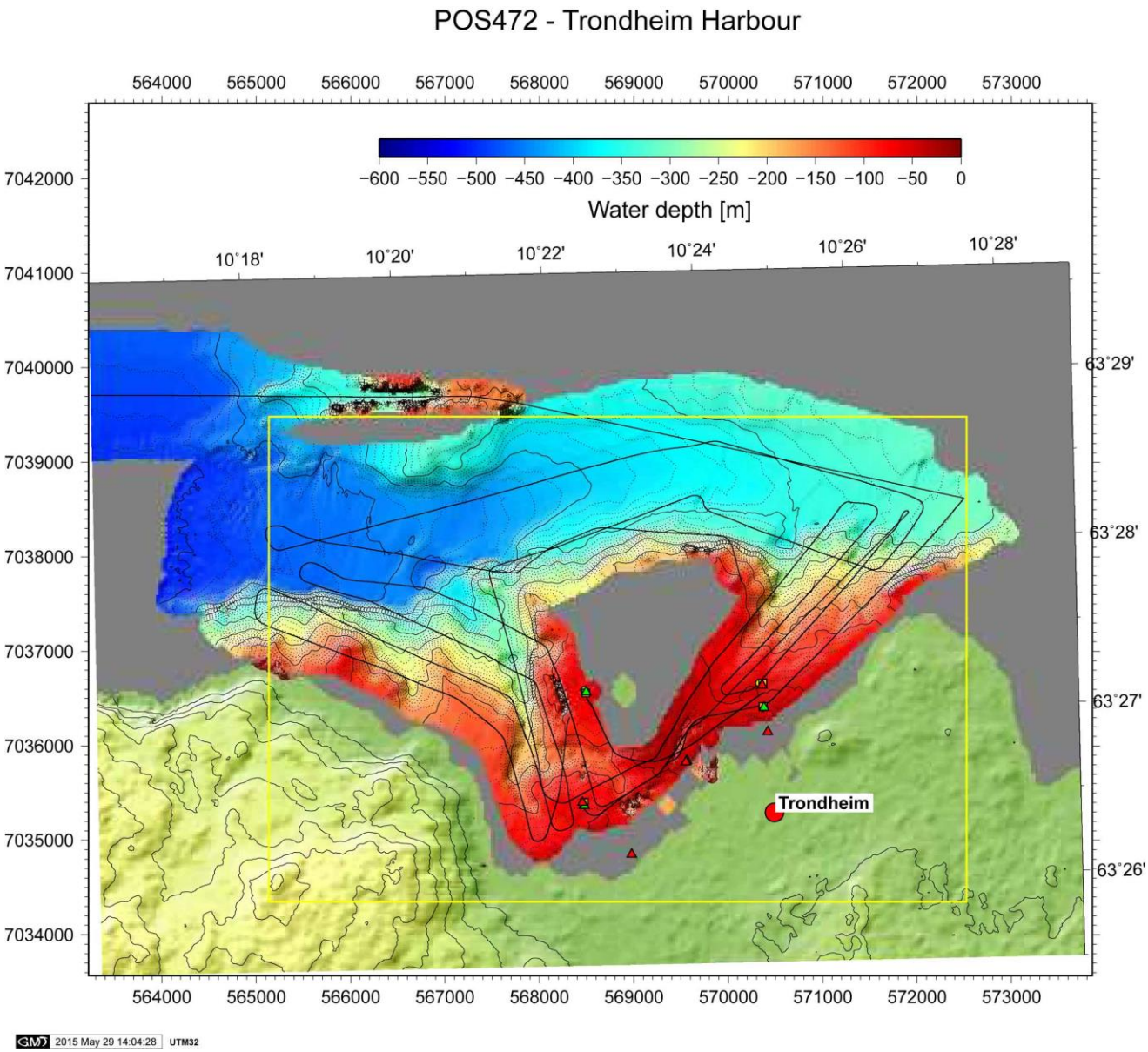

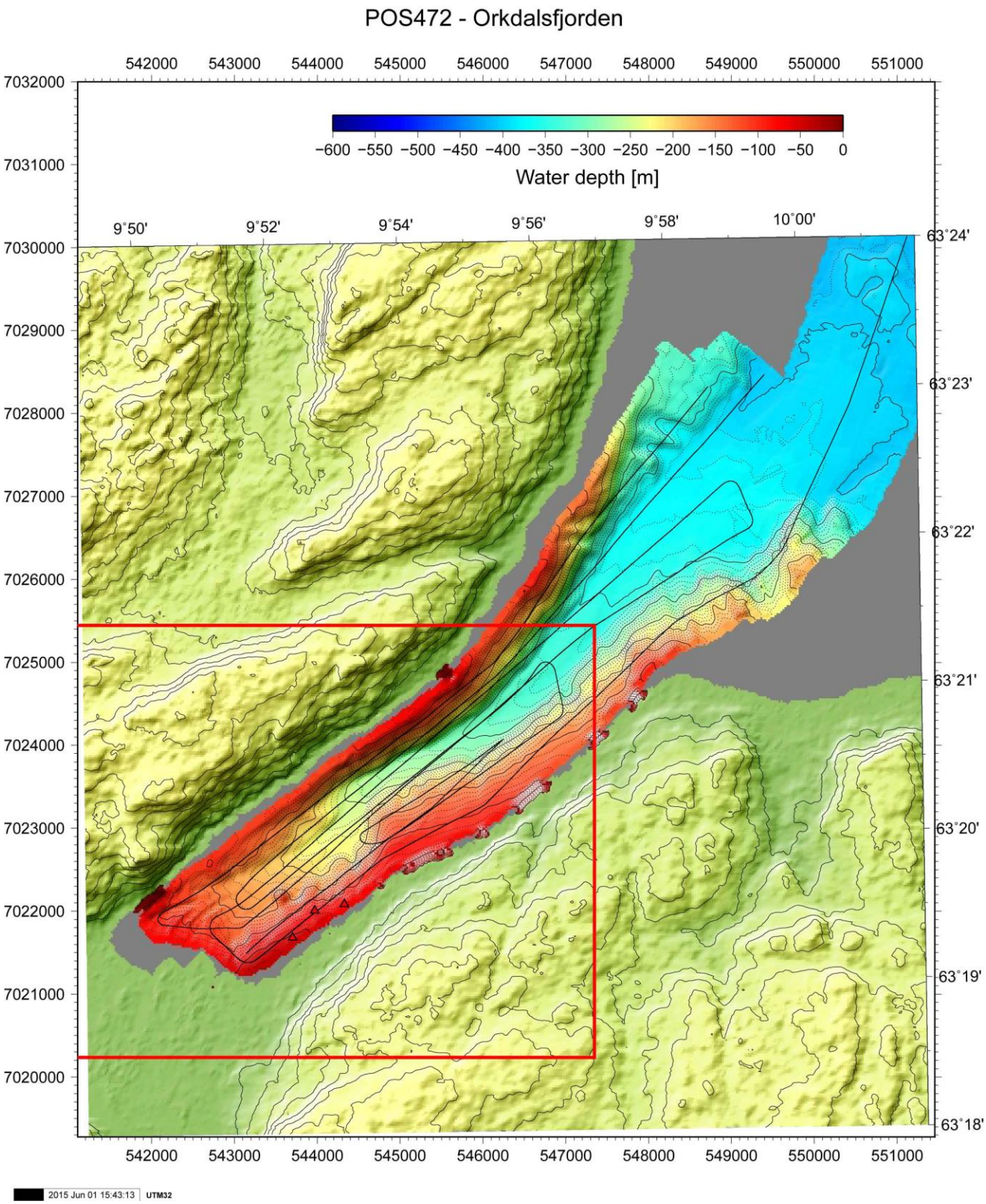
POS472 - Orkdalsfjorden
542000
543000
544000
545000
546000
547000
548000
549000
550000
551000
7032000
7031000
7030000
7029000
7028000
7027000
7026000
7025000
7024000
7023000
7022000
7021000
7020000
−600 −550 −500 −450 −400 −350 −300 −250 −200 −150 −100 −50 0
Water depth [m]
9°50'
9°52'
9°54'
9°56'
9°58'
10°00'
63°24'
63°23'
63°22'
63°21'
63°20'
63°19'
63°18'
2015 Jun 01 15:43:13
UTM32

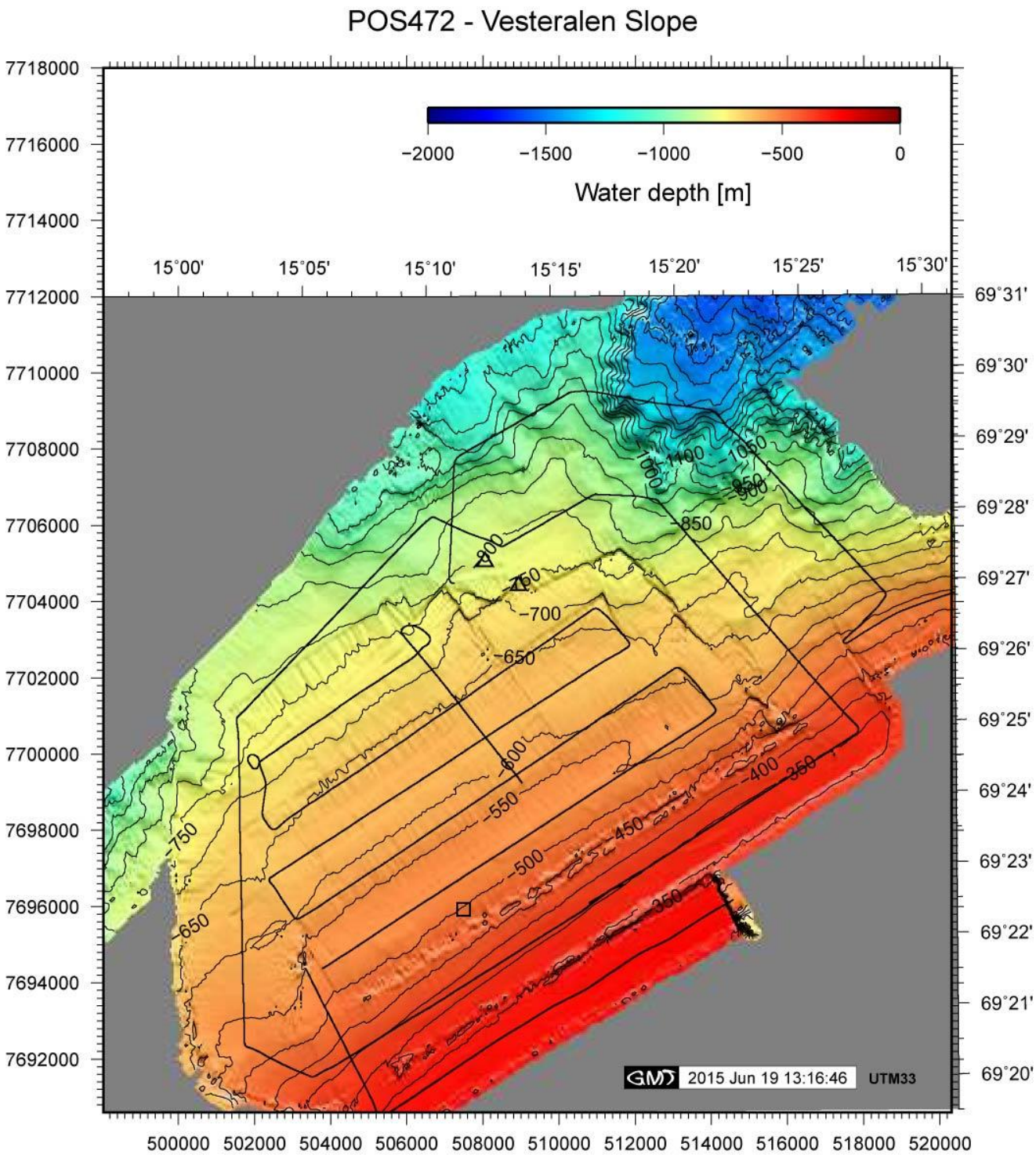
POS472 - Vesteralen Slope
−2000
−1500
−1000
−500
0
Water depth [m]
15°00'
15°05'
15°10'
15°15'
15°20'
15°25'
15°30'
69°31'
69°30'
69°29'
69°28'
69°27'
69°26'
69°25'
69°24'
69°23'
69°22'
69°21'
69°20'
7718000
7716000
7714000
7712000
7710000
7708000
7706000
7704000
7702000
7700000
7698000
7696000
7694000
7692000
500000
502000
504000
506000
508000
510000
512000
514000
516000
518000
520000
GMT 2015 Jun 19 13:16:46
UTM33

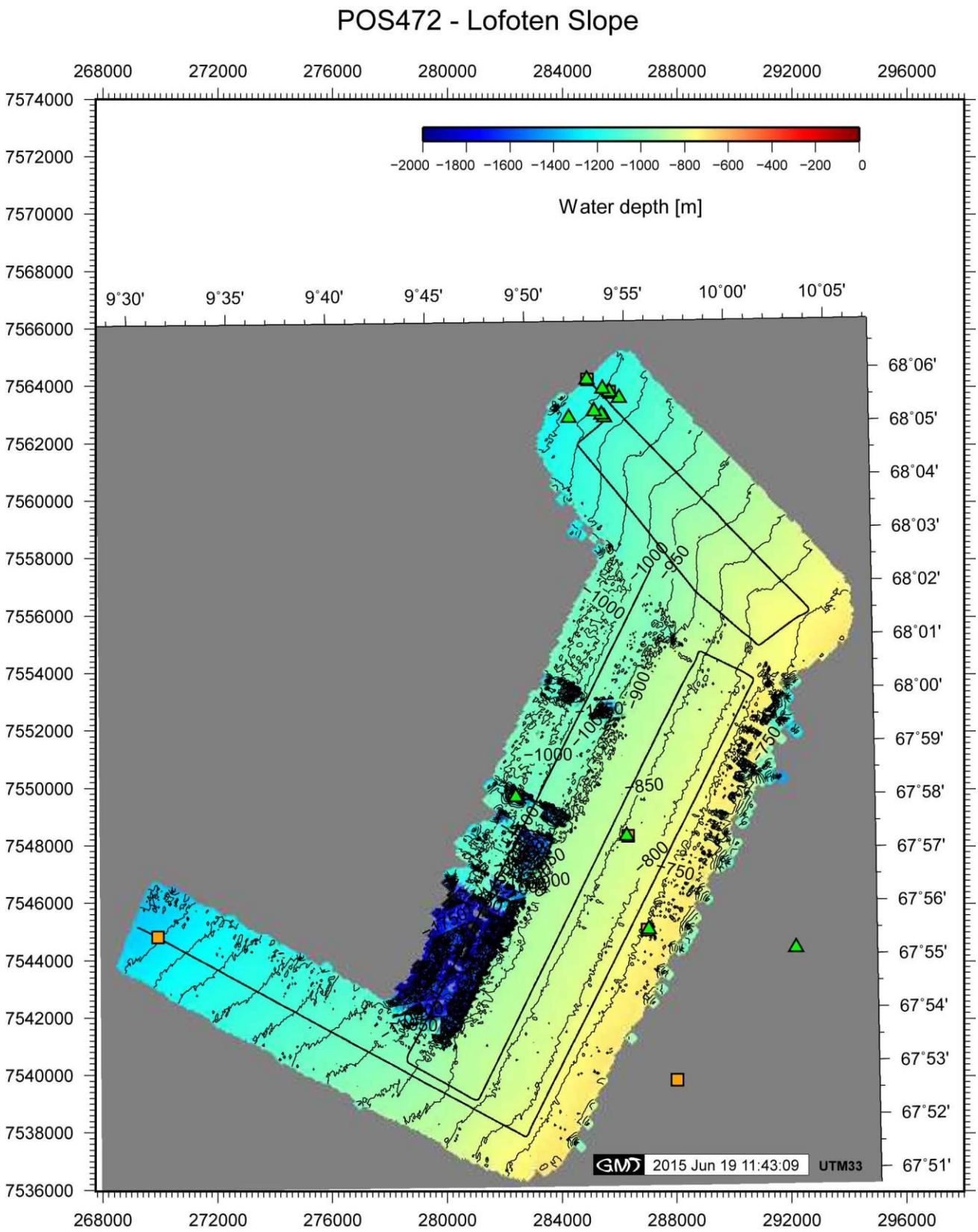
POS472 - Lofoten Slope
268000
272000
276000
280000
284000
288000
292000
296000
7574000
7572000
7570000
7568000
7566000
7564000
7562000
7560000
7558000
7556000
7554000
7552000
7550000
7548000
7546000
7544000
7542000
7540000
7538000
7536000
−2000 −1800 −1600 −1400 −1200 −1000 −800 −600 −400 −200 0
Water depth [m]
9°30'
9°35'
9°40'
9°45'
9°50'
9°55'
10°00'
10°05'
68°06'
68°05'
68°04'
68°03'
68°02'
68°01'
68°00'
67°59'
67°58'
67°57'
67°56'
67°55'
67°54'
67°53'
67°52'
67°51'
−1000
−950
−900
−850
−800
−750
GMT 2015 Jun 19 11:43:09
UTM33

From report No. 289 onwards this series is published under the new title:
Berichte aus dem MARUM und dem Fachbereich Geowissenschaften der Universität Bremen
A complete list of all publications of this series from no. 1 to 292 (1986 – 2012) was printed at last in issue no. 292.

No. 289 – Mohtadi, M. and cruise participants (2012). Report and preliminary results of RV SONNE Cruise SO 223T. TransGeoBiOc. Pusan – Suva, 09.09.2012 – 08.10.2012. 47 pages.
No. 290 – Hebbeln, D., Wienberg, C. and cruise participants (2012). Report and preliminary results of R/V Maria S. Merian cruise MSM20-4. WACOM – West-Atlantic Cold-water Corals Ecosystems: The West Side Story. Bridgetown – Freeport, 14 March – 7 April 2012. 120 pages.
No. 291 – Sahling, H. and cruise participants (2012). R/V Heincke Cruise Report HE-387. Gas emissions at the Svalbard continental margin. Longyearbyen – Bremerhaven, 20 August – 16 September 2012. 170 pages.
No. 292 – Pichler, T., Häusler, S. and Tsuonis, G. (2013). Abstracts of the 3rd International Workshop "Research in Shallow Marine and Fresh Water Systems". 134 pages.
No. 293 – Kucera, M. and cruise participants (2013). Cruise report of RV Sonne Cruise SO-226-3. Dip-FIP - The extent and structure of cryptic diversity in morphospecies of planktonic Foraminifera of the Indopacific Warm Pool. Wellington – Kaohsiung, 04.03.2013 - 28.03.2013. 39 pages.
No. 294 – Wienberg, C. and cruise participants (2013). Report and preliminary results of R/V Poseidon cruise P451-2. Practical training cruise onboard R/V Poseidon - From cruise organisation to marine geological sampling: Shipboard training for PhD students on R/V Poseidon in the Gulf of Cádiz, Spain. Portimao – Lisbon, 24 April – 1 May 2013. 65 pages.
No. 295 – Mohtadi, M. and cruise participants (2013). Report and preliminary results of R/V SONNE cruise SO-228, Kaohsiung-Townsville, 04.05.2013-23.06.2013, EISPAC-WESTWIND-SIODP. 107 pages.
No. 296 – Zonneveld, K. and cruise participants (2013). Report and preliminary results of R/V POSEIDON cruise POS448. CAPRICCIO – Calabrian and Adriatic Past River Input and Carbon ConversIOn In the Eastern Mediterranean. Messina – Messina, 6 – 23 March 2013. 47 pages.
No. 297 – Kopf, A. and cruise participants (2013). Report and preliminary results of R/V SONNE cruise SO222. MEMO: MeBo drilling and in situ Long-term Monitoring in the Nankai Trough accretionary complex, Japan. Leg A: Hong Kong, PR China, 09.06.2012 – Nagoya, Japan, 30.06.2012. Leg B: Nagoya, Japan, 04.07.2012 – Pusan, Korea, 18.07.2012. 121 pages.
No. 298 – Fischer, G. and cruise participants (2013). Report and preliminary results of R/V POSEIDON cruise POS445. Las Palmas – Las Palmas, 19.01.2013 – 01.02.2013. 30 pages.
No. 299 – Hanebuth, T.J.J. and cruise participants (2013). CORIBAR – Ice dynamics and meltwater deposits: coring in the Kveithola Trough, NW Barents Sea. Cruise MSM30. 16.07. – 15.08.2013, Tromsø (Norway) – Tromsø (Norway). 74 pages.
No. 300 – Bohrmann, G. and cruise participants (2014). Report and Preliminary Results of R/V POSEIDON Cruise P462, Izmir – Izmir, 28 October – 21 November, 2013. Gas Hydrate Dynamics of Mud Volcanoes in the Submarine Anaximander Mountains (Eastern Mediterranean). 51 pages.
No. 301 – Wefer, G. and cruise participants (2014). Report and preliminary results of R/V SONNE Cruise SO219A, Tohoku-Oki Earthquake – Japan Trench, Yokohama – Yokohama, 08.03.2012 – 06.04.2012. 83 pages.
No. 302 – Meinecke, G. (2014). HROV: Entwicklung und Bau eines hybriden Unterwasserfahrzeugs – Schlussbericht. 10 pages.
No. 303 – Meinecke, G. (2014). Inverse hydroakustische USBL-Navigation mit integrierter Kommunikation – Schlussbericht. 10 pages.
No. 304 – Fischer, G. and cruise participants (2014). Report and preliminary results of R/V POSEIDON cruise POS464, Las Palmas (Canary Islands) – Las Palmas (Canary Islands), 03.02.2014 – 18.02.2014. 29 pages.
No. 305 – Heuer, V.B. and cruise participants (2014). Report and preliminary results of R/V POSEIDON cruise POS450, DARCSEAS II – Deep subseafloor Archaea in the Western Mediterranean Sea: Carbon Cycle, Life Strategies, and Role in Sedimentary Ecosystems, Barcelona (Spain) – Malaga (Spain), April 2 – 13, 2013. 42 pages.
No. 306 – Bohrmann, G. and cruise participants (2015). Report and preliminary results of R/V METEOR cruise M112, Dynamic of Mud Volcanoes and Seeps in the Calabrian Accretionary Prism, Ionian Sea, Catania (Italy) – Catania (Italy), November 6 – December 15, 2014. 217 pages.
No. 307 – Fischer, G. and cruise participants (2015). Report and preliminary results of R/V POSEIDON cruise POS481, Las Palmas (Canary Islands) – Las Palmas (Canary Islands), 15.02.2015 – 03.03.2015. 33 pages.
No. 308 – Wefer, G. and Freudenthal, T. (2016). MeBo200 – Entwicklung und Bau eines ferngesteuerten Bohrgerätes für Kernbohrungen am Meeresboden bis 200 m Bohrteufe, Schlussbericht. 9 pages.
No. 309 – Sahling, H. and cruise participants (2016). R/V POSEIDON cruise POS498, Recovery of Observatories at Athina Mud Volcano, Izmir (Turkey) – Catania (Italy), 18 April – 1 May, 2016. 63 pages.
No. 310 – Fischer, G. and cruise participants (2016). Report and preliminary results of R/V POSEIDON cruise POS495, Las Palmas (Canary Islands) – Las Palmas (Canary Islands), 18.02.2016 – 02.03.2016. 29 pages.
No. 311 – Bohrmann, G. and cruise participants (2016). Report and preliminary results of R/V POSEIDON cruise POS499, Calabrian Mud Volcanoes, Catania (Italy) – Catania (Italy), 04 May – 22 May, 2016. 76 pages.
No. 312 – Kopf, A., Fleischmann, T. and cruise participants (2016). Report and preliminary results of R/V POSEIDON cruise POS500, LISA, Ligurian Slope AUV mapping, gravity coring and seismic reflection, Catania (Italy) – Malaga (Spain), 25.05.2016 – 09.06.2016. 58 pages.
No. 313 – Stegmann, S. and cruise participants (2017). Report and preliminary results of R/V POSEIDON cruise POS472, NORGEotech, Geotechnical in situ investigation of slope stability in Norway, Trondheim (Norway) – Tromsø (Norway), 27.07.2014 – 12.08.2014. 103 pages.